GROWTH OF MAGNETITE
ON STEEL
in high temperature aqueous environments.

by

MICHAEL JOSEPH LONGSTER, A.I.M.

A thesis submitted for the degree of Doctor of
Philosophy of The University of Aston in Birmingham.

January 1970.

SUMMARY

Previous studies on the oxidation of steel in high temperature aqueous environments have shown that the morphology and kinetics of formation of the corrosion product are dependent to a large extent on the environment. In alkaline solutions, oxidation in the presence of an external cathode resulted in the formation of a duplex layered oxide, whereas in the absence of an external cathode only a single layered oxide was formed. Furthermore, oxidation in ferrous chloride environments produced very much faster rates of oxidation.

This work was undertaken to provide more information on the principles involved in the production of various oxide forms.

The oxidation of mild steel in deionized water, 3.5M NaOH and ferrous chloride solutions at 316°C have been investigated using principally electron microscopy and Fe^{55} and Fe^{59} radioactive tracers. These new data are used to discuss differences in oxide morphology. A mechanism for the oxidation of steel in the absence of an external cathode has been proposed, which involves a two stage process of pore blocking followed by solid state diffusion. Regarding the oxidation of steel in the presence of an external cathode, the kinetics and mode of outer layer formation have been determined; these results are consistent with oxidation controlled by solution transport of iron. The oxidation of iron in ferrous chloride solutions is discussed, emphasis being placed on the effect of nickel in the early stages.

CONTENTS

CHAPTER II EXPERIMENTAL PROCEDURE AND TECHNIQUES

2.6. Electron microscopy

2.7. Weight change and thickness determinations

CHAPTER III RESULTS: GROWTH OF MAGNETITE IN CONDITIONED PRESSURE VESSELS

3.2. Radioactive tracer experiments

3.4. Electron microscopy

CHAPTER IV RESULTS: GROWTH IN P.T.F.E. LINED PRESSURE VESSELS

4.2. Nucleation and growth studies

4.3. Radioactive tracer experiments

CHAPTER V RESULTS: OXIDATION IN CHLORIDE ENVIRONMENTS

CHAPTER VI RESULTS: OXIDATION OF IRON ELECTRODEPOSITS

INTRODUCTION

The iron-water reaction has been extensively studied in recent years[1-6]. The chief reason being that greater use has been made of iron and its alloys in growth industries such as conventional and nuclear power generation for high temperature water heat exchangers. There would however appear to be a contradiction here because it is a well known feature of the iron-water system that it is thermodynamically unstable. The thermodynamics of a system will only predict the feasibility of a reaction whilst giving no information on the rate; it is for this reason that the most useful studies in this field have been biased towards the kinetics and morphology of the products of reaction. In general, the end product of the reaction between iron and water (in the absence of oxygen and at temperatures below 570°C) is magnetite. Fortunately the rate of the reaction is of a sufficiently low order to enable iron to be used for many high temperature water applications; under these conditions the magnetite layer is behaving protectively. Occasionally the magnetite becomes unprotective and leads to failure of the component. In an attempt to eliminate the breakdown of magnetite in boilers, a tremendous amount of research work both on static systems and also simulated boilers has been carried out, resulting in significant reductions in the incidence of failures.

In 1961 Potter and Mann[7] at the Central Electricity Research Laboratories, Leatherhead studied the oxidation behaviour of steel in sodium hydroxide solutions at temperatures between 250 and 350°C. The conditions of their experiments involved block specimens in conditioned pressure vessels; i.e. mild steel pressure vessels whose internal surfaces were covered with preformed magnetite oxide. Oxidation in these conditions produced a two layered oxide; the layer adjacent to the metal was found to be compact whilst the outer layer consisted of a loose assembly of magnetite crystals many of which showed a tetrahedral form. The fact that inert pearlite markers originally present in the steel retained their original position in the inner layer after oxidation suggested that the inner layer formed with zero volume change. More recent investigations[8-10] have shown the inner layer to be porous and permeated in such a way that iron could be transported across it in soluble form and produce the outer layer. The driving force for this mechanism arises because the first formed products after dissolution of iron have a greater solubility than the magnetite which eventually forms. Very much faster rates of oxidation were observed when iron was oxidised in ferrous chloride/nickel chloride solutions[11]. The oxide formed was lamellar, consisting of alternate layers of crystalline and porous oxide, it also closely resembled the oxide frequently found in boiler tubes suffering enhanced corrosion.

Bloom[12] obtained a compact single layered oxide on mild steel after oxidation in sodium hydroxide solutions of similar composition to those used by Potter and Mann; the experimental conditions were different in that the oxide was grown on the internal walls of a mild steel capsule. These irregular single layered oxides are commonly referred to as "Bloom" growths to distinguish them from the duplex Potter and Mann growths. Marsh[13] was able to reproduce "Bloom" growth by oxidising mild steel specimens in either an unconditioned pressure vessel or in a P.T.F.E. capsule contained in a normal mild steel pressure vessel. Using the results of these and further experiments, he attributed the formation of a porous inner layer to effects of electrical polarisation, a fact that contrasts with the work of Castle and Mann[10] who consider the external cathode functions as a diffusion sink for iron ions.

In an attempt to determine the way in which the two types of oxide were nucleated, Friggens and Holmes[14] investigated the early stages of oxide growth in deionized water using scanning and transmission electron microscopy. It was concluded that in the presence of an external cathode, the growth process was predominately 3-dimensional whereas in the absence of an external cathode, the process was 2- dimensional. These differences were ascribed to different surface mobilities of the reaction products.

The purpose of this present work can now be described. The basis is derived from several points arising from a study of the literature. To prevent undue repetition, these topics may be found at the end of the literature survey (Chapter I).

(1) At the present time there is no information on the kinetics and mode in which the outer layer forms nor is there any information on the extent of iron transport between the specimen and environment under Potter and Mann conditions. In this work attempts have been made to determine the factors affecting outer layer formation and also the extent of iron transport within the experimental system and the oxide itself. These results are discussed in conjunction with an electron microscopical study of the surface of the specimen after various times of oxidation.

(2) Subsidiary experiments showed that when a steel sample was oxidised in a P.T.F.E. lined pressure vessel containing sodium hydroxide solution at 316°C, the surface was covered with magnetite tetrahedra at a much earlier stage than if the same specimen was oxidised under Potter and Mann conditions (compare Fig. 4.6a. with b.); if similar experiments were performed in deionized water, no change was observed on the specimen oxidised in a P.T.F.E. capsule at times exceeding 40 minutes, yet

the specimen oxidised under Potter and Mann conditions showed nucleation and growth of an outer layer (compare Fig. 3.22. with Fig. 4.10.). In order to explain these observations a growth model is proposed to describe the oxidation of steel in the absence of an external cathode (in a P.T.F.E. lined pressure vessel). The model is based on a mechanism in which the rate is dependent initially on pore blocking and then by solid state diffusion.

(3) The oxidation of iron in chloride environments has been investigated because of the similarity between the morphology of the oxide formed under these conditions and the oxidation product found in boiler tube corrosion. This environment is vastly different from sodium hydroxide solutions because of its ability to support very much higher concentrations of ferrous ions. In this system experiments have been conducted to determine (a) how transport mechanisms are affected by a high ferrous ion concentration and (b) the influence of nickel additions especially in the early stages.

The experimental techniques principally used were scanning and transmission electron microscopy and radioactive iron tracers previously unused in similar investigations.

This thesis is divided into three parts, these are: survey of literature, experimental techniques and results, and finally a discussion and conclusions. Chapter I is devoted to a survey of the relevant literature but it also contains a critique of the knowledge of the subject at the present time. Chapter II commences with the experimental research programme and then describes the experimental procedures and techniques, as well as discussing the principles governing their use. There follow four chapters on the experimental results, each one devoted to a particular system. The growth of magnetite in both conditioned pressure vessels and in P.T.F.E. lined capsules, in ferrous chloride/nickel chloride solutions as well as the oxidation of iron electrodeposits are the subjects of individual chapters. In the final chapter the results of Chapters III,IV,V and VI are discussed. There follows a section devoted to conclusions, and two appendices: the first one is on boiler corrosion and the second one describes the analytical method used for the determination of iron.

CHAPTER I

LITERATURE SURVEY

1.1. The iron-water reaction.

The equilibrium attained when iron reacts with water, was the basis of a classic investigation by Chaudron[15] in 1921. In the reaction involving the conversion of iron into magnetite in high temperature water,

$$\text{i.e.} \quad 3Fe + 4H_2O \rightarrow Fe_3O_4 + 4H_2$$

equilibrium is reached when the pH_2/pH_2O ratio reaches a certain temperature dependent value.

Fig. 1.1. shows the variation of pH_2/pH_2O ratio with temperature. Using a value of the pH_2/pH_2O ratio found in normal boiler operation (10^{-9} to 10^{-7} max.), Homig[16] suggested that iron or wüstite will proceed to react with water to completion. Having established the necessary equilibrium conditions for the formation of magnetite, it would be prudent at this stage to examine in more detail the magnetite forming reaction.

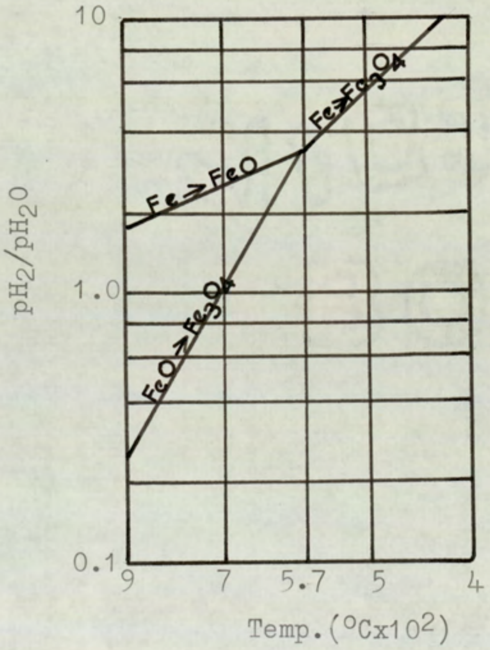

Fig. 1.1.
Variation of pH_2/pH_2O with temperature after Chaudron[15]

The reaction mechanism between iron and water has been investigated by Linnenbom[17] in the temperature range 25-300°C. Whilst it is thermodynamically feasible for the direct formation of magnetite at room temperature (Reaction I), it is rarely if ever found.

e.g.

$$3Fe + 4H_2O \longrightarrow Fe_3O_4 + 4H_2 \quad \Delta F^{o}_{298^{o}K} = -15640 \text{ cal......I}$$

$$Fe + 2H_2O \longrightarrow Fe(OH)_2 + H_2 \quad \Delta F^{o}_{298^{o}K} = -2190 \text{ cal.....II}$$

$$3Fe(OH)_2 \longrightarrow Fe_3O_4 + 2H_2O + H_2 \quad \Delta F^{o}_{298^{o}K} = -9070 \text{ cal...III}$$

However, a more likely reaction that is favoured by many workers[17,18] is the formation of ferrous hydroxide by Reaction II.

At normal boiler operating temperatures there is thermodynamic evidence that Reaction I can occur which would of course mean that magnetite forms directly from iron. Alternatively there is a possibility that magnetite forms by Reaction III which is known as the Schikorr[19] reaction. Ferrous hydroxide would then be an intermediate in the formation of magnetite. The concentration of ferrous hydroxide at any time on a corroding sample would of course be a function of the overall iron corrosion rate. There may be some basis for this argument, since ferrous hydroxide converts to magnetite[20] in accordance with the Schikorr reaction with an activation energy of 30±3 kcal./mole.

over the temperature range 150-210°C.

1.2. The growth of magnetite films.

1.2.1. Introduction.

A tremendous amount of literature has been published on this topic and it would be appropriate to survey the literature in terms of kinetics and structure. Direct comparisons between the results of different workers are made extremely difficult because relatively minor differences in oxidation conditions have been shown to radically affect both the kinetics and morphology of the magnetite formed[13]. Nevertheless, an attempt is made to review the relevant literature underlining any important conclusions and topics of a controversial nature. The method of oxidation in high temperature water generally involves the use of static pressure vessels heated either by a muffle furnace or alternatively by some independent electrical method.

1.2.2. Growth in high temperature water.

The definition of high temperature water implies oxidation in water at temperatures between 300 and 350°C.

Before 1960 very little systematic work had been performed on the oxidation of steel in high temperature aqueous environments. In the United States Kaufmann, Marcy and Trautmann[21] investigated the corrosion of mild steel in heated pressure vessels by measuring the residual pressure produced by the liberation of hydrogen. Bloom and Fraser[22] determined the corrosion rate of steel in concentrated caustic soda solutions by measuring the rate of hydrogen diffusion through the thin wall of the pressure vessel. The majority of the other work before 1961 had been performed on stressed mild steel in an effort to investigate caustic embrittlement[23].

Investigations by Potter and Mann[7] and later extended by Adams, Field, Holmes and Stanley[8] into the oxidation of small specimens in aqueous environments containing additions of sodium hydroxide invariably showed that an oxide containing two magnetite layers was formed. These two layers had different visual and physical properties (Fig. 1.2a.). The layer adjacent to the steel was found to be protective, adherent and free from cracks, whilst the outer layer was of coarse grained crystalline magnetite. Fig. 1.2b. illustrates this crystalline magnetite layer formed in 3.5M NaOH after 125 hours oxidation at 316°C.

Using weight change experiments Potter found the following general relationships (see Fig. 1.3.) for the oxidation of steel in 13% sodium hydroxide solutions at 340°C. Furthermore, increased concentrations of sodium hydroxide up to 40% resulted in a corresponding increase in the total corrosion rate, although the ratio between total oxidation and adherent oxide remained constant. Under these conditions the total oxidation

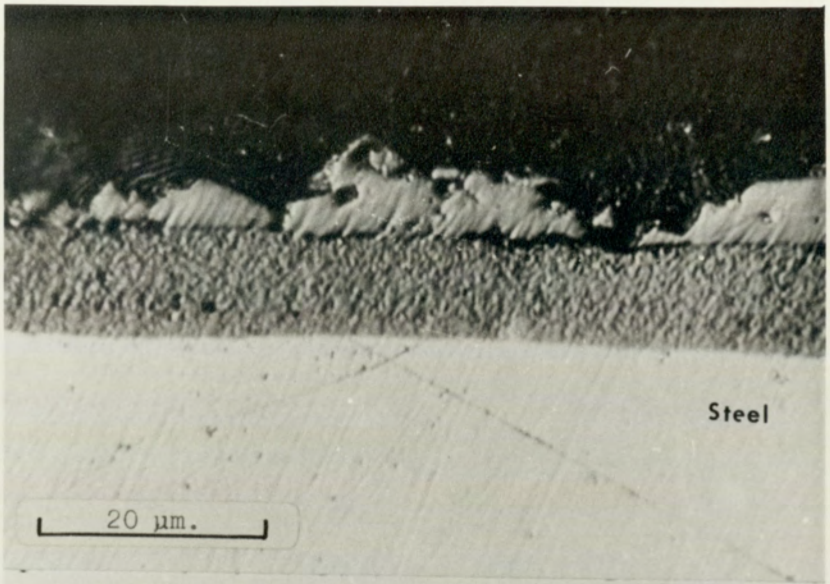

Fig. 1.2a. Cross section of steel oxidised in a conditioned pressure vessel. (3.5M NaOH, 316°C, 125 hours.)

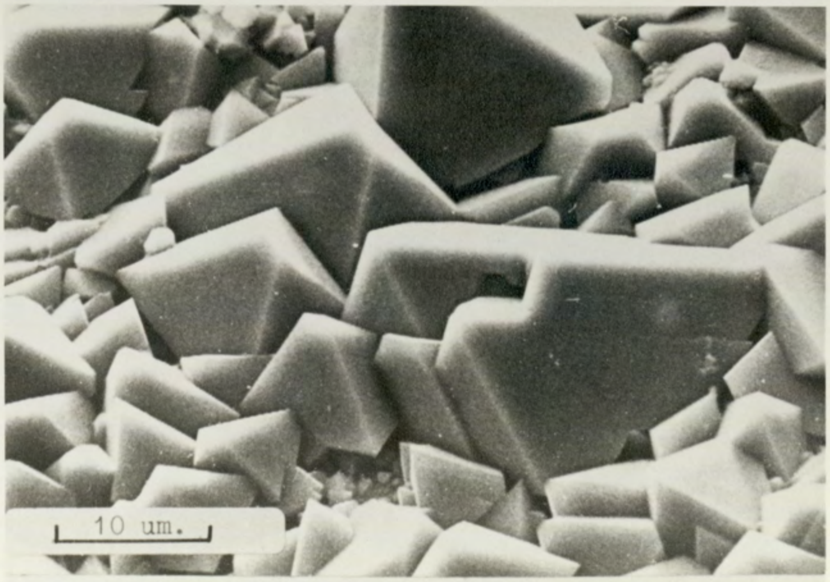

Fig. 1.2b. Scanning electron micrograph of the surface shown in Fig. 1.2a.

obeyed the parabolic growth law $x = kt^n$ where x equals total iron oxidised, t is the time, k is the constant and n is the power and was found to equal 0.6 by statistical treatment. An interesting feature of oxidation under these conditions is that the pearlite present in the steel retained its original position in the inner layer in spite of a Pilling-Bedworth[24] ratio of 2.1:1. This situation occurred because approximately half the iron left the corroding sample (Fig. 1.3.) leaving the inner layer virtually stress free. The iron atoms responsible for building up the inner layer were ionized and reacted to form magnetite at their original position on the lattice.

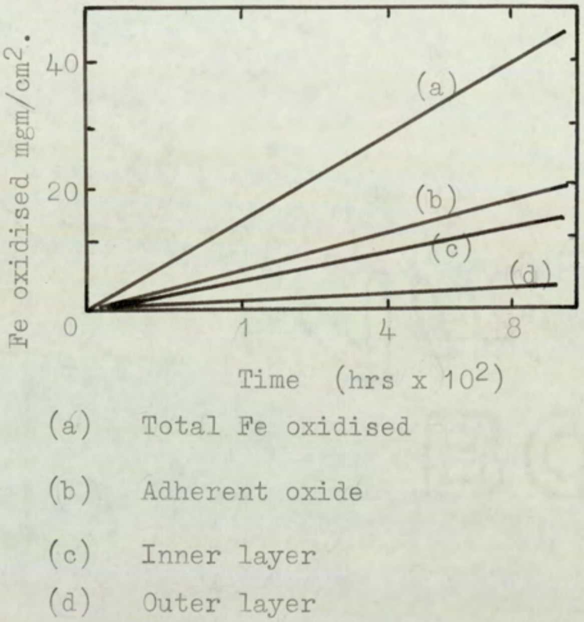

Fig. 1.3. Distribution of oxidised iron after oxidation of mild steel in 13% NaOH at 340°C. After Potter and Mann[7].

1.2.3. Transport mechanisms.

The activation energy for the oxidation of iron in 13% sodium hydroxide solution over the temperature range 250-350°C was found to be 30 kcal/mole* whereas the activation energy for the growth of magnetite by a solid state diffusion process was the order of 50-55 kcal/mole[25,26]. This implied that the magnetite formation mechanisms were somewhat different in these two cases. For this reason research workers[7,8] have attempted to reconcile the lower value of activation energy observed in high temperature aqeous oxidation with differences in morphology and physical aspects of the oxide layers. Observations by Adams, Field, Holmes and Stanley[8] on the changes in thickness of the inner layer with time suggested that it could be mathematically represented by the logarithmic growth law:

$$x = k1 \ln(1 + k2t)$$

where $k1$ and $k2$ are constants and x is oxide thickness after time t. This law which was first suggested by Evans[27] and later modified by Harrison[28] represents mutually-blocking pores where the compressional stress in one pore exerts a pressure on an adjacent pore such that it may become blocked. This might at first seem reasonable since there is ample evidence of the production of a porous inner layer from direct observations such as electron microscopy[9,29,30], and indirect observations which have included density[8] and gas adsorption[9] measurements.

---

* originally quoted in ref. 7 as 15±2 kcal/mole. was found to be in error and was later corrected to 30±2 kcal/mole.

In order to explain their observations, Adams et al proposed a model hypothesis which is depicted in Fig. 1.4. Primary attack takes place at lattice defects such as screw dislocations. The screw dislocation may become completely oxidised since the attack could spread downwards into the iron and along the length of the step. Shear forces were introduced between the magnetite and iron which resulted in iron particles being detached thereby leaving a pore to allow further access of the oxidising medium. The detached iron was thought to be dissolved by the oxidising medium which resulted in the formation of the magnetite outer layer by a solution transport process. An advantage of this model was that it could predict and explain many observations encountered in high temperature aqueous oxidation of iron. Perhaps the most important of the predictions was the magnetite grain size, which was actually found to be between 250Å and 5000Å. Similar dimensions were calculated by equating the parameter of the unit spinel lattice with the iron lattice to mismatch, assuming that no distortion of the crystal lattice occurred at the interface. Perhaps the most serious disadvantage is that there is no evidence that initial attack of the iron surface occurs in the way postulated, certainly the dimensions suggested would be easily resolvable by modern electron microscopical techniques and instruments. Secondly the model

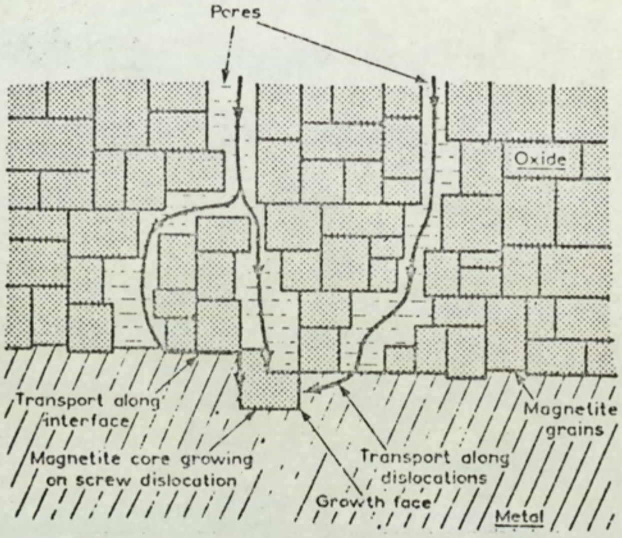

Fig. 1.4. Showing suggested diffusion paths to growth interface for oxygen-bearing ions. (After Adams et al.[8]).

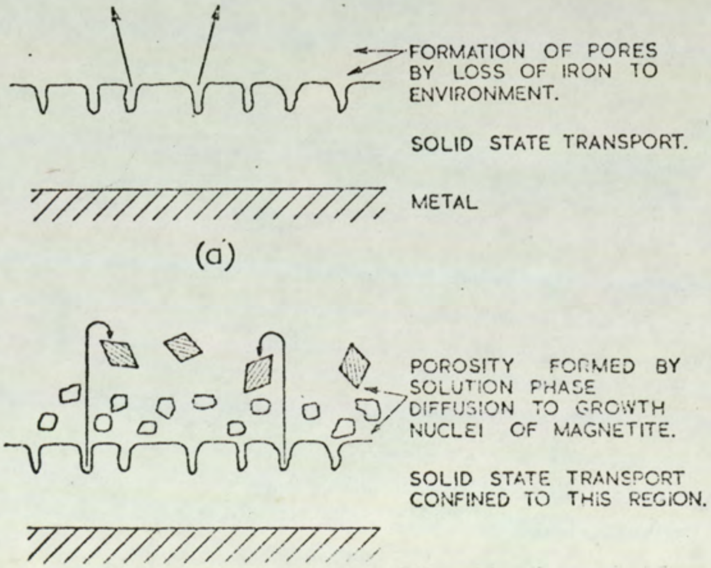

Fig. 1.5. Representing the formation of a two layered magnetite film on steel. (After Castle and Mann[10].).

takes no account of the effect of the air formed ferric oxide film that is present on the iron surface, which would suffer dissolution before the iron substrate and would infer some form of transition region.

Effect of alkalinity on iron transport.

Castle and Masterson[9] have adequately explained the influence of alkalinity on the corrosion rate at high temperatures. The inner magnetite layer is assumed to be porous allowing the oxidising medium close access to the metal during oxidation. They produced evidence that the equilibrium concentration of iron ions with iron metal depends on the hydroxyl ion concentration; applying this important result to the hypothesis that the overall corrosion rate is controlled by the outward transport of these iron-containing ions under a concentration gradient then for a constant period of time they obtained the following relationship:-

$$\ln W = K + \tfrac{1}{2}\ln S$$

where W = weight of iron corroded in a given time

S = equilibrium solubility of iron

K = constant

In this form the relationship is linear and was proved experimentally by plotting the weight of iron oxidised after 50 hours against the solubility of iron in sodium hydroxide solutions ranging from 0-20%. This must be regarded as an extremely important result in the oxidation of iron in these conditions. It would seem appropriate at this stage to examine schematically the mechanism by which a double layered oxide grows. Fig. 1.5. represents the stages and conditions from nucleation to subsequent growth of a porous oxide proposed by Castle and Mann[10]. The steel surface was assumed to be covered with an air formed film of ferric oxide. On immersion of the steel in an electrolyte at high temperature, the initial stages of oxidation were characterised by two competing factors, they were: (a) the thickening of the film by solid state diffusion and (b) dissolution of the film by the electrolyte. In sodium hydroxide environments at temperatures around 360°C the effect of (a) would be very slow compared to (b). At an early stage in the process, magnetite nuclei developed at the oxide-electrolyte interface and perpetuated iron transport away from the dissolution region. A feature of this mechanism was that the oxidation process became independent of the experimental container as soon as the growth nuclei and dissolving interface were separated by the porous inner layer. The driving force for the transport of iron could be well explained from Linnenbom's[17] work which showed that the apparent solubility of iron in water falls by a factor of ten when magnetite is nucleated in the solution. To test their model Castle and Mann performed the following experiment: two similar iron specimens were oxidised for

168 hours in static pressure vessels at 300°C in 13% sodium hydroxide solution. One of the specimens was transferred to another pressure vessel containing deionized water and both were reoxidised for 48 hours. As expected the specimen in deionized water had soluble iron transport suppressed (iron has lower solubility in deionized water than in sodium hydroxide solution at 300°C) and therefore could not maintain porous oxide growth. A layer of non porous oxide had formed at the oxide metal interface.

The Castle, Mann[10] model gave an explanation for the differences in morphology of magnetite grown by Bloom and co-workers[12,22]. In Bloom's experiments where the ratio of surface area to volume of electrolyte was large a non porous film was produced. A similar film was produced in a P.T.F.E. lined pressure vessel where the ratio of surface area to volume of electrolyte was 1 cm^2. to 1 ml. When the pressure vessel containing the P.T.F.E. capsule was mechanically shaken a porous Potter and Mann type oxide was produced. In this system the solution would rapidly saturate with iron, removing the iron ions away from their emergent sites; this was found sufficient to perpetuate a porous layer.

In the absence of mechanical shaking, a porous inner layer could still be induced by the introduction of a diffusion sink, i.e. a surface capable of supporting the Schikorr reaction.

Platinum foil was used and after a period of time it was found to be covered with magnetite crystals. Evans[31] considers that the platinum surface supports a cathodic reaction, the production of hydrogen e.g. $2H^+ + 2e = H_2$

and balanced by the anodic reaction:-

$$FeO_2^{2-} = FeO_2^- + e$$

The liquid would then become supersaturated with regard to magnetite and deposition occurs by the following reaction:-

$$FeO_2^{2-} + 2FeO_2^- + 4H^+ = Fe_3O_4 + 2H_2O$$

Growth in unconditioned pressure vessels.

The experimental work reviewed so far has been concerned with the oxidation of independent samples in pressure vessels, the internal surfaces of which were covered with magnetite by a pre-oxidation treatment. Oxidation of iron samples in unconditioned or new pressure vessels gave vastly different results[13]. The chief difference being that only a single layer was produced which was much more protective. These protective single layers could also be achieved by oxidising the specimen inside a P.T.F.E. capsule placed inside a normal pressure vessel (see Fig. 1.6.). This single layered growth was extremely similar to that obtained by Bloom[12,32] during his investigation of the alkaline corrosion of steel. His technique involved the continuous measurement of hydrogen produced from the corrosion reaction. The pressure

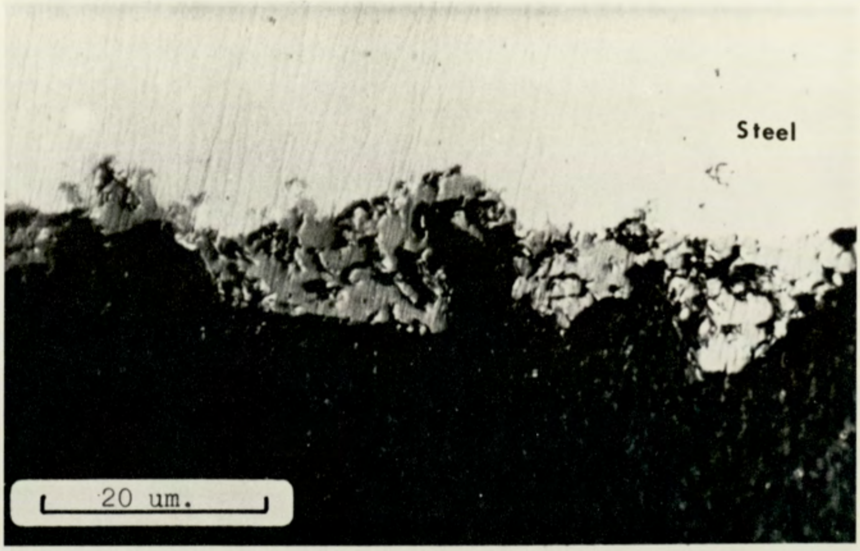

Fig. 1.6a. Cross section of steel oxidised in a P.T.F.E. lined pressure vessel. (3.5M NaOH, 316°C, 100 hours.)

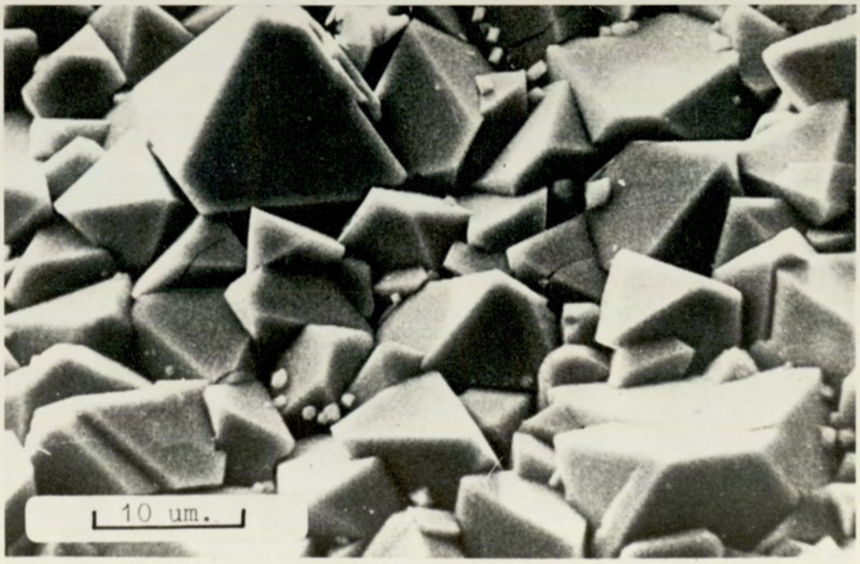

Fig. 1.6b. Scanning electron micrograph of surface shown in Fig. 1.6a.

vessel was constructed from a tube flattened at both ends and spot welded to seal in the liquid. In these experiments the internal surfaces of the tube constituted the specimen. The tube walls were thin such that hydrogen evolved from the magnetite forming reaction could diffuse through the walls and be measured continuously. This type of growth is now commonly referred to as "Bloom" growth to distinguish it from the two layered "Potter and Mann" growth. A further interesting feature of "Bloom" growth is the incidence of hemispherical pits; any theory explaining the differences between the two types of growth must adequately account for the observed pitting.

In an attempt to resolve the differences between the two types of oxide growth, Marsh[13] carried out experiments involving different experimental conditions which were capable of producing both oxide forms and under certain conditions mixtures of both types. It would appear from Marsh's work that when a mild steel specimen has no contact with a suitable cathode capable of supporting the following reactions:-

$$2e + 2H_2O \rightarrow 2OH^- + H_2$$

or $4e + 2H_2O + O_2 \rightarrow 4OH^-$ (in the initial stages when there is some dissolved oxygen present) non porous irregular film is formed (Bloom type). The pitting formed is thought to arise from defects in the film exposing the underlying steel. The magnetite already formed acts as an external cathode and would account for the similarity that exists between the magnetite in the pit and the inner layer of Potter and Mann magnetite.

In contrast to the work of Marsh, Castle and Mann[10] considered that electrical polarisation was not necessary for the formation of a porous oxide, although it may have constituted an additional driving force.

1.2.4. Oxidation in deionized water between 300 and 360°C.

The rates of oxidation of iron in deionized water were found to be extremely low. Potter[4] reported a magnetite layer of only four microns thick after 2500 hours at 360°C, but claimed a close similarity in morphology with the double layer formed in alkaline solutions. This would be in accordance with the work of Douglas and Zyzes[1] if the reduction in surface activity of their inert radioactive markers could be attributed to residence between an inner and outer layer. This would of course be extremely difficult because it was seen that the oxides grown in deionized water were very thin.

Katō and Arai[33] claimed that oxidation in an electrolyte of pH 11 resulted in a mechanism similar to that of dry oxidation. It would be difficult to compare this work with that of other workers on two accounts, firstly the pressure vessels and solution were kept saturated with oxygen which would of course allow oxygen to react directly with the steel as in normal dry oxidation and secondly, the corrosion of iron is lowest in water where additions of sodium hydroxide have been made to pH 11. It is of interest that their electron micrographs of the iron surface oxidised under these conditions differed greatly from specimens where solution transport has been known to occur, in that the crystalline outer layer was absent. It would appear therefore that because of the low corrosion rate of iron in the electrolyte, iron transport had been suppressed.

1.2.5. Oxidation in superheated steam and water.

Oxidation under these conditions has been the subject of close attention by many workers[4,34,35], particularly those associated with high pressure and temperature steam plant where these conditions are frequently encountered. It would appear from the literature that the corrosion rate can usually be attributed to the general growth law $w = kt^n$, where w is the weight gain after time t, k is a constant and n is the power which is found to vary under these conditions between 0.3 and 0.5. A parabolic growth law (where $n = 0.5$) would indicate a diffusional process where the diffusion path that one or more of the reactants must take is increasing with time. If the corrosion rates are ascribed to a cubic law (where $n = 0.3$)

then the oxidation mechanism would have to be explained by some mechanism other than simple diffusion.

Experimental determinations of the self diffusion of oxygen in magnetite by Castle and Surman[36,37] did not satisfy the growth rates actually observed in superheated steam. The calculated value of $D_{450} = 7 \times 10^{-14}$ cm.^{2} sec^{-1}. being about five orders of magnitude greater than the experimental value at 450°C indicates that solid state oxygen diffusion is not rate controlling.

1.2.6. Oxidation in ferrous chloride environments.

Fast linear rates of oxidation have sometimes been observed in environments capable of holding a high ferrous ion content in solution[11]. The presence of nickel ions at only a low concentration (10^{-4}M) assured that fast linear oxidation took place in 0.1M ferrous chloride. The magnetite that formed under these conditions was invariably thick and laminated; the laminations consisting of oxide similar to the inner and outer layer formed in alkaline environments under normal Potter and Mann conditions. Crazing was also observed which Potter and Mann[11] concluded was the chief reason for the non-protectiveness. Furthermore, they supposed that the suppression of the outward migration of iron cations was such as to cause the film to grow completely at the metal/oxide interface. This supposition rather contrasted with the model proposed by Castle and Mann, which suggested that the nickel present on the outer surface of the oxide encouraged iron transport away from the corroding steel interface. This would adequately explain the observation that oxidation in ferrous chloride environments is erratic in the absence of nickel, but reproducible when a layer of nickel is present. The linear kinetics that were observed would only be coincidental if the Castle, Mann model trully described the oxidation under these conditions.

1.3. Nucleation and growth.

1.3.1. Introduction.

The nucleation and growth of magnetite films on iron oxidised in conditioned and P.T.F.E. lined pressure vessels have been investigated by electron microscopy, to provide more information on these early stages[14]. As with most microscopical techniques the results must be interpreted with great caution, as the phases and structures present during the active oxidation process cannot be viewed with a microscope without changing their environment considerably. Obviously some techniqes are much to be preferred in this respect than others, for instance, scanning electron microscopy has the advantage over other electron microscopical techniques in that the surface can be viewed without any further preparation. Even this technique suffers the serious disadvantage that the sample has to be cooled from high temperature washed and dried before viewing.

1.3.2. Nucleation of Potter and Mann films.

Transmission electron microscopy by Field and Holmes[29] showed that magnetite crystallites between 300Å and 1000Å in size formed on annealed iron when oxidised in deionized water at 250°C after only 20 minutes. The nucleation density was found to be $10^{10}/\text{cm.}^2$; at this density dislocation sites would not be responsible for nucleation. On impingement of the growing crystallites, small pores were left between 0-300Å in diameter. In later studies Friggens and Holmes[14] could distinguish between two different types of particles after only 20 minutes oxidation. The particles were observed to grow both laterally and outwards perpendicular to the metal substrate. Pores were again observed to remain after impingement of the first formed crystallites, whilst larger particles falling in the size range 1000-2000Å were thought to be the commencement of the large regular crystals found in Potter and Mann type films.

1.3.3. Nucleation of Bloom films.

Although initial nucleation of Bloom films appeared to be in a similar way to that observed in Potter and Mann films, their subsequent growth seemed to be markedly different. There was evidence that the growth was essentially 2-dimensional and that the particles merely merged forming a continuous film. It is not clear why these differences occur but Marsh's theory that the conditioned pressure vessel walls acted as a cathode for the electrochemical magnetite forming reaction does seem credible especially where the difference in the transport of iron ions may not be so significant in the two cases.

1.3.4. Epitaxial relationships.

The epitaxial relationships[38] normally observed for magnetite growth on iron are:-

$$(001)_{Fe} \quad \| \quad (001)_{Fe_3O_4}$$
$$[110]_{Fe} \quad \| \quad [100]_{Fe_3O_4}$$

There was some evidence that the oxidation of iron in high temperature aqueous environments followed this pattern since the recrystallisation textures most usually found in iron were $\{100\}$ 15° from $\langle 011\rangle$ and $\{112\}$ 15° from $\langle 110\rangle$; on oxidation these would result in $\langle 110\rangle$ magnetite reflections which in fact were found to predominate[14].

Summary.

The main points which arise from a study of the relevant literature describing the oxidation of iron in high temperature aqueous environments are as follows:-

(1) Recent theories do not explain why the outer surface of inner layer oxide formed on large grained annealed steel has the appearance of saucer shaped depressions (see Fig. 3.15.). It has been suggested that large outer layer crystals offer a degree of

protection (see Fig. 10 ref. 29), this would only account for depressions at the inner oxide/metal interface. At higher magnifications pits were found in the inner layer (see Fig. 3.16.) which represent the seat of outer layer crystals; these are not easily explained on existing theories.

(2) No account is taken of the influence of external polarisation on the nucleation and growth of outer layer; (see Chapter VI where experiments are described which show that the state of the surface can affect outer layer formation.

(3) It is still not clear why pores in the inner layer remain open during oxidation under Potter and Mann conditions, although they allegedly contain iron in solution which subsequently deposits magnetite to form outer layer.

(4) In attempts to differentiate between the early stages of oxidation under both Potter and Mann, and Bloom conditions, conclusions have been drawn from transmission electron microscopy of oxides stripped from their substrates by the iodine/methanol technique[39]. This method could modify the oxide structure and for this reason results must be viewed with caution until they have been confirmed by some other technique.

(5) A mechanism is required to describe the oxidation of iron in the absence of an external cathode. Any such mechanism must be consistent with both weight change data and electron

microscopical studies of the surface. It must also account for the irregular metal/oxide interface (compare Fig. 1.2a. with 1.6a.).

(6) No systematic study has been made of the effect of nickel during the early stages of oxidation in ferrous chloride environments, nor has the effect on iron transport in electrolytes containing a high concentration of ferrous ions been investigated.

CHAPTER II

EXPERIMENTAL PROCEDURE AND TECHNIQUES

2.1. Introduction.

This chapter on experimental procedure and techniques describes all the experimental techniques included in this thesis, and also the principles governing their use. The first part is devoted to an account of the experimental research programme in order to prevent repetition of experimental details. The section following contains a description of the oxidation system, and materials and treatments. Finally, actual experiments are discussed with sections on radioactive tracer experiments, electron microscopy and oxide thickness determination.

2.2. Experimental research programme.

2.2.1. Radioactive tracer studies.

Radioactive tracers provide a powerful tool for the research worker in oxidation studies, and even more so if they are of similar species to the metal under investigation. There would seem every justification to use radio tracers in a study of the oxidation of iron in high temperature water, providing suitable isotopes are readily available. Under these conditions tracers could be favourably used to ascertain the movement of iron ions within the experimental system and also the distribution through the actual oxide.

Fortunately there are two iron isotopes readily available, Fe^{55} and Fe^{59}, both of which are eminently suitable for oxidation studies.

The systems investigated by tracers were:-

(1) oxidation of mild steel in a conditioned pressure vessel

(2) oxidation of mild steel in a pressure vessel lined with P.T.F.E.

(3) oxidation of mild steel in ferrous chloride solution containing nickel additions.

The experimental conditions generally involved temperatures of 316°C for times up to 1000 hours.

2.2.2. Electron microscopy.

Most of the electron microscopy carried out on the nucleation of these oxides so far, has been carried out on thin layers stripped from the iron surface by the iodine/methanol technique[39]. Under these conditions damage or alternatively modification of the oxides could occur which would undoubtedly affect interpretation of the oxidation mechanism.

In this work a direct carbon replication technique has been used which is thought to give a more satisfactory representation of the structure. In this respect the scanning electron microscope is even better than any replication technique but unfortunately suffers a limitation from inferior resolution. Nevertheless, valuable information may be obtained of the initial stages of oxidation, for this reason studies by both scanning and electron microscopy were made of the following systems:-

(1) oxidation of mild steel in a conditioned pressure vessel

(2) oxidation of mild steel in a pressure vessel lined with P.T.F.E.

(3) oxidation of mild steel in ferrous chloride solution.

The experimental conditions involved 3.5M sodium hydroxide solution or deionized water (except where otherwise stated) at 316°C.

2.2.3. Weight change and oxide thickness data.

These determinations were made whenever necessary to interpret results gained from electron microscopy or tracer experiments. Although adequate information is available in the literature regarding the kinetics of oxidation, certain redeterminations were justified on the grounds that it is extremely difficult to obtain inter-laboratory reproducibility.

2.2.4. Oxidation of electrodeposited iron.

The oxidation of electrodeposited iron was found to give quite uncharacteristic results, especially with regard to the formation of the outer crystalline layer. Some of these deviations could be attributed to the strong (111) preferred orientation, as well as the very small grain size, both of which are common features of these electrodeposits[40]. A morphological study of the different oxides produced on iron deposited from various types of plating baths were made. Several critical experiments were performed in order to explain these differences.

2.2.5. Examination of magnetite produced in a boiler.

An examination was made of the internal surfaces of a boiler tube that had been in service for 4000 hours. This tube was selected because a portion of it had been in a position of high heat transfer. Both optical metallography and electron microprobe analysis were made of sections of the tube. The results were compared to the laboratory scale experiments to see how valid these are in the control of corrosion.

2.3. The oxidation system.

2.3.1. Pressure vessels.

The pressure vessels were machined from $\frac{3}{4}$" mild steel rod to En3B specification; the actual analysis being:-

C 0.18% , S 0.054% , Si 0.18% , P 0.012% , Mn 0.70%

The open end was sealed with an Ermeto* blanking cap; Fig. 2.1. illustrates the complete pressure vessel together with a P.T.F.E. capsule that was used in some of the experiments. Both the P.T.F.E. capsule and its loose fitting lid were machined from $\frac{1}{2}$" P.T.F.E. rod. Some of the pressure vessels were conditioned by sealing in

---

* Manufactured by British Ermeto Corporation Ltd., Maidenhead, Berkshire, England.

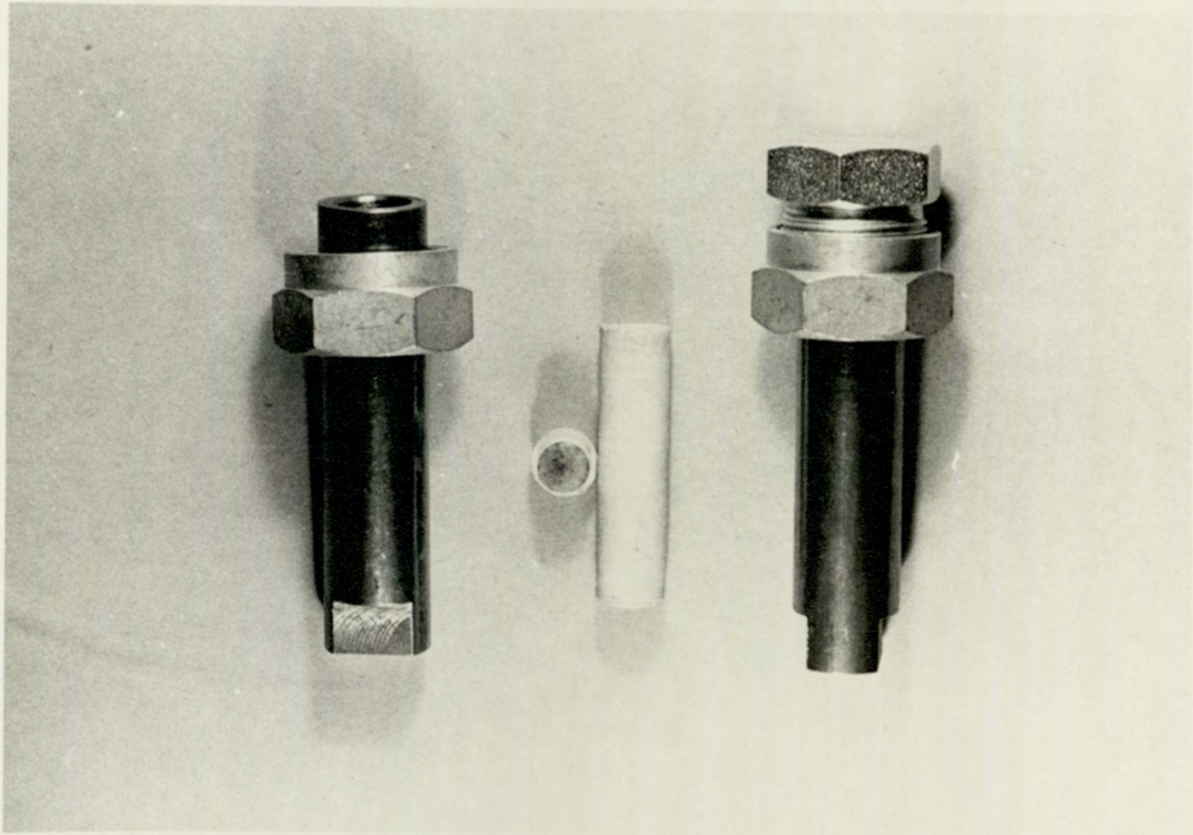

Fig. 2.1. Pressure vessel and P.T.F.E. capsule.

six mls. of 3.5M sodium hydroxide solution and holding them at 316°C for 500 hours. This ensured that the walls of the pressure vessel were covered with a thick layer of magnetite. The internal volume of each pressure vessel was about ten mls., but in general they were only filled with six mls. of liquid before sealing and subsequent heating. Under these conditions the immersed surface area was about 18 cms^2. During a run the vessels were placed in a muffle furnace that was capable of attaining any temperature between 250-350°C to an accuracy of ± 2°C. In long term tests, the temperature of the furnace was frequently checked with an independent thermocouple/potentiometer system.

Fig. 2.2. shows how the inside temperature of a pressure vessel varied with time when placed in a furnace set at 316°C; after 20 minutes, the temperature inside was about 300°C and approached the temperature of the furnace after 25 minutes.

The pressure inside the vessel was dependent on the saturation vapour pressure of water at the test temperature; Fig. 2.3. illustrates the variation in pressure with temperature, at 316°C the pressure inside the pressure vessel was about 1500psi ($10MN/m^2$).

2.3.2. Solutions.

The solutions were made up from A.R. grade chemicals to the concentrations stated for each experiment with deionized

Fig. 2.2. Variation of temperature of pressure vessel with time.

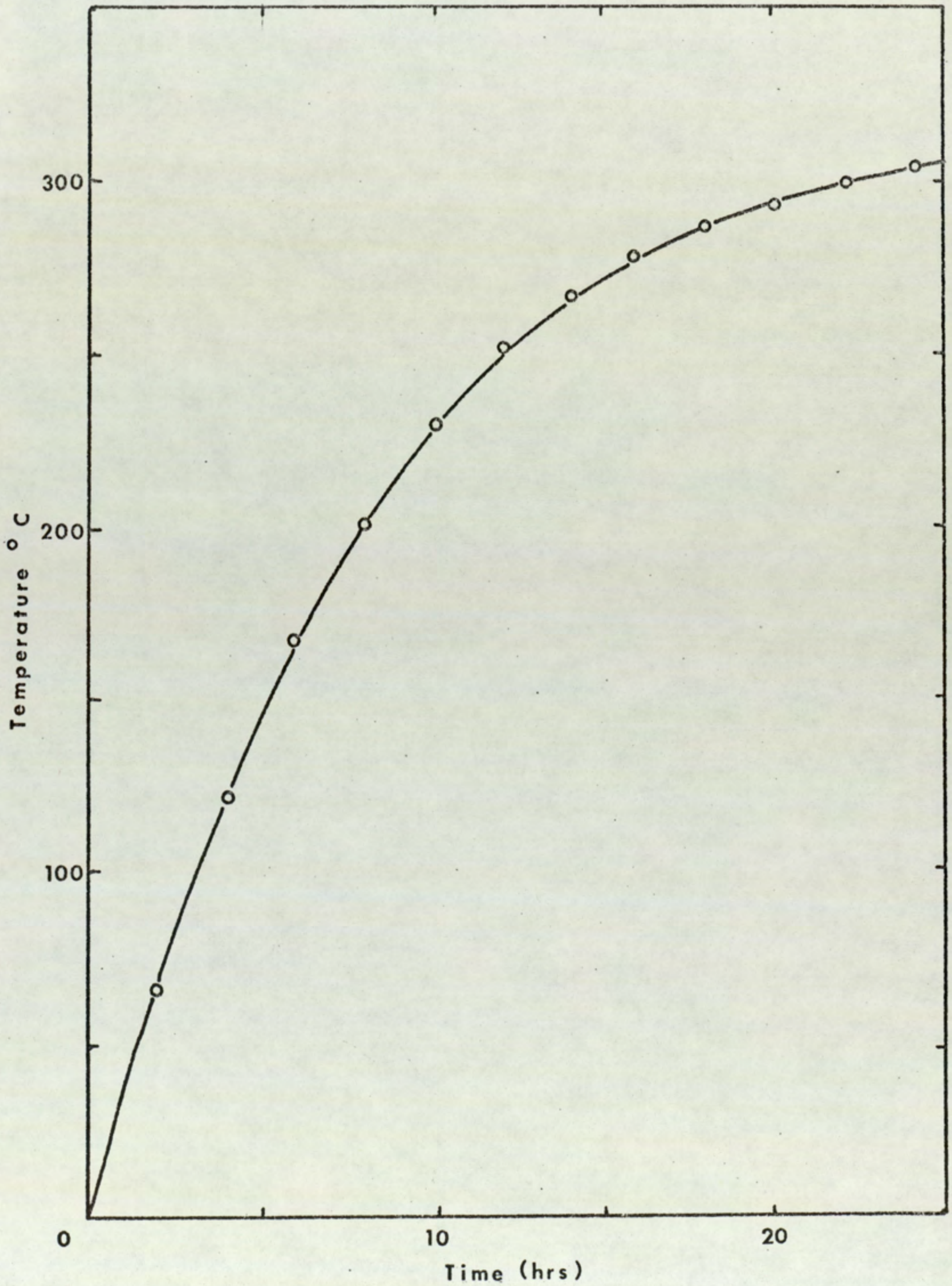

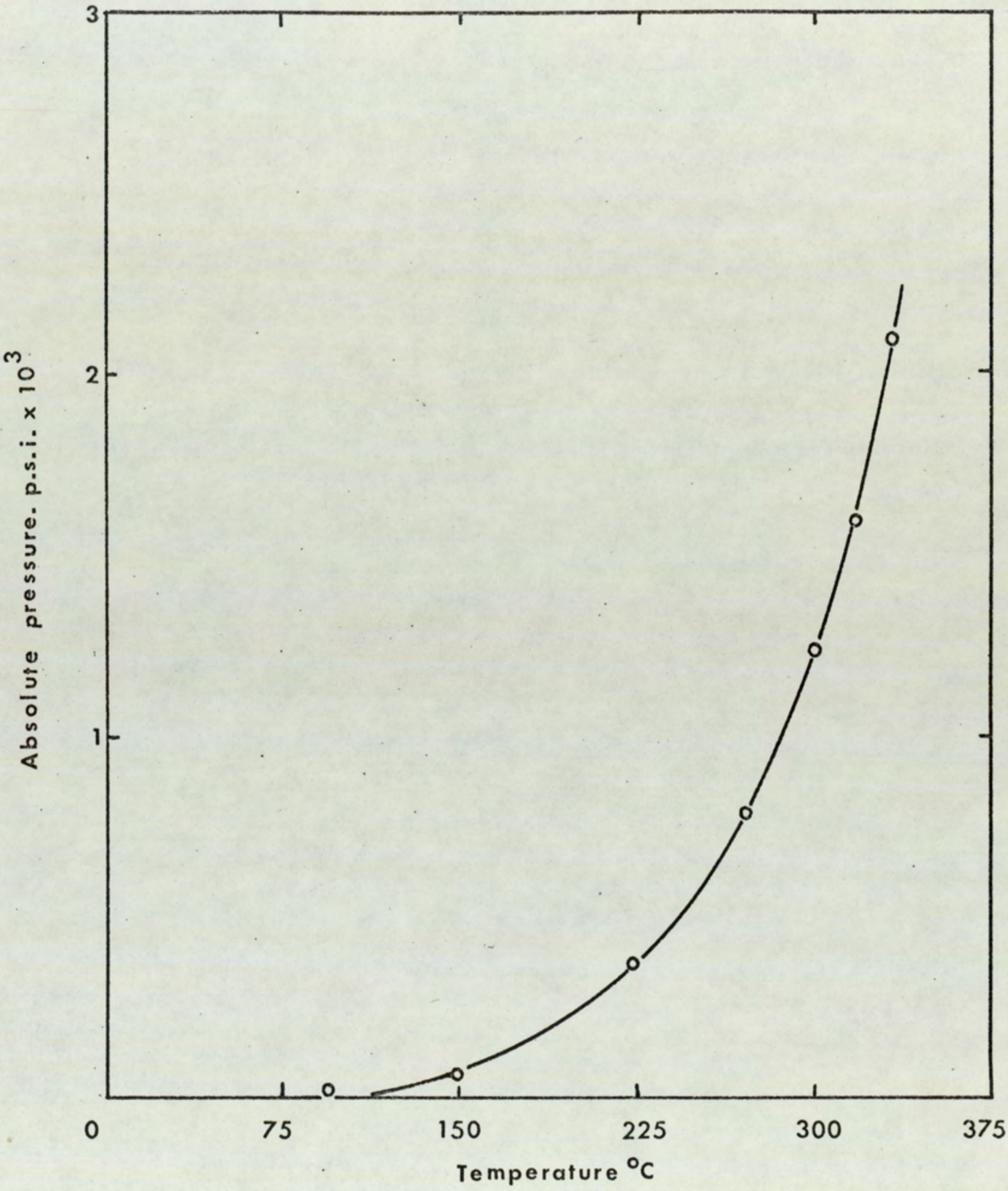

Fig. 2.3. Showing variation of saturation vapour pressure[41] with temperature.

water. When storage was necessary for any length of time, stoppered air tight polythene bottles were used.

2.4. Materials and treatments.

All the corrosion samples were prepared from a single stock of steel in sheet form (0.056 cms.) specifically kept for this purpose: analysis,

C 0.06% , S 0.024% , Si trace , P 0.007% , Mn 0.29%

The steel was either used in the "as received" condition (annealed but small grained) or alternatively given a further anneal (Fig.2.4a). This second annealing treatment was carried out under vacuum for 40 minutes at 940°C. Back reflection X-ray photographs of the steel in the two conditions indicate a much increased grain size as well as a slight preferred orientation in the annealed condition (Fig. 2.4b.).

The steel in the "as received" condition was found to give a more uniform and reproducible duplex Potter and Mann oxide, that was much more suitable for the radioactive tracer experiments. The steel in the annealed condition was used for the preparation of oxides that were examined by electron microscopy.

2.4.1. Oxidation procedure.

The steel sheet was guillotined to the dimensions required by each test. The strips were degreased in acetone before sealing in a pressure vessel. After removal of the pressure vessel from the

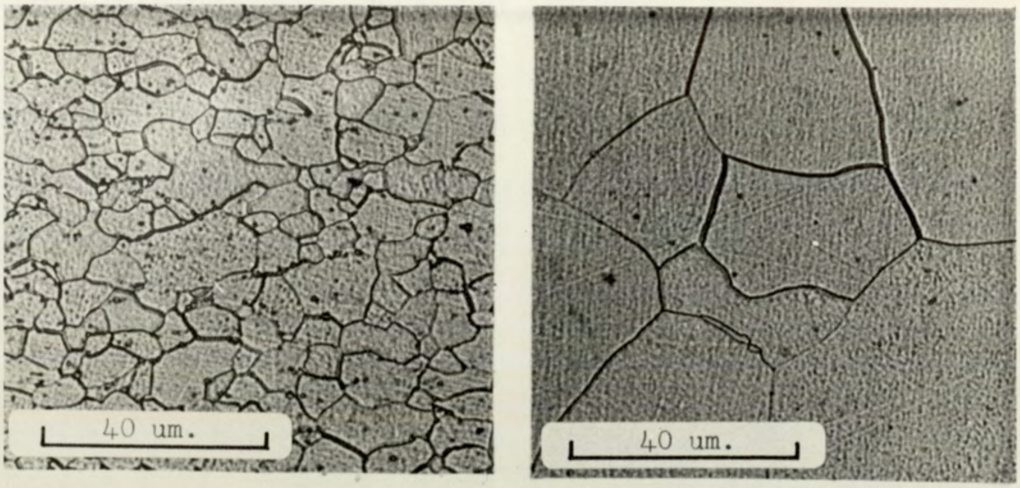

(a) as received

(a) annealed

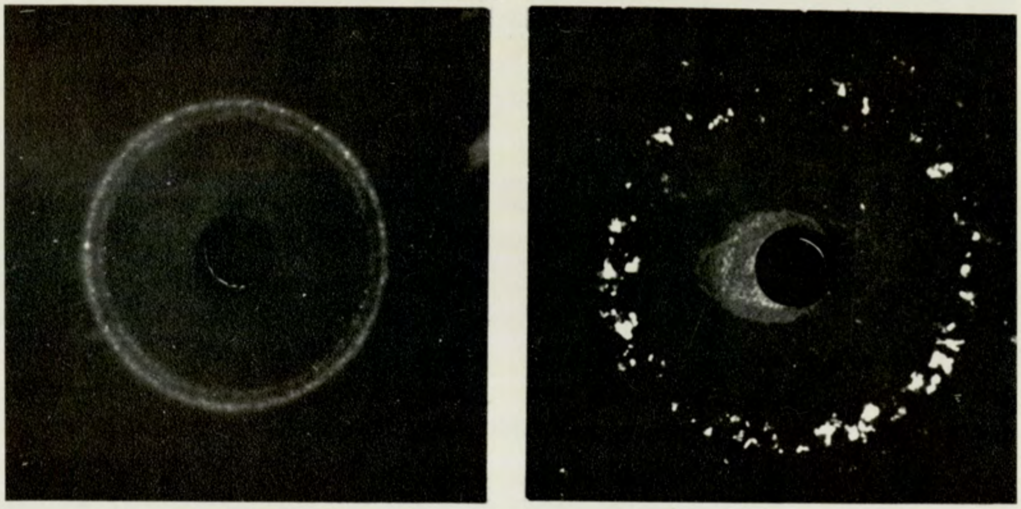

(b) as received

(b) annealed

Fig. 2.4(a) Optical micrographs of steel in the as received and annealed conditions.

Fig. 2.4(b) Back reflection X-ray photographs of steel sheet in the as received and annealed conditions.

furnace, it was cooled down to room temperature in a stream of water before unsealing. The specimens were removed, washed with water and alcohol before drying in warm air. The specimens were then stored in a desiccator before examination.

2.5. Radioactive tracer experiments.

2.5.1. Introduction.

Table I lists the properties of the radioactive isotopes of iron. It is seen that there are two isotopes, Fe^{55} and Fe^{59}, both of which are available in a solution of ferric chloride from the Radiochemical Centre, Amersham, Bucks. The experiments were designed to make full use of the individual properties of the isotopes.

TABLE I *

Isotope	Principal radiations	Energies	half life
Fe^{55}	X-ray	5.9 KeV	2.7 yrs
Fe^{59}	β γ	0.27,0.46,MeV 1.1, 1.3, MeV	45 days

* data obtained from reference 42.

2.5.2. Investigation of the movement of iron within the experimental system.

Fe^{59} was used in these experiments, the emission of two gamma rays of 1.1 and 1.3 MeV. respectively made detection relatively simple. The active iron was electroplated onto one side of a steel panel (that had first been anodically cleaned and rinsed in 2% HCl) from an active iron chloride solution. The bath was made up by adding 4.35 mls. of a ferric chloride solution (specific activity 11.0 curies/gm Fe) to 75 mls. of a standard ferrous chloride iron plating bath containing 300 gms/l of $FeCl_2$ and 335 gms/l of $CaCl_2$*. The thickness of the deposit was calculated to be about 0.1 micron. It is very difficult to give an exact figure for the thickness since the cathodic current efficiency was not determined during electrodeposition. An estimate of the real thickness derived from cathodic current efficiencies as quoted in the literature[43] would be in the order of 0.09 microns. In any case these very thin deposits of iron did not affect the normal oxidation mechanism in any way; in fact tests were carried out on deposits up to four times this thickness and it was found that the deposit had to be about 0.5 microns thick before oxidation was affected.

The test pieces measuring 3 cms. by 2 cms. were cut from the larger plated panels; this procedure was adopted to obviate edge effects incurred during electrodeposition. The test pieces were then counted for total activity using a sodium iodide

---

* The bath contained 4000 micro curies of Fe^{59}.

crystal (Th) scintillation counter fitted with a perspex specimen holder that ensured reproducible geometry. Higher sample to background count ratios were obtained by discriminating for the 1.1 and 1.3 MeV. gamma emission (see Fig. 2.5.). In this way, the counts for each sample fell in the range 5000-8000 counts per minute above background. Some of the test pieces were over plated with approximately 1 micron of non active iron for some additional sandwich tests.

Testing procedure.

The samples were placed in conditioned pressure vessels containing 6 mls. of 3.5M sodium hydroxide solution. They were sealed and placed in the furnace at 316°C. Withdrawals of duplicate samples each in its own pressure vessel, were made at set intervals of time. After cooling in a stream of cold water the pressure vessel was opened and the sample removed. The sample was washed with deionized water and alcohol, dried and counted for total activity. The electrolyte in the pressure vessel was washed out, added to the washings from the sample, then filtered through a Whatman No. 1 filter paper and made up to 100 mls. in a graduated flask. All the magnetite inside the pressure vessel and cap was dissolved out with concentrated HCl and similarly made up to 100 mls. The two liquid samples were counted for total activity in the arrangement shown in Fig. 2.6.; the time for 20,000 counts was

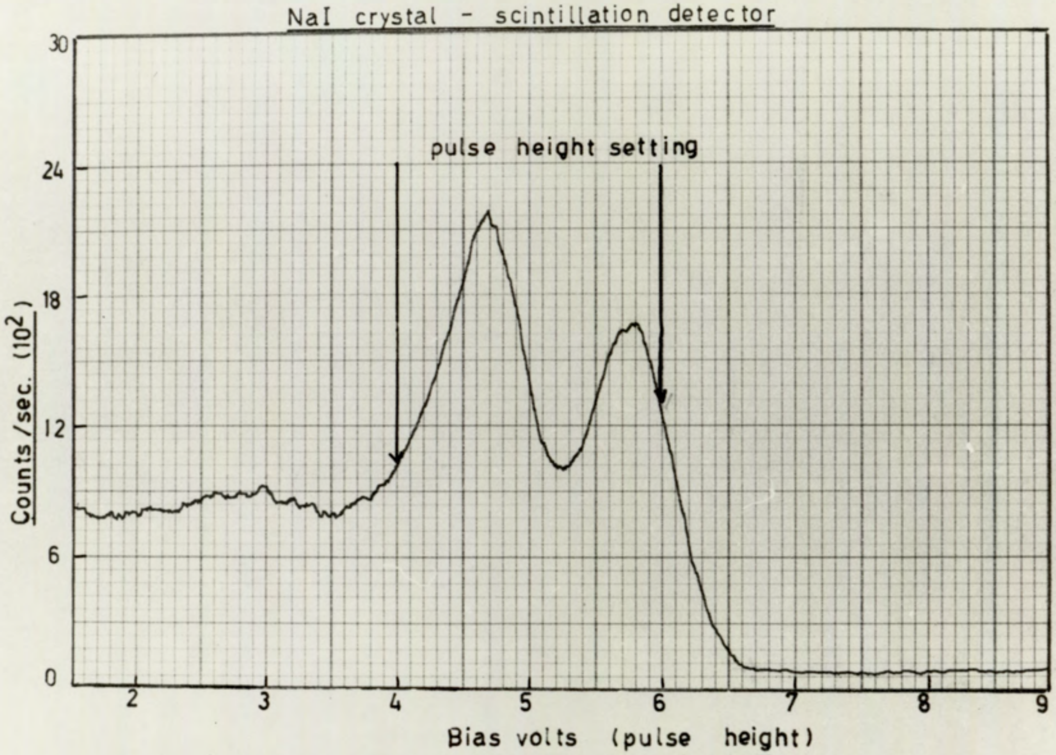

FIG. 2.5. GAMMA RAY SPECTRA Fe^{59} SOURCE

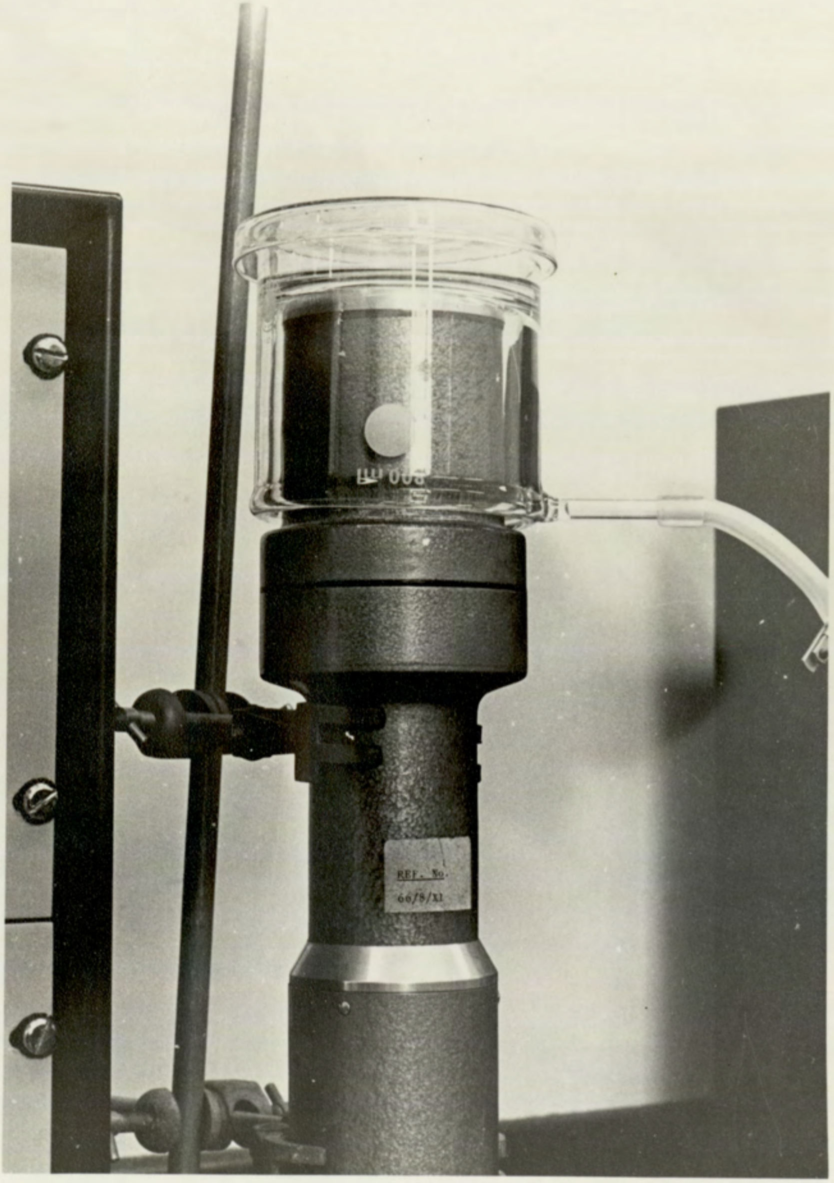

Fig. 2.6. Showing arrangement to obtain maximum counting geometry for liquid samples.

taken to reduce the statistical error to below 1%. An activity balance could be achieved once the factor relating the apparent activity of the solid sample to the apparent activity of the liquid sample was known. This was determined by first counting a solid sample, dissolving it in concentrated HCl followed by recounting it as a liquid sample. The relationship was found to be:-

counts (solid sample) = counts (liquid sample) x 1.79

(all counts corrected for background).

The high concentration of iron in solution did not significantly affect the observed activity of the liquid sample; no correction was found necessary. Furthermore, the residue retained by the filter paper was never found to contain any significant activity in any of the experiments. The percentage activity existing between the sample, the electrolyte and the pressure vessel wall after oxidation, was calculated and recorded as a function of time.

To determine the extent of iron ion movement between the two sides of the oxidised sample, a different technique was used. The active side was stopped off with lacquer before dissolving off the magnetite from the non active side. The active iron movement was detected by a lowering of the total activity.

2.5.3. Transportation of iron within the oxide.

A thin layer of radioactive iron initially deposited on an iron surface would be redistributed through the oxide after oxidation. Determination of this redistribution would allow us to predict with some certainty the oxidation mechanism.

The two cases of solid state lattice diffusion and transportation of iron as the ferroate ion via a porous inner layer would give radically different redistribution[44,45]. Figs. 2.7a. and 2,7b, show the two types of redistribution that would occur under these two conditions. Deviations from these two idealised situations could occur if both of these mechanisms were active, or alternatively if there were chemical or physical interactions between different phases as the oxide formed. Fortunately, direct observations of the oxide from electron microscopy allow better and more informative interpretations of the redistribution data.

Two completely different techniques may be used in these studies, they are (a) sectioning method and (b) decrease in surface activity method. During this investigation it was found advantageous to use both methods.

2.5.3.1. Sectioning technique.

Sectioning techniques have been used previously[45,46] to determine the diffusion of copper in copper oxide, it involved the removal of uniform thin layers of the bulk oxide for radiochemical analysis.

It became prohibitively difficult to produce test pieces for these experiments by electrodeposition of the active layer onto

Fig. 2.7.

Schematic representation of the redistribution of an active iron tracer after oxidation.

(a) Transport via solution filled pores.

(b) Solid state diffusion.[44,45]

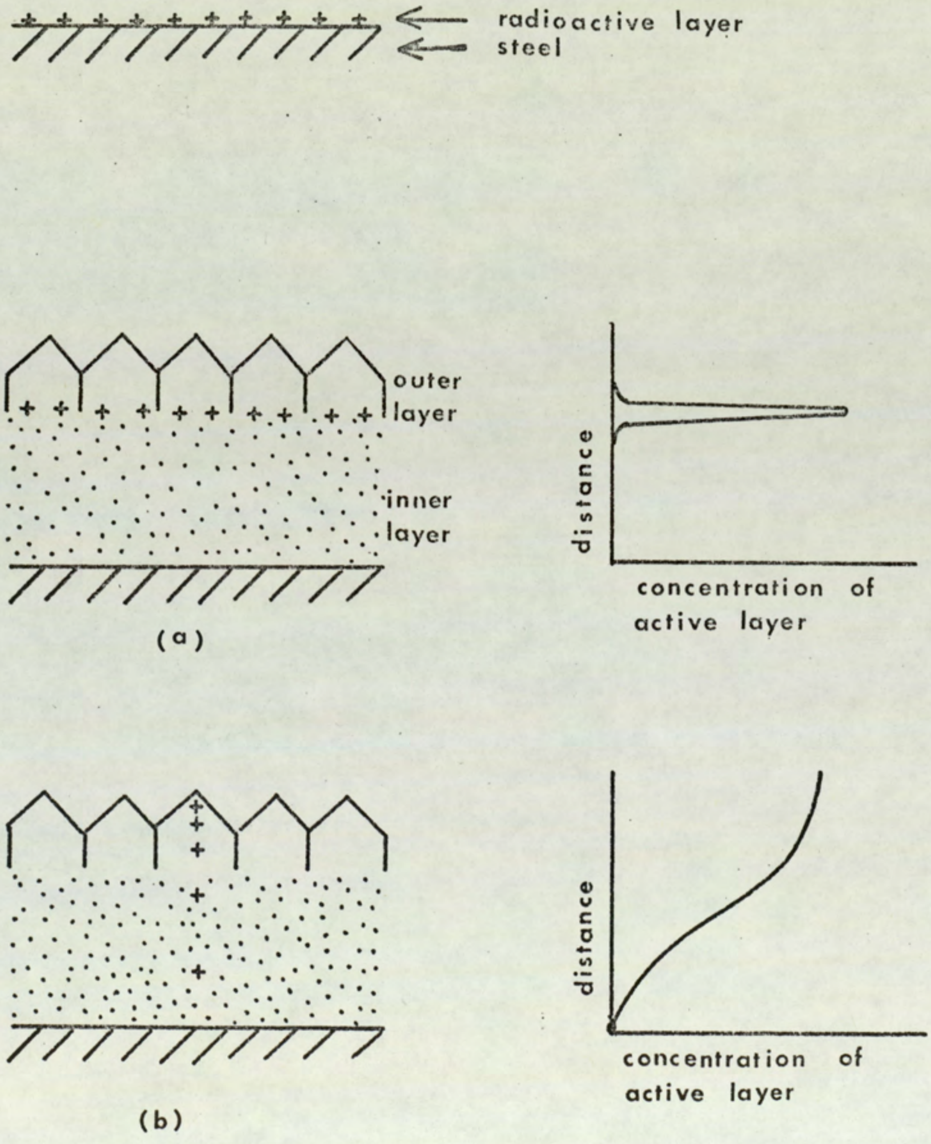

the iron surface, since on oxidation up to 85% of the total activity was lost to the experimental system. A technique involving laying down the active layer as an oxide was developed. Pieces of the steel from which the test samples were to be cut were bolted together with spacers and placed in a pressure vessel containing 5.0 mls. of 3.5M sodium hydroxide solution. An active iron solution, containing 100 micro-curies of Fe^{59} was added in the form of 1.5 mls. of ferric chloride solution*. After agitation the pressure vessel was sealed and oxidised for 2 hours at 300°C. The pressure vessel was then opened and the test pieces were removed. Both the test pieces were found to be active, the solution however, was completely inactive. The following reactions describe how magnetite would be laid down in an active form.

$$FeCl_3 \text{ (active)} + NaOH \rightarrow Fe(OH)_3$$

$$Fe(OH)_3 + NaOH \rightarrow NaFeO_2 + 2H_2O$$

$$2NaFeO_2 + H_2O \rightarrow Fe_3O_4 \text{ (active)} + NaOH \text{ (in the absence of oxygen)}$$

Test pieces measuring 1 cm. x 1.4 cms. were cut from the active samples and oxidised in conditioned pressure vessels at 316°C for 2 hours. After oxidation they were washed in deionized water and dried with alcohol.

---

* The specific activity of the ferric chloride solution was 9.5 curies/gm. of Fe.

2.5.3.2. Cathodic reduction.

The dissolution of iron oxide films in acidic solution has been studied by many workers[47,48,49]. If the iron is in contact with the oxide, the process may be described as being one of reduction and dissolution.

For magnetite the reduction could occur by the following reactions:-

$$Fe_3O_4 + 6H^+ + 2e \rightleftharpoons FeO + 2Fe^{2+} + 3H_2O$$

$$Fe_3O_4 + 8H^+ + 2e \rightleftharpoons Fe^{2+} + 4H_2O$$

$$FeO + 2H^+ + 2e \rightleftharpoons Fe + H_2O$$

In the absence of an applied E.M.F. the anodic process i.e. the corrosion of iron ($Fe \rightarrow Fe^{2+} + 2e$) offers a supply of electrons required by the cathodic reaction. This complete process is termed "auto-reduction".

The application of an external cathodic potential would suppress the anodic corrosion process and supply the necessary electrons required by the reductive process. However, in certain acid environments the cathodic reaction, $2H^+ + 2e \rightarrow H_2$ may take place; the extent depending on the applied potential and also the favourability of sites capable of supporting this reaction.

To test the practical validity of this dissolution process for bulk duplex layered magnetite, a series of trials were performed in $\frac{N}{50}$ and $\frac{N}{25}$ HCl solutions.

Standard iron specimens were oxidised as described earlier, for 200 hours. Electrical contact was made to the sample with a thin pair of tweezers before stopping off with "Lacomit"* all but 1 cm^2. This oxide surface was placed in a normal potentiostatic cell as the working electrode. The cell had a volume capable of containing 100 mls. of electrolyte that could be agitated at a speed of 200 rpm. Cathodic potentiostatic polarisation curves were plotted in the normal way except that the time held at each increment in potential was 7 minutes. After each 7 minutes the electrolyte was removed and a fresh 100 mls. of electrolyte sample was immediately put in its place. An aliquot of the sample was analysed colorimetrically for iron by the thioglycollic acid method (outlined in Appendix II). Fig. 2.8a. shows the rate of iron dissolution in $\frac{N}{25}$ HCl. At the rest potential, it is seen that iron is readily going into solution, this in fact is "auto-reduction" as described earlier. At a potential of -1.45 V.S.C.E. the oxide dissolution was at a maximum, cathodic reduction of the magnetite was taking place in the presence of an applied cathodic E.M.F. The electrons supplied by this external cathodic current were suppressing the anodic corrosion of iron. On increasing the potential (more negative) the rate of iron going

---

* Trade name for lacquer manufactured by W. Cannings Ltd., Birmingham, England.

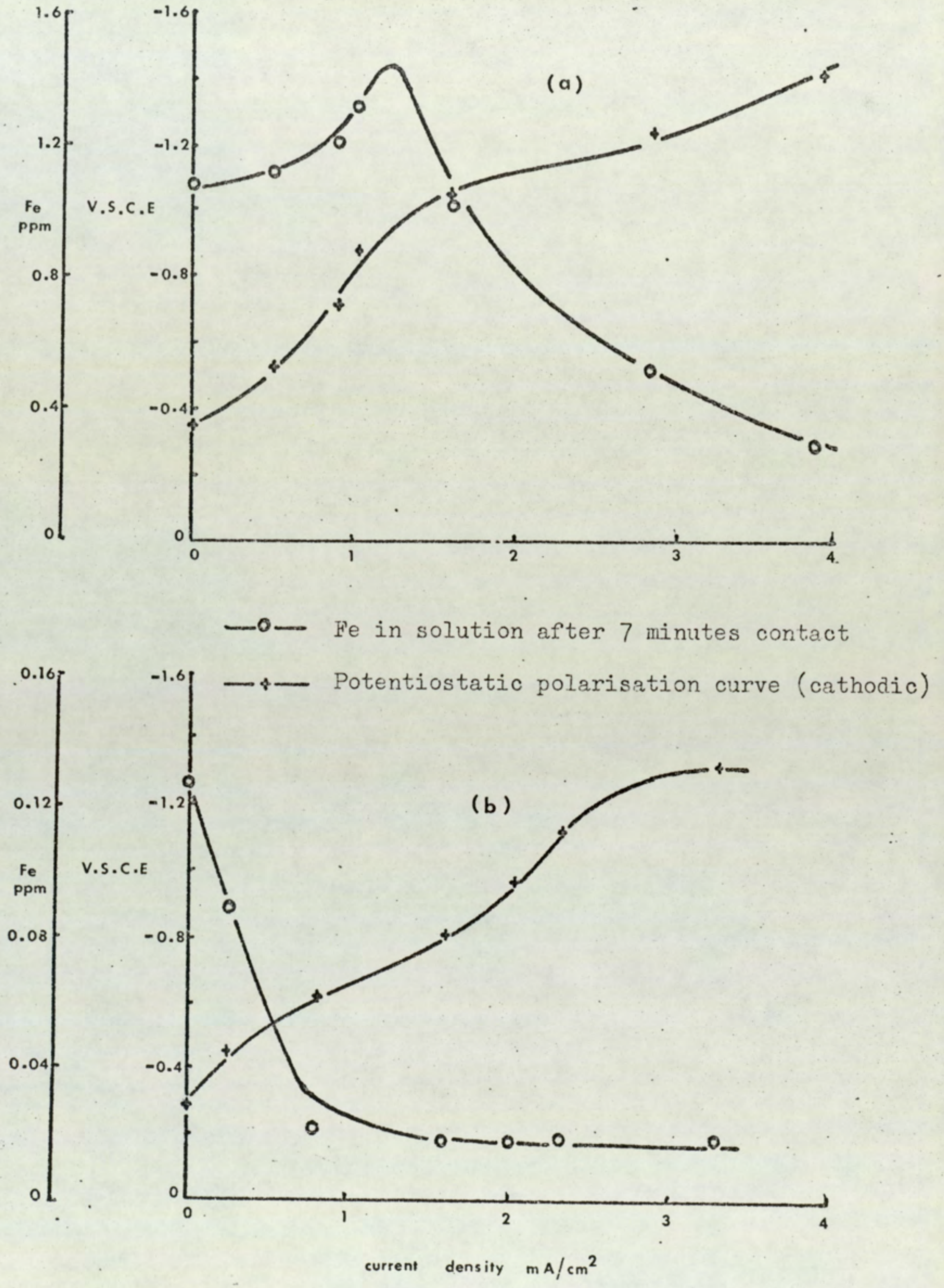

Fig. 2.8. Cathodic reduction of (a) Fe_3O_4 and (b) iron in $\frac{N}{25}$ HCl + 0.2% hexamine.

into solution rapidly diminished, and the cathodic reaction $2H^+ + 2e \rightarrow H_2$ became more prominent. The potential used for the reduction of the radioactive samples was the one that gave maximum dissolution rates; at this potential the dissolution of the iron substrate was virtually zero. Fig. 2.8b. illustrates the suppression of the $Fe \rightarrow Fe^{2+} + 2e$ reaction.

The usefulness of this technique depends to a large extent on the uniformity of the dissolution. Fig. 2.9. shows the oxide surface after successive increments of time in the dissolution cell. It is seen that initial attack occurred on the faces of the large outer crystals at many different sites. The sites grew larger with several forming triangular etch pits. Eventually the whole crystal was consumed but it is seen that at some stage before all the outer layer was dissolved, attack had commenced on the porous inner layer; this was certainly a disadvantage and was taken into account when interpreting the radiochemical analysis.

The oxidised radioactive samples were treated in a similar way. The activity of each sample was measured with a scintillation counter using the arrangement shown in Fig. 2.6. An aliquot of each sample was taken for total iron analysis; this was necessary in order to calculate the thickness of oxide representing the activity. In this way the results could be displayed in histogram form.

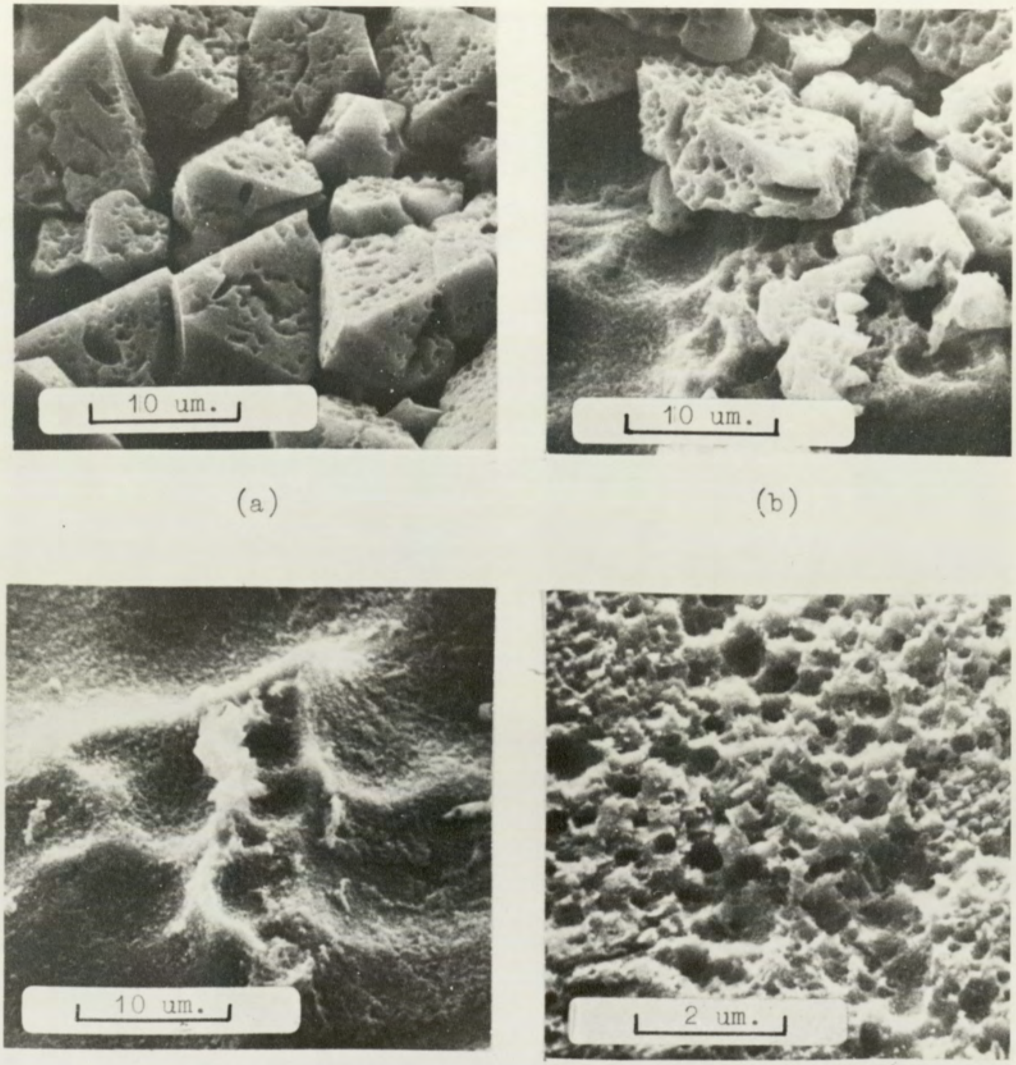

(a) (b)

(c) (d)

Fig. 2.9. Magnetite surface after cathodic reduction in $\frac{N}{25}$ HCl.

(a) and (b) showing dissolution of outer layer.

(c) and (d) showing dissolution of inner layer.

2.5.3.3. Surface activity measurements.

The decrease in surface activity technique has been selected by many research workers for the determination of diffusion coefficients in both oxides[26,50] and metals[51]. The change in surface activity of a sample after oxidation may be regarded as a function of the oxidation mechanism. For instance, the two oxidation mechanisms of solid state diffusion and iron transportation through solution filled pores give two radically different distributions and hence different decreases in surface activity.

Fig. 2.7. illustrates the distribution of radioactive iron expected if oxidation occurs via transportation through a porous inner layer. Providing the original radioactive layer remains infinitely small then:-

$$\log F = \mu x$$

where x = thickness of outer layer

μ = absorption coefficient of magnetite

$F = \frac{I}{Io}$ I = surface activity after oxidation

Io = surface activity before oxidation

The successful application of this formula depends therefore on the accurate determination of μ and x.

If oxidation occurs by solid state diffusion, then a more complex mathematical analysis is required. Steigman, Shockley and Nix[52] have provided an analysis relating the diffusion coefficient D to the decrease in surface activity and the absorption coefficient μ for the medium concerned i.e.

$$F = e^{Z} \left[1 - \Theta(\sqrt{Z}) \right] \quad \ldots\ldots\ldots\ldots\ldots(I)$$

where Θ is the Gauss error integral

$Z = \mu^{2}Dt$

F is the fraction of activity remaining at the surface after diffusion

t is the time at the diffusion temperature.

For equation (I) to hold, the following assumptions must first be satisfied:-

(1) the measured surface activity must decrease exponentially with absorber thickness; this will depend to a large extent on the experimental set up, especially the detector geometry.

(2) the distribution of the radioactive iron through the oxide at any given time and temperature will be the same as that obtained if an equivalent amount of radioactive magnetite were deposited on a magnetite surface in a similar experiment. This would be satisfied if the thickness of the original layer was very much smaller than the final oxide.

The validity of these experiments depends to a great extent on there being a suitable isotope available; this implies that the isotope should give reasonable measurable changes in surface activity under the conditions of the experiment. Fortunately, Fe^{55} which emits a 5.9 KeV X-ray was found suitable.

2.5.3.4. Measurement of μ for Fe^{55} in magnetite.

The measurement was made by determining the reduction in activity of an Fe^{55} source after placing magnetite filters between the source and the detector. The magnetite filters were constructed by building up layers of magnetite powder on a thin aluminium foil. The absorption coefficient of aluminium was determined by placing increasing thicknesses of aluminium foils between an Fe^{55} source and a Geiger-Müller counter. The time for 20,000 counts was recorded for each increment in thickness. Fig. 2.10. illustrates a plot of log I against absorber thickness in mgms./cm^2. From this graph, a foil was selected that was sufficiently rigid to support magnetite layers adequately, but less than the half thickness for Fe^{55} radiation. A 4.50 mgms./cm^2. foil was chosen; it was then cut into squares of 6 cms., coated with collodion and dipped into a fluidised bed of finely ground magnetite. Magnetite filters ranging from 0-12.6 mgms./cm^2. were produced in this way; Fig. 2.11a. illustrates four of these filters. The structure of the magnetite is clearly seen in the Scanning Electron Micrographs (S.E.M.) of a 0.5 and a 3.6 mgms./cm^2. filter respectively (Fig. 2.11b.). A plot of log (surface activity)

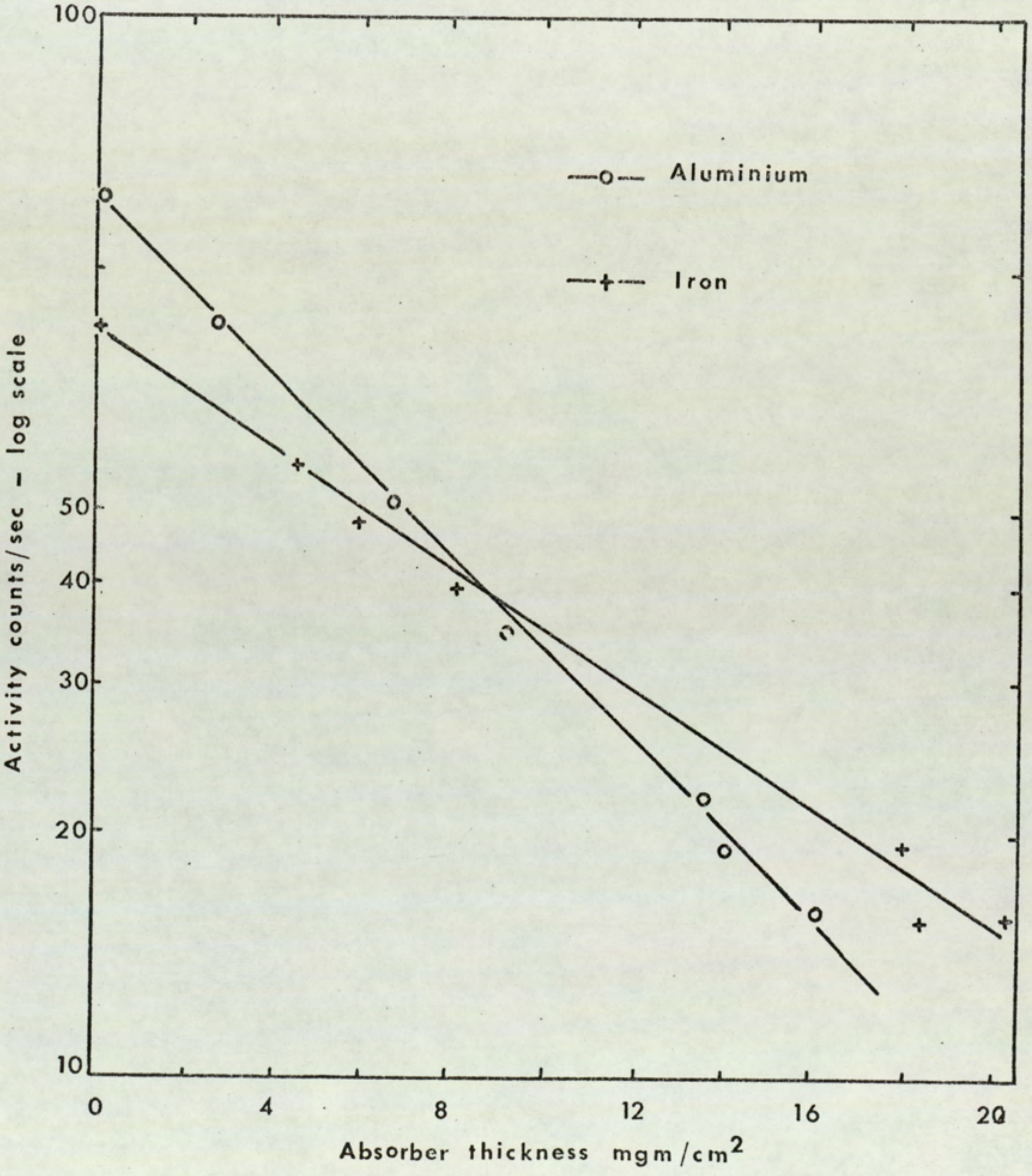

Fig. 2.10. Absorption of X-ray emitted from Fe^{55}.

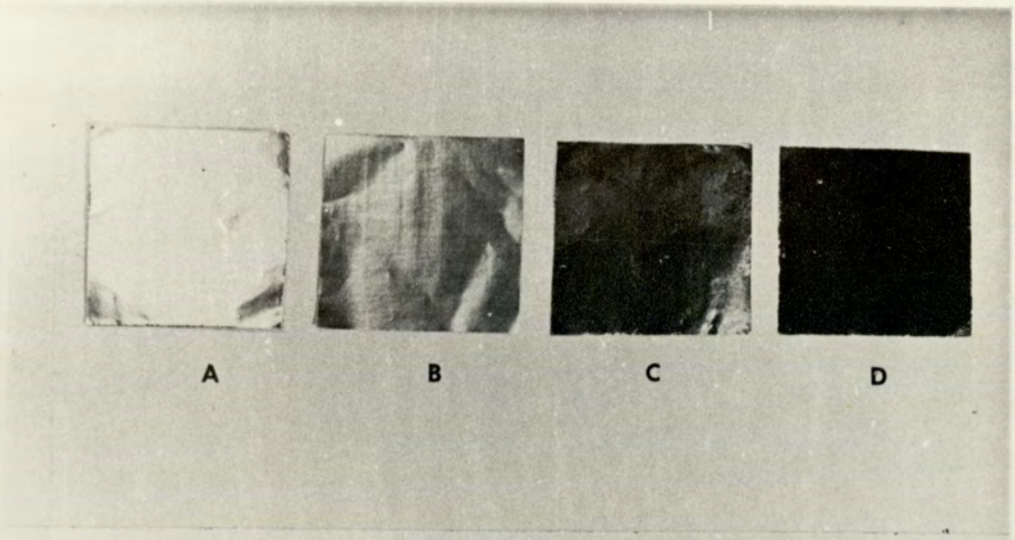

Fig. 2.11a.

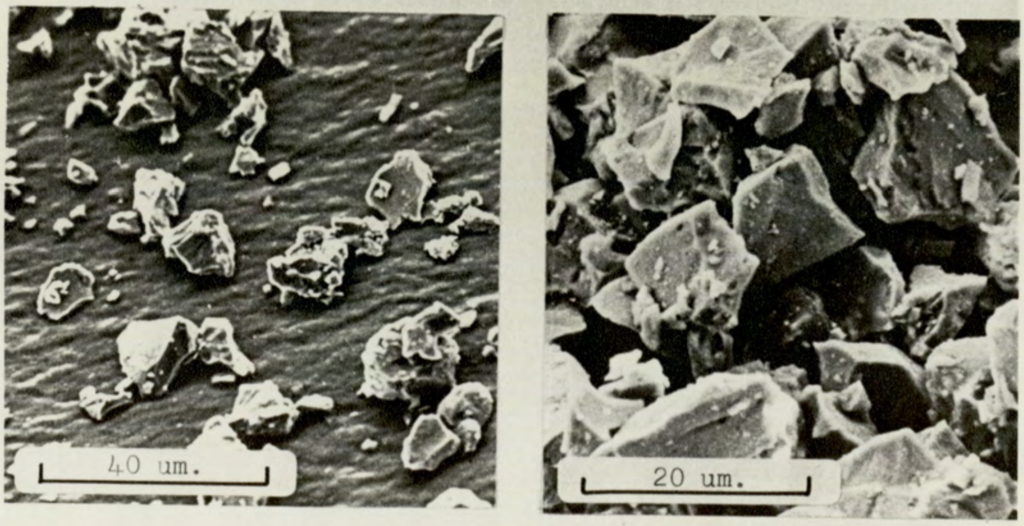

Fig. 2.11b.

Fig. 2.11. Magnetite on aluminium foil.

(a) A - 0, B - 0.5, C - 3.6, D - 12.6, mgm./cm.^{2} Fe_3O_4.

(b) S.E.M. of magnetite on aluminium foil.
LHS, 0.5 mgm./cm.^{2}, RHS, 3.6 mgm./cm.^{2} Fe_3O_4

with magnetite thickness is shown in Fig. 2.12. There are two important results from this graph; firstly the measured surface activity decreased exponentially with absorber thickness and secondly, the calculated experimental linear absorption coefficient

$$\text{for magnetite} = \frac{0.693 \times 1000 \times 5.18^{53}}{9.5}$$

$$= \underline{378 \text{ cms}.^{-1}}$$

The absorption properties of Al and Fe for the radiation by Fe^{55} were found to agree reasonably well with the known X-ray mass absorption coefficients of Al and Fe for MnKα radiation. This would justify the use of the equation:-

$$\mu = \rho(90.9f_{Fe} + 32.2f_0)$$

where μ = linear absorption coefficient

ρ = density of magnetite (5.18)[53]

f_{Fe} and f_0 are weight fractions of iron and oxygen respectively.

Using this formula, μ is calculated to be 387 $cm.^{-1}$, and the decay line this represents is also shown in Fig. 2.12. The discrepancy between the experimental and the calculated value of μ is possibly due to the magnetite being in a finely divided state which would cause X-ray reflections. The magnetite formed in these oxidation experiments is finely divided or crystalline and would justify the use of the experimental value with confidence.

Fig. 2.12. Absorption of X-ray emitted from Fe^{55}.

Magnetite absorber.

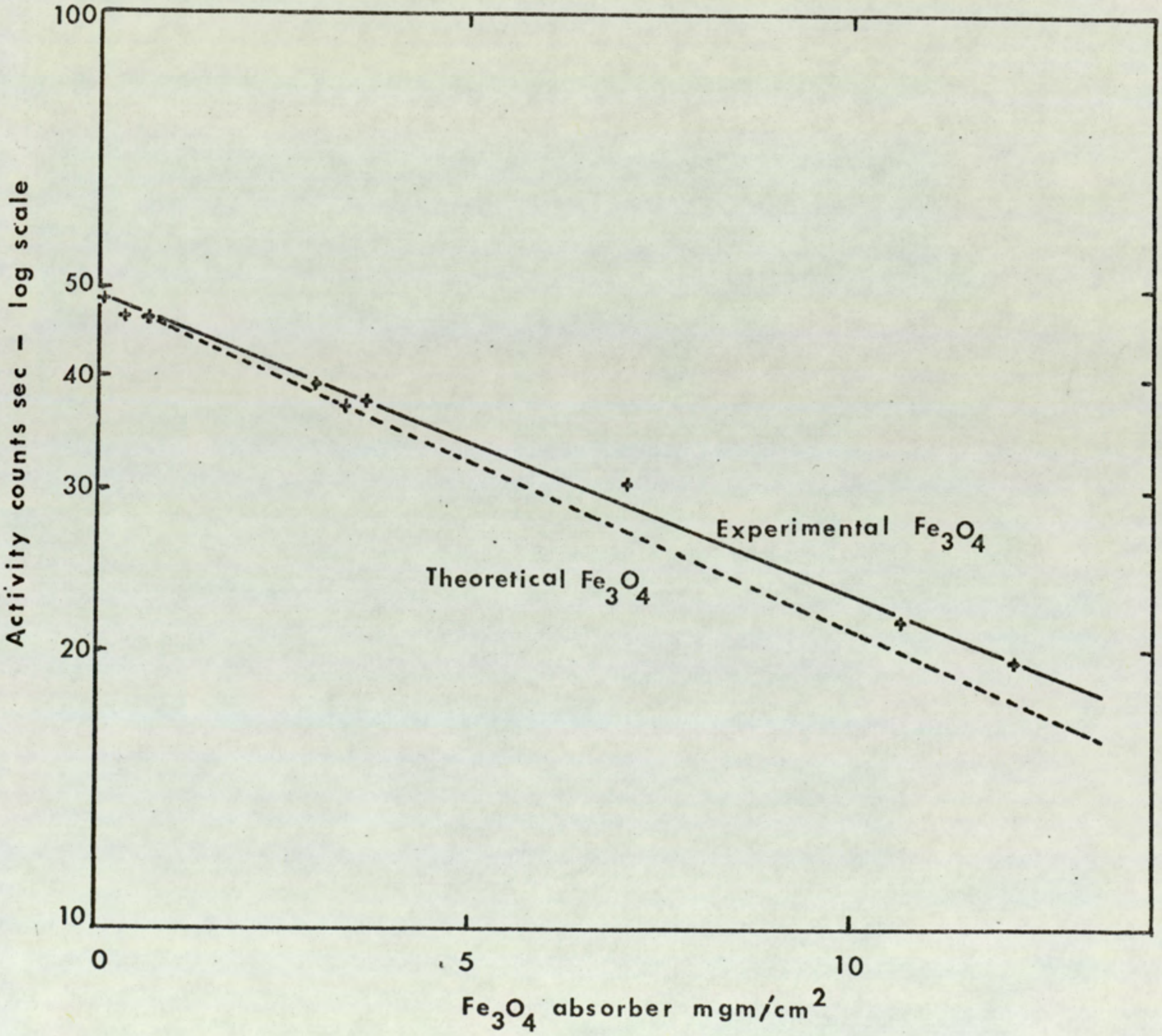

2.5.3.5. Experimental procedure.

The test pieces were prepared in a similar way as those used in the Fe^{59} experiments (see p.38); the only difference being that 100 micro-curies of Fe^{55} contained in a ferric chloride solution of specific activity 9.5 curies/gm. Fe was injected into the pressure vessel. The test pieces of approximate size 1.1 x 1.1 cms. were then oxidised in the usual way for different lengths of time*. The activity of the sample was determined both before and after oxidation. It was found quite satisfactory to use the same sample for each oxidation run, in fact better reproducibility could be obtained in this way. Initially samples were counted for surface activity on two different types of counting apparatus. The arrangements used were (a) a Geiger-Müller detector and (b) an argon/methane proportional counter. Using arrangement (a) the counts fell in the range 3000-6000 per minute, and (b) 24,000-33,000 per minute.

The deposition of the active layer was found to be extremely uniform; Fig. 2.13. shows a scan across the specimen surface in both an x and y direction. An argon/methane

---

* To account for the 2 hours pretreatment used in laying down the active isotope, the surface activity was extrapolated back to zero time; in this way a true value of I could be achieved.

FIG. 2.13. ACTIVITY SCAN

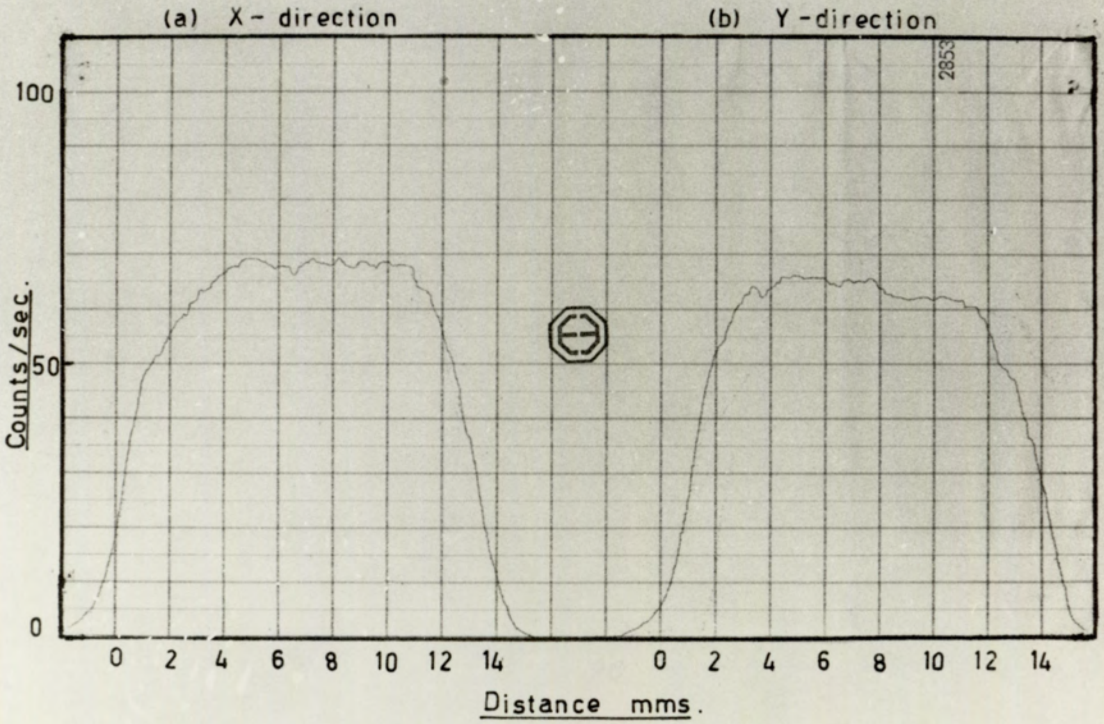

proportional counter with a 1 mm. slit was used for these scans. A uniform deposit was necessary for reproducibility and in this respect the practical results were very encouraging.

Surface activity determinations were undertaken in the following systems:-

(1) conditioned pressure vessels containing either 3.5M NaOH or 0.1M $FeCl_2$ + 0.001M $NiCl_2$ at 316°C

(2) P.T.F.E. lined pressure vessels containing 3.5M NaOH at 316°C

2.5.3.6. Experimental precautions and corrections.

The following corrections were made on all surface activity determinations:-

(1) correction for background

(2) correction for radioactive decay especially important in long term tests

(3) correction for day to day variation in instrument electronics; this was made by reference to a standard test piece kept in a desiccator for this purpose.

Geometry.

Reproducible geometry was attained by using a perspex holder constructed in such a way that during counting it held the test piece in only one position under the detector (Fig. 2.14.).

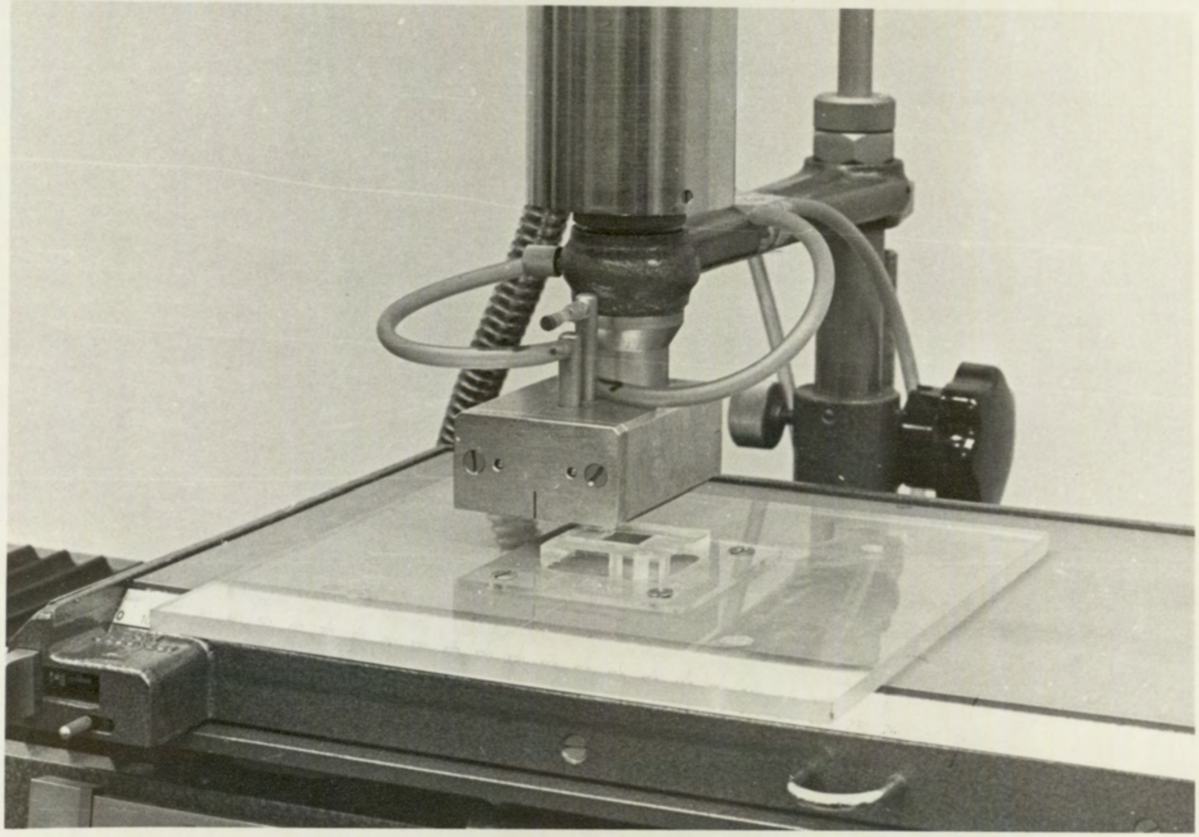

Fig. 2.14. Showing the experimental arrangement used for surface activity measurements using a proportional detector.

Back reflection.

The influence of back reflection on the counting rate was determined for an Fe^{55} source for different thicknesses of iron and magnetite.

An Fe^{55} source was deposited onto a 50 micron thick film of "Mylar"; successive increments of iron and magnetite filters were placed directly beneath the source, and counts were recorded at each increment. The results are given in Table II and indicate that the effect of back reflection is negligible and can be ignored in these studies.

TABLE II

Back-scatter data from iron and magnetite filters; Fe^{55} source.

Iron

thickness of filter mgm/cm^2.	0	2.6	6.6	8.4	18.0	20.0
activity c/sec.	50.4	50.8	50.0	49.6	50.4	49.0

Magnetite

thickness of filter mgm/cm^2.	0	0.60	3.26	6.90	10.6	12.1
activity c/sec.	50.0	50.1	50.1	49.3	49.7	49.5

Effect of working distance.

The working distance which may be defined as the distance between the active source and the window of the detector was relatively small in these experiments (approximately 0.3-0.5 cms.).

The relationship between detected activity and distance is given by the inverse square law $A \propto \frac{1}{d^2}$, where A is detected activity and d is the distance between the source and the detector. If a constant is introduced for the experimental arrangement the equation may be written

$$A = K \frac{1}{d^2}$$

Any change in d caused by either oxidation or positioning could have severe consequences, the extent being dependent on the nominal value of d and K. In order to determine the effect changes in d would have, a series of activities were measured for incremental decreases in d. Fig. 2.15. shows the percentage increase in surface activity observed for diminishing values of d. It is seen that there is less than 1% increase in activity for an increase in d of 100 microns. The working distance chosen therefore was quite satisfactory in this respect.

Edge effects.

To ascertain the influence of edge effects during oxidation, some of the samples in the initial runs were counted with their edges blanked off. The blanking plate constructed of perspex was

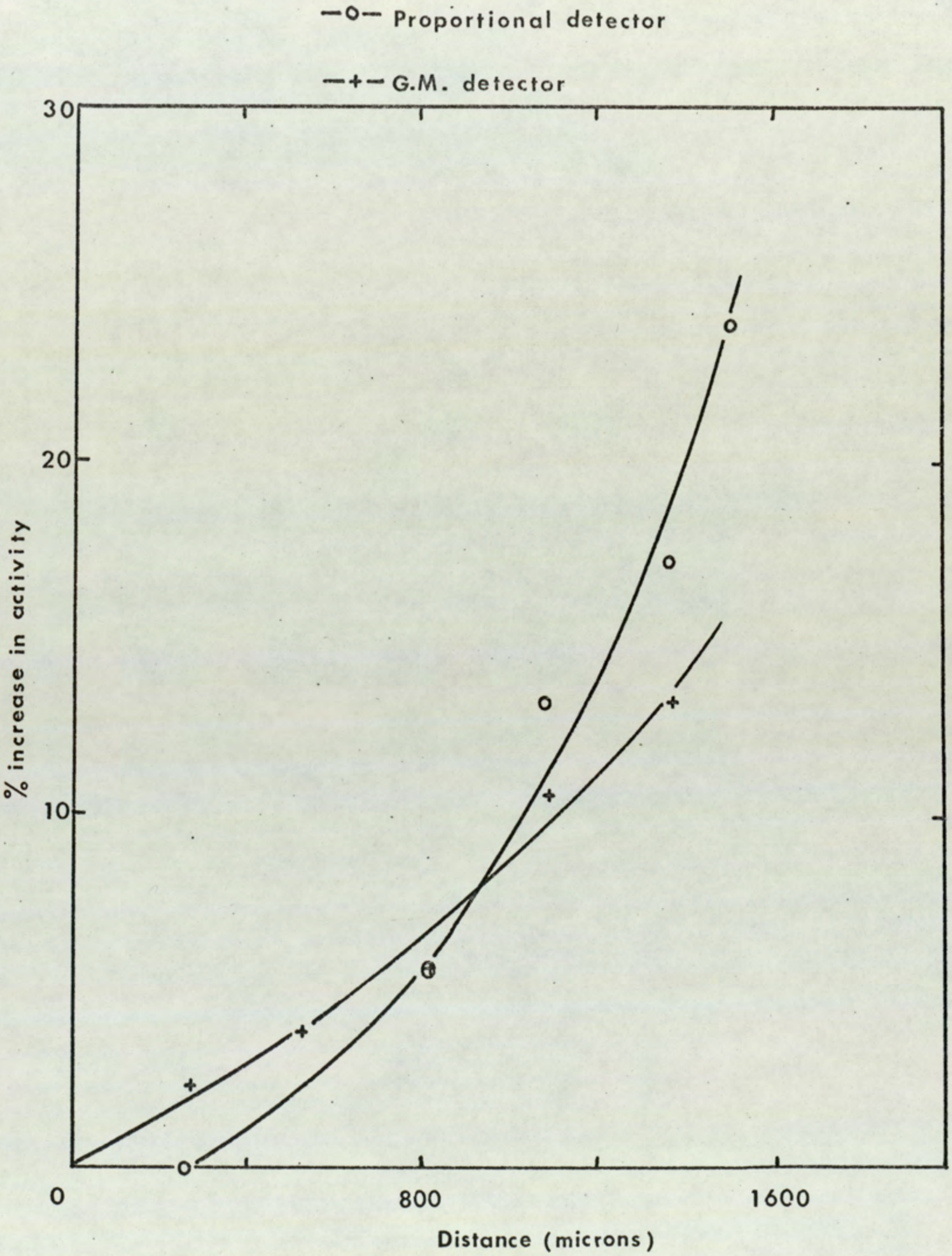

Fig. 2.15. Showing % increase in activity for variations in distance between source and detector.

provided with a 1 cm. hole. These comparative results are described in Chapter III.

2.5.3.7. Surface activity measurements after removal of successive oxide layers.

It was found possible to remove uniform layers of the crystalline oxide by polishing on a cloth impregnated with 1 micron diamond abrasive; Fig. 2.16. illustrates the surface of the oxide treated in this way. The actual test pieces for these radioactive experiments were machnined from mild steel bar of composition and treatments used previously. Duplicate test pieces measuring 1.2 x 1.2 x 0.2 cms. had one of the larger faces ground with 1 micron diamond paste before laying down the Fe^{55}. Oxidation of duplicate samples was then performed in 3.5M NaOH at 316°C for 500 hours. The test pieces were weighed and counted for surface activity before and after removal of a layer of oxide. A perspex jig was used to hold the specimen during the grinding operation to ensure the removal of uniform layers. The sample was agitated in diamond paste cleaning fluid to remove the last traces of grinding compound; the efficiency of this process was very good, since little trace of the abrasive could be observed on the surface of the specimen even at higher magnifications.

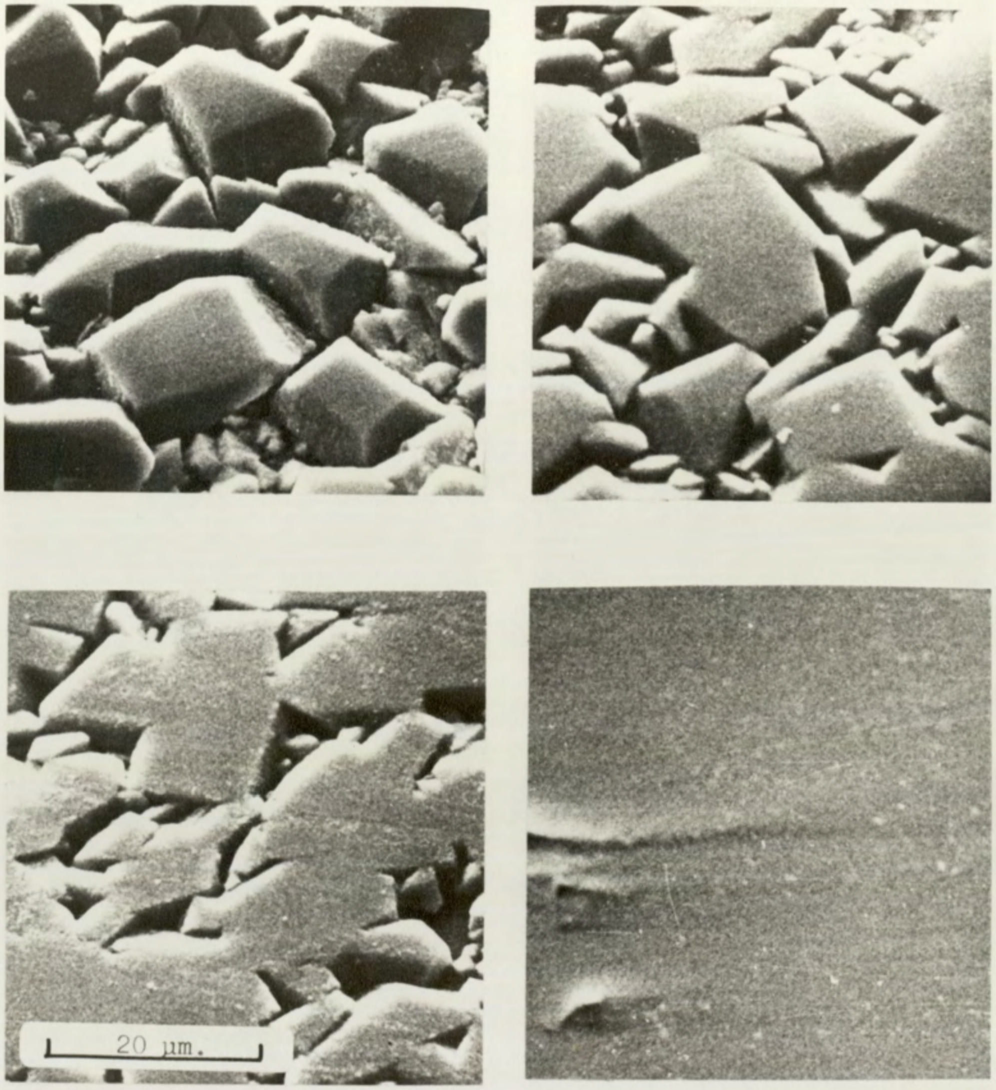

Fig. 2.16. Showing surface of the oxide after polishing with 1 micron diamond paste.

2.6. Electron microscopy.

2.6.1. Preparation of test pieces.

The vacuum annealed steel was cut into strips 1 cm. x 3 cms. x 0.06 cms. which were then electropolished in a 10% perchloric acid in glacial acetic acid at 35 volts and current density of 0.8 amps/cm^2. The strips were then oxidised at 316°C for times ranging from 7 minutes to 8 hours. The oxidation environment was either deionized water, 3.5M NaOH or 0.1M ferrous chloride with nickel additions in either conditioned or P.T.F.E. lined pressure vessels. After oxidation a portion of each specimen was retained for direct examination in the scanning electron microscope; the remainder was coated with a thin evaporated layer of carbon.

2.6.2. Replica preparation.

The carbon replica was removed by electropolishing the surface in a 10% HCl in ethyl alcohol solution, removal being assisted by immersion of the specimen in deionized water. At this stage the oxide particles were adherent to the carbon replica and were removed by immersion in a 70% HCl in water solution. The replica was well washed with deionized water and alcohol before it was mounted on a copper grid.

Examination of the replicas was carried out at 80KV in a Phillip's E.M. 200 microscope. Five replicas, each from a different area of a specimen were examined; the photomicrographs shown can therefore be considered as being completely representative.

2.7. Weight change and thickness determinations.

2.7.1. Weight change experiments.

The specimens were degreased and weighed both before and after oxidation. To overcome the hygroscopic effects of the oxide layer, specimens were dried in an oven at 80°C followed by reweighing after cooling in a desiccator. The oxide scale was then removed potentiostatically in 1N H_2SO_4 solution followed by reweighing.

2.7.2. Thickness measurements.

The oxidised samples were mounted in "Araldite"* under vacuum, to ensure that the outer surface of the oxide was adequately supported. Cross sections were prepared in the usual metallurgical way with final polishing to $\frac{1}{4}$ micron. The cross sections were examined in a Vicker's projection microscope, fitted with a graticuled screen.

2.8. Oxidation of electrodeposited iron.

The oxidation of iron deposited from two different baths was made, the two baths being:-

---

* Araldite: AY103, hardener HY 951. Supplied by C.I.B.A. (A.R.L.) Ltd., Duxford, Cambridge, England.

(1) ferrous chloride bath[54]

$FeCl_2\ 4H_2O$	300 gms./l.
$CaCl_2$	335 gms./l.
Tp. 90°C	pH 0.8-1.5

cathodic current density 6.5 A/dm^2.

(2) ferrous sulphate bath[54]

ammonium ferrous sulphate	350 gms./l.
Tp. 25°C	pH 2.8-3.4

cathodic current density 2 A/dm^2.

In both cases a 12 micron layer of iron was plated onto a steel surface that had been anodically cleaned in "Anodax"* followed by rinsing in a 2% HCl solution.

---

* Anodax: Proprietary anodic cleaner, supplied by W. Cannings Ltd., Birmingham, England.

CHAPTER III

RESULTS: GROWTH OF MAGNETITE IN CONDITIONED PRESSURE VESSELS

3.1. Introduction.

This chapter on the growth of magnetite in conditioned pressure vessels is divided into three sections. In the first two sections results of experiments to determine the redistribution of radioactive iron tracers are described. It is shown that the tracer resides beneath the outer layer after oxidation, a result which is used to calculate the kinetics of outer layer formation. Comparisons are made with weight change data described in the following section. Finally, the results of an electron microscopy investigation of the oxides grown after various times in 3.5M sodium hydroxide solutions are described.

3.2. Radioactive tracer experiments.

3.2.1. Distribution of iron about the experimental system.

Fig. 3.1. shows the radioactive iron distribution after oxidation in sodium hydroxide solution at 316°C; it is seen that although the initially active sample had lost some of its activity both the electrolyte and the pressure vessel had gained activity. This gain experienced by the electrolyte increased at a very rapid rate with time; it must be remembered however that the temperature of the pressure vessel rapidly increases when placed in the furnace. The maximum amount of activity recorded was about 25% of the total after 20 minutes. From this point on the electrolyte rapidly lost most of its activity both to the sample and to the pressure vessel

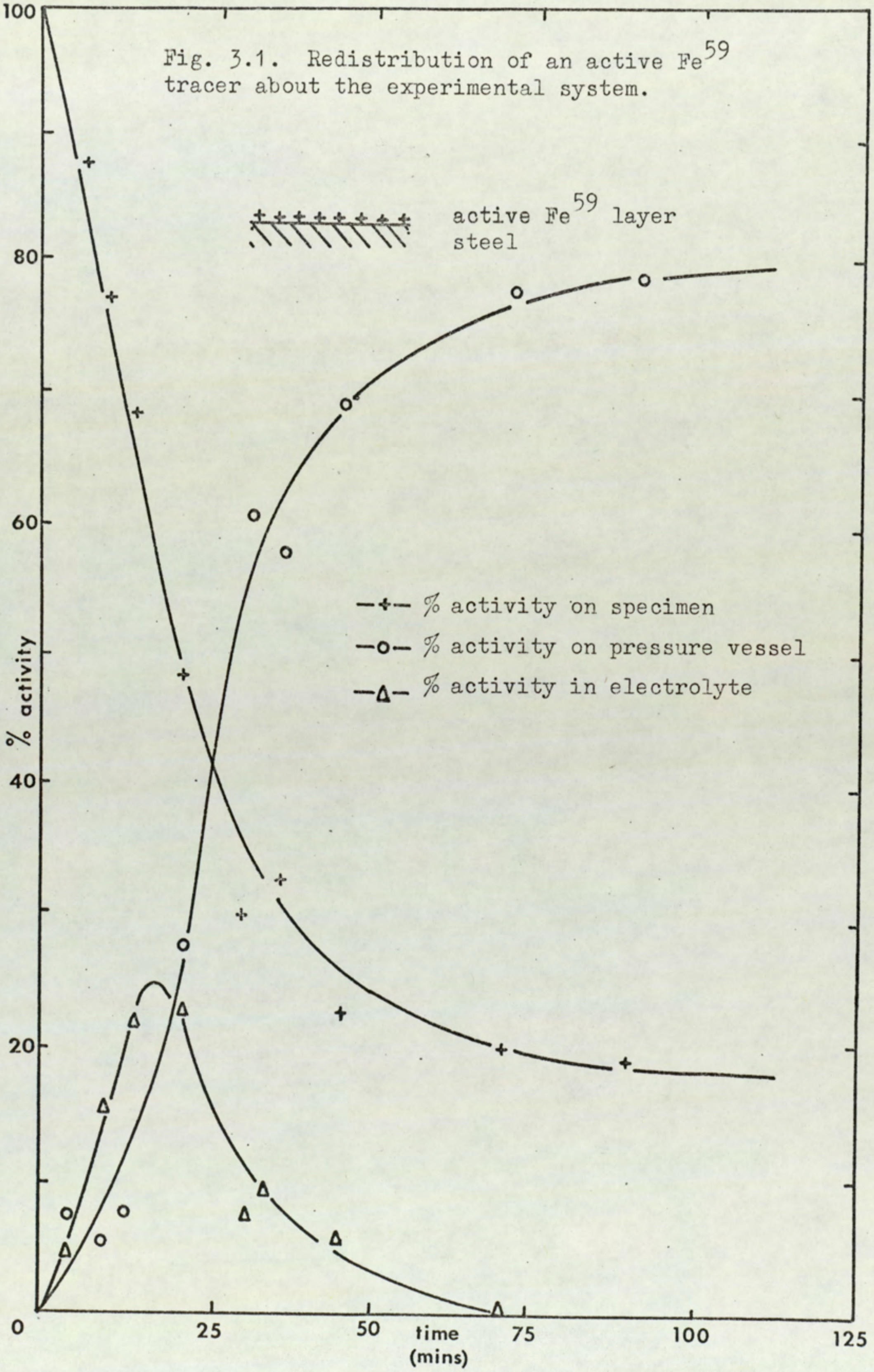

Fig. 3.1. Redistribution of an active Fe^{59} tracer about the experimental system.

wall. After 75 minutes, very little interchange took place presumably because all the active iron had been converted to magnetite. The following reactions describe these early stages:-

$$2Fe + 2NaOH + 2H_2O \rightarrow NaFeO_2 + 3H_2$$

$$2NaFeO_2 + H_2O \rightarrow Fe_2O_3 + 2NaOH$$

$$3Fe_2O_3 + H_2 \rightarrow 2Fe_3O_4 + H_2O$$

The surface area to volume used in these experiments was approximately 1 cm^2./1 ml. (neglecting any growth on the vessel walls, which would of course be small in a conditioned pressure vessel.) If it is assumed that the original radioactive layer was 0.09 microns thick, then on total dissolution the electrolyte would contain 71 ppm. of iron in solution. In fact the maximum achieved by the electrolyte was 25% of the total activity which would be equivalent to 18 ppm. of iron in solution. It must be remembered that the radioactive measurements were made at room temperature where the effects of supersaturation of iron dissolved in sodium hydroxide solution were not known. Nevertheless it is significant that although there was iron still present in a radioactive form the activity in the electrolyte started to decrease after 20 minutes. This is consistent with Linnenbom's[18] observation that the solubility of iron in a solution decreases when magnetite is nucleated. After the active layer had been oxidised the radioactive iron ions would be diluted with iron from beneath the active layer. When the radioactive layer was plated over with a 1 micron layer of iron, activity was first detected in the electrolyte after some 20 to 25 minutes; the activity on the specimen only dropped to 40% (Fig. 3.2.) as compared to 20% on a non plated specimen. This could be attributed to the fact that initial rapid dissolution, followed by nucleation of magnetite had taken place before the active layer was reached. It is also significant that the activity in the electrolyte did not reach the same high values as experienced with the exposed active layer. This may be explained by considering the formation of the oxide to be well underway at this stage and thereby offering a degree of protection.

The degree of mobility of iron ions in the experimental system was found to be quite remarkable in the early stages of oxidation; any theory of nucleation and growth of these studies must be able to account for this. Fig. 3.3. illustrates the percentage of activity picked up by the non active side of a test specimen. The maximum of 15% was recorded after about 50 minutes. An interesting feature was that the non active side of the specimen was not as efficient as the magnetite on the pressure vessel wall for the removal of iron in solution. This would be in accord with the observation that a nucleated magnetite surface acts as a sink[11] by supporting the magnetite forming reaction.

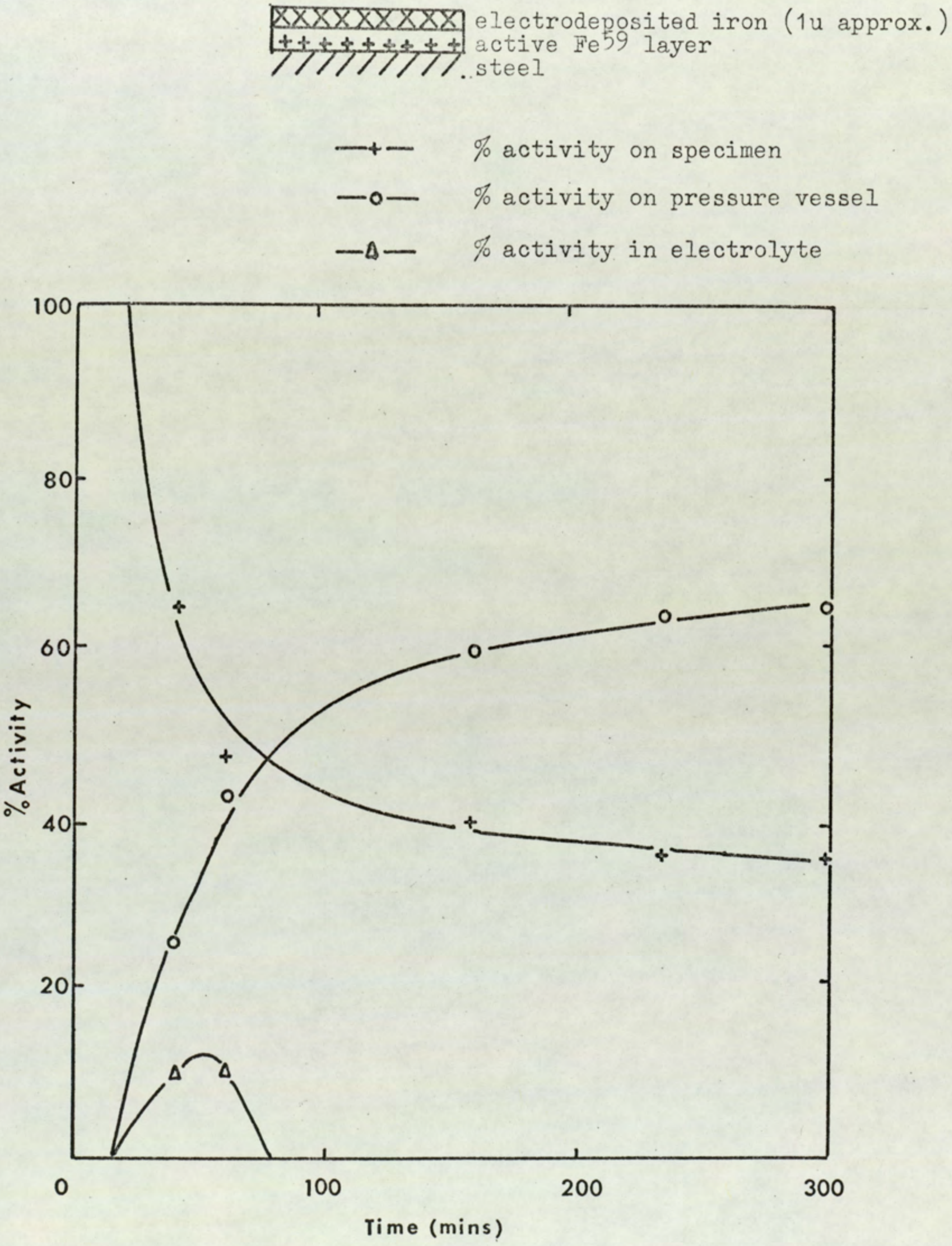

Fig. 3.2. Redistribution of an active Fe^{59} tracer.

Fig. 3.3. Showing increase in activity of side of specimen not plated with Fe^{59}.

NB. percentages are based on specimen only.

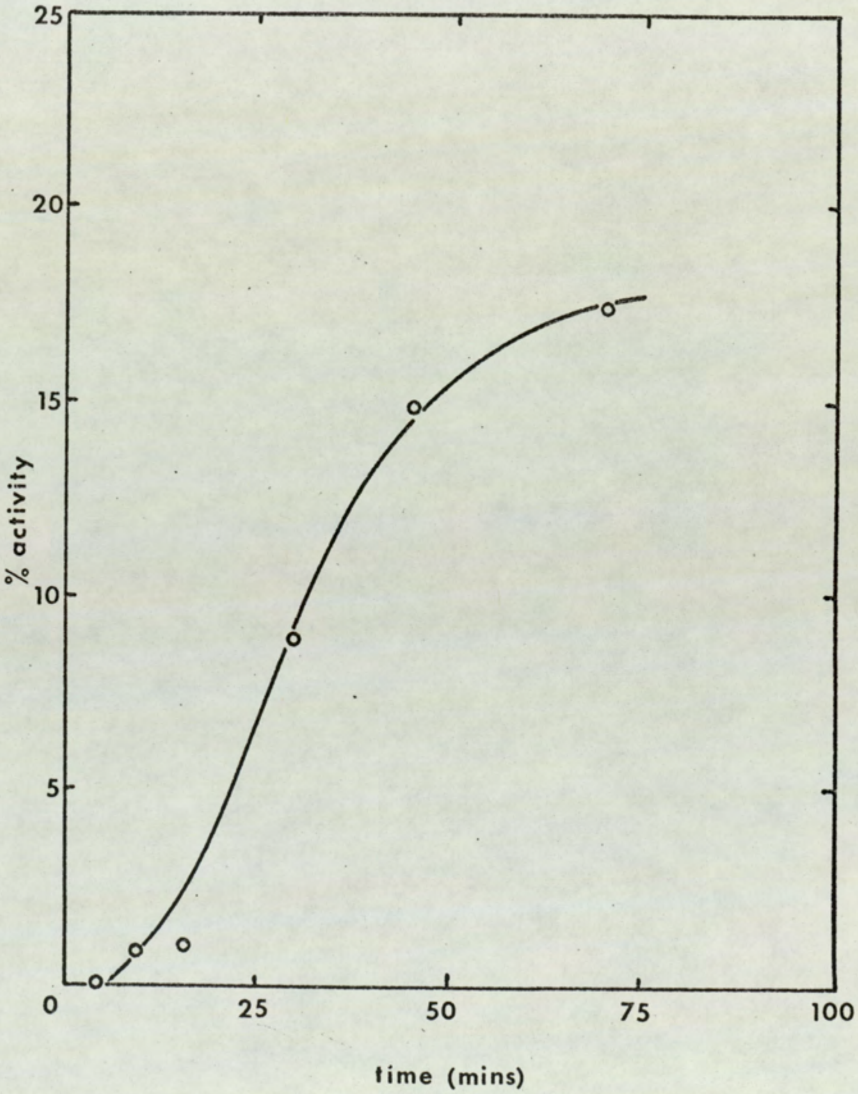

3.2.2. Distribution of radioactive iron within the oxide.

The results of the Fe^{55} surface activity tracer experiments are given in Table III. Duplicate coupons were used for each run; the practice of using the same coupon for each oxidation period was found to be quite satisfactory from comparisons with individual coupons that had had their oxidation interrupted at set intervals of time.

The observed decrease in surface activity

$$\frac{I}{Io} = e^{-\frac{\mu}{p} d}$$

where Io = surface activity with no absorber

I = surface activity after oxidation

$\frac{\mu}{p}$ = mass absorption coefficient

d = thickness of the absorbing layer

assuming the active layer retains its original dimensions even though it may be covered with oxide.

Taking logs

$$\ln \frac{I}{Io} = -\frac{\mu}{p} d \ln e^{e}$$

therefore $$\ln \frac{I}{Io} = -\frac{\mu}{p} d$$

therefore $\ln F$ plotted against d should be linear ($F = \frac{I}{Io}$).

Fig. 3.4. shows the data of Fig. 2.12. (magnetite layers

TABLE III Surface activity data

Sample I					Sample II				
time (hrs)	counting arrangement	fractional surface activity $F = \frac{I}{Io}$	$\log_{10}F$	magnetite mgm/cm^2.	time (hrs)	counting arrangement	fractional surface activity $F = \frac{I}{Io}$	$\log_{10}F$	magnetite mgm/cm^2.
21	a	0.959	$\bar{1}.9818$	0.60	2	a	0.986	$\bar{1}.9939$	0.25
21	b	0.928	.9675	1.05	2	b	0.935	.9708	0.96
21	c	0.957	.9809	0.65	2	c	0.988	.9948	0.26
39	a	0.873	$\bar{1}.9410$	1.90	42	a	0.851	$\bar{1}.9299$	2.23
39	b	0.875	.9420	1.85	42	b	0.861	.9350	2.05
39	c	0.905	.9566	1.38	42	c	0.894	.9513	1.55
154	a	0.789	$\bar{1}.8971$	3.22	157	a	0.793	$\bar{1}.8993$	3.16
154	b	0.808	.9074	2.90	157	b	0.804	.9053	2.98
154	c	0.839	.9238	2.40	157	c	0.815	.9112	2.80
290	a	0.714	$\bar{1}.8537$	4.60	293	a	0.735	$\bar{1}.8663$	4.20
290	b	0.737	.8675	4.15	293	b	0.755	.8779	3.80
290	c	0.781	.8927	3.35	293	c	0.780	.8921	3.40
449	a	0.670	$\bar{1}.8261$	5.42	452	a	0.678	$\bar{1}.8312$	5.25
449	b	0.701	.8457	4.88	452	b	0.701	.8457	4.88
449	c	0.718	.8561	4.50	452	c	0.717	.8555	4.51
1212	a	0.560	$\bar{1}.7482$	7.80	1215	a	0.585	$\bar{1}.7672$	7.20
1956	a	0.549	$\bar{1}.7396$	8.10					

a - G.M. counter b - G.M.counter (specimen edge masked) c - propl. counter (edge masked)

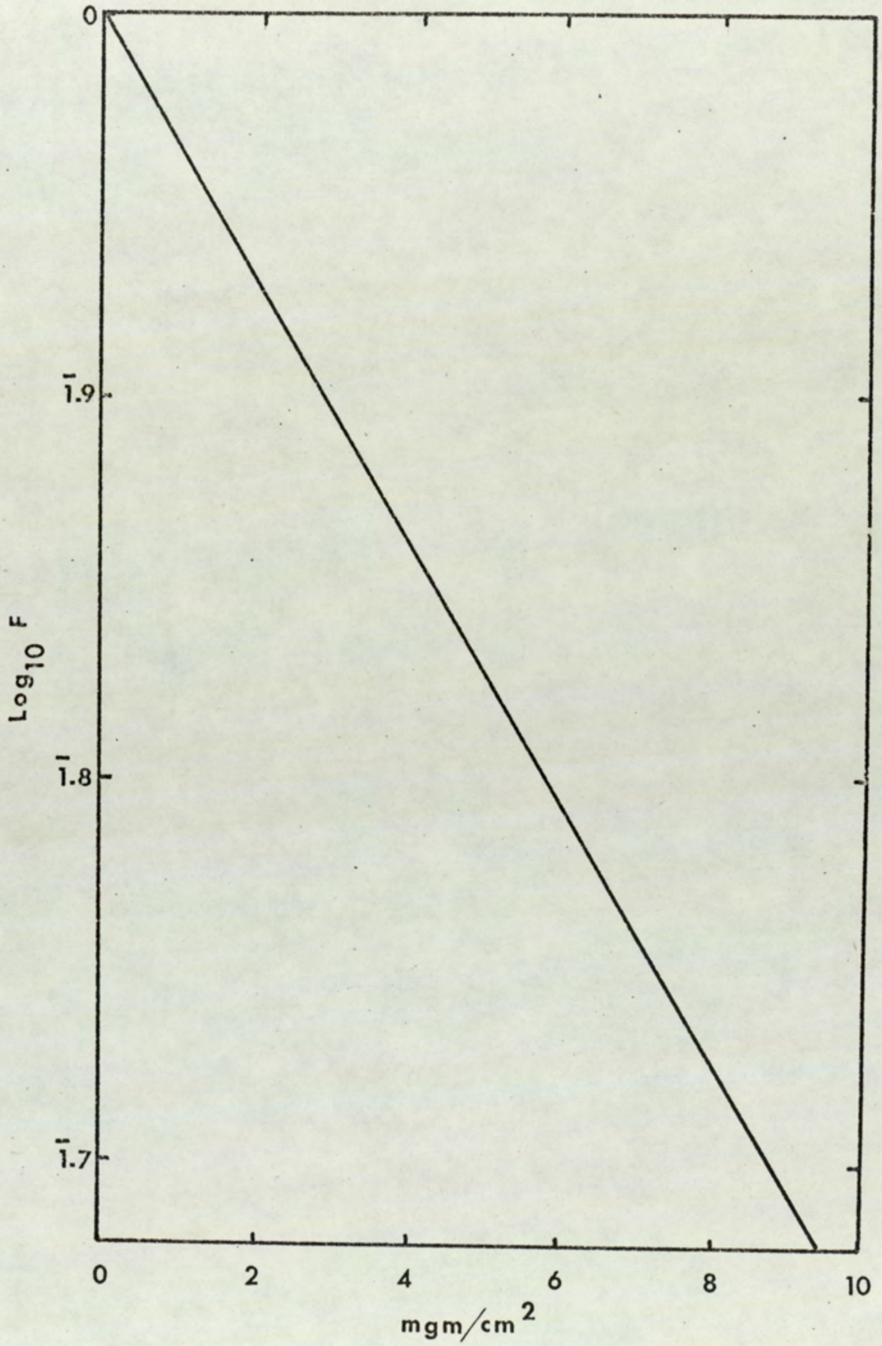

Fig. 3.4. Showing relationship between $\log_{10}F$ and magnetite thickness: data derived from Fig. 2.12.

built up on aluminium foil) plotted in this form. This curve can be used to calculate the absorber thickness on an oxidised specimen providing of course the active layer retains its original dimensions.

If the values of log d derived from each value of F (Table III, duplicate samples I and II) are plotted against log time, the relationship is found to be linear. Statistical treatment gives gradients of 0.53 and 0.46 with product moment correlation coefficients[55] of 0.99 and 0.98 respectively.

From Figs.3.5a & b $x = 0.22t^{0.49}$

where x is outer layer in mgm./cm.^2 and t is time (hours); this is consistent with parabolic kinetics and was the criterion for iron transport through a porous inner layer.

The values of x at any time are in fairly good agreement with values of outer layer thickness obtained from weight change and inner layer thickness measurements (Table IV, columns 5 and 6 and Fig. 3.6.).

It is noticeable that the outer layer thicknesses calculated from the surface activity data are a few percent greater than those actually observed. Nevertheless, these results provide strong evidence for an oxidation mechanism being described as iron transport through solution filled pores. Certainly, it would seem that there is no evidence of solid state diffusion predominating.

Duplicate sample (1)

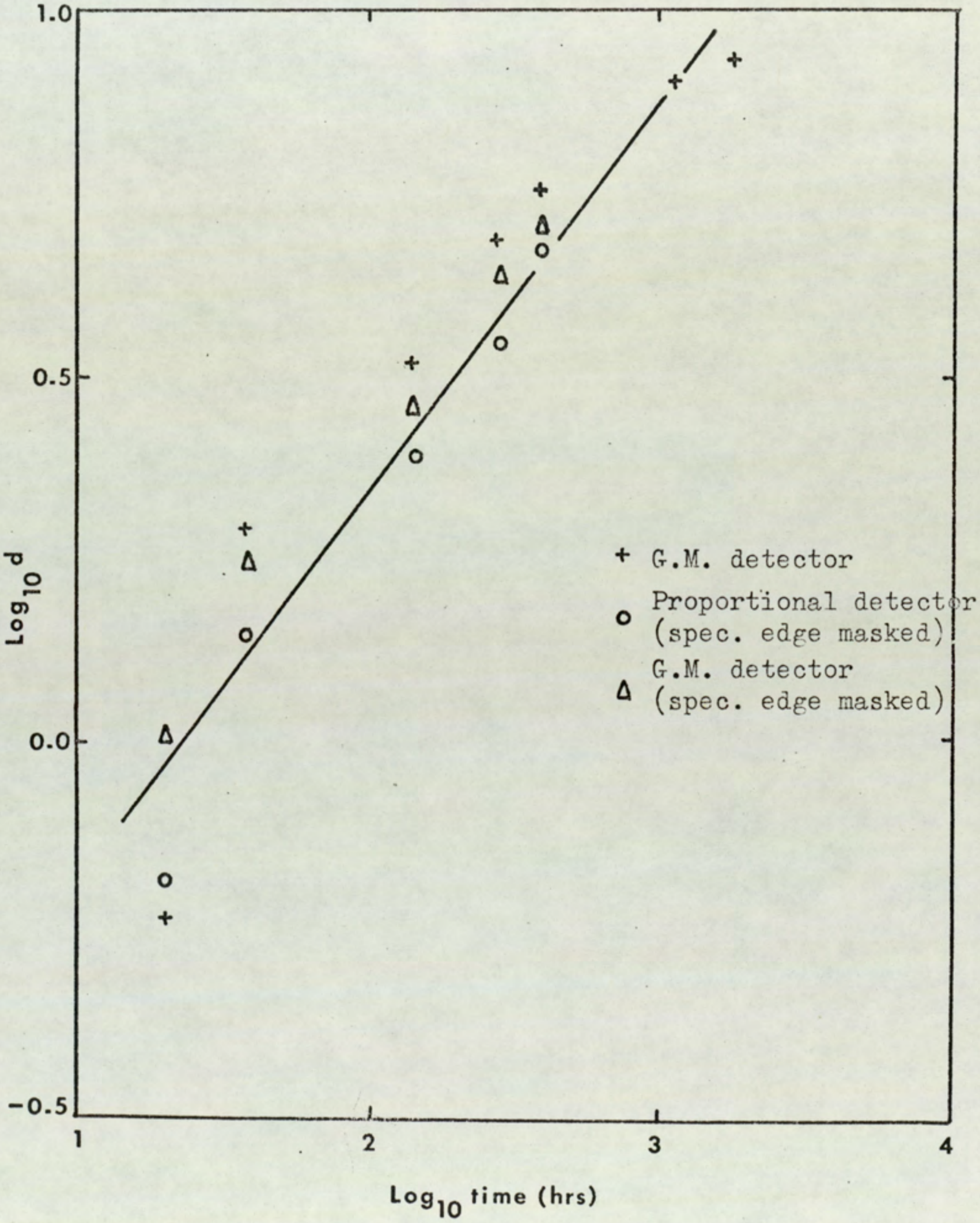

Fig. 3.5a. Showing relationship between magnetite thickness (derived from surface activity measurements) and time.

Duplicate sample (2)

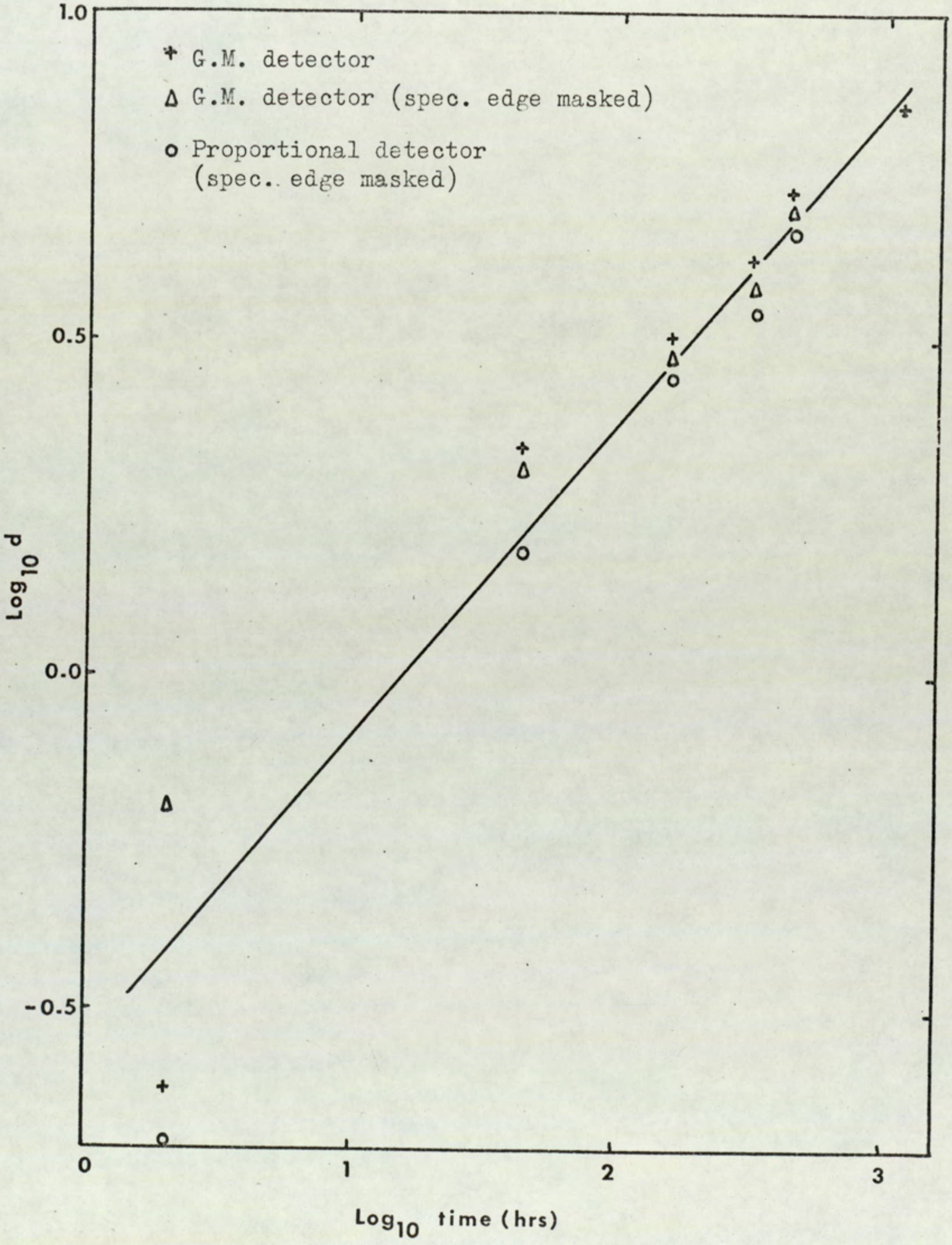

Fig. 3.5b. Showing relationship between magnetite thickness (derived from surface activity measurements) and time.

TABLE IV Oxidation of iron in a conditioned pressure vessel

(3.5M NaOH 316°C)

time (hrs)	mean thickness of inner layer (microns)		average thickness of inner layer mgm/cm². *	experimental thickness of outer layer mgm/cm².	outer layer calculated from surface activities
	Section I	Section II			
47	6.3	8.1	3.4	1.2	1.5
90	10.4	11.4	5.1	1.8	2.0
260	18.1	17.5	8.4	2.7	3.5
504	25.8	24.4	11.8	3.3	4.8
980	28.0	26.0	12.7	4.7	6.8

* density of magnetite, 4.7 from ref.8.

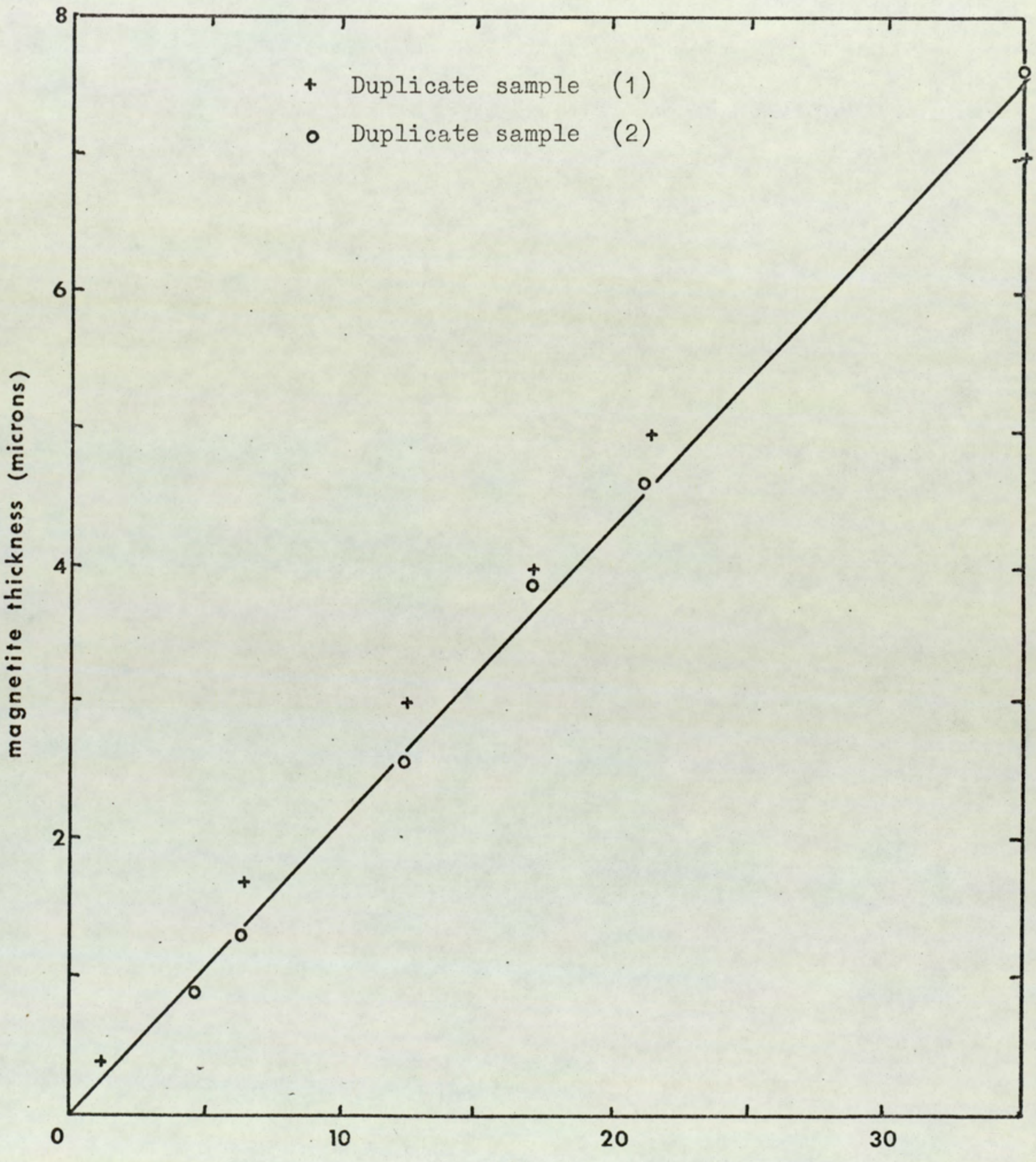

Fig. 3.6. Variation of outer layer thickness (from surface activity data) with time.

The two experiments involving sectioning of the oxide whilst perhaps lacking in precision, both confirm the absence of high activities in the outer layers. Fig. 3.7. is a histogram showing the redistribution of an active Fe^{59} tracer after oxidation. Although activity in small amounts was found in the first samples (representing the outermost layers), the highest activities were found midway between the two layers.

Fig. 3.8. illustrates the increase in surface activity after the removal of successive oxide layers. The theoretical increase in activity for a radioactive layer in residence between the inner and outer layer is also shown on Fig. 3.8. The agreement is sufficiently good to confirm the deductions from the previous results (p.59).

3.3. Weight change data and thickness measurements.

This data was required for the interpretation of the tracer experiments. Duplicate samples were oxidised as described previously at 316°C for up to 1000 hours. One sample at each time was mounted in "Araldite" and two cross sections were taken at right angles to each other. The other sample was used for weight change experiments. Five inner layer thicknesses were recorded for each cross section. The thickness of the outer layer was calculated by subtracting the inner layer oxide from the total oxide; the results are shown in Table IV.

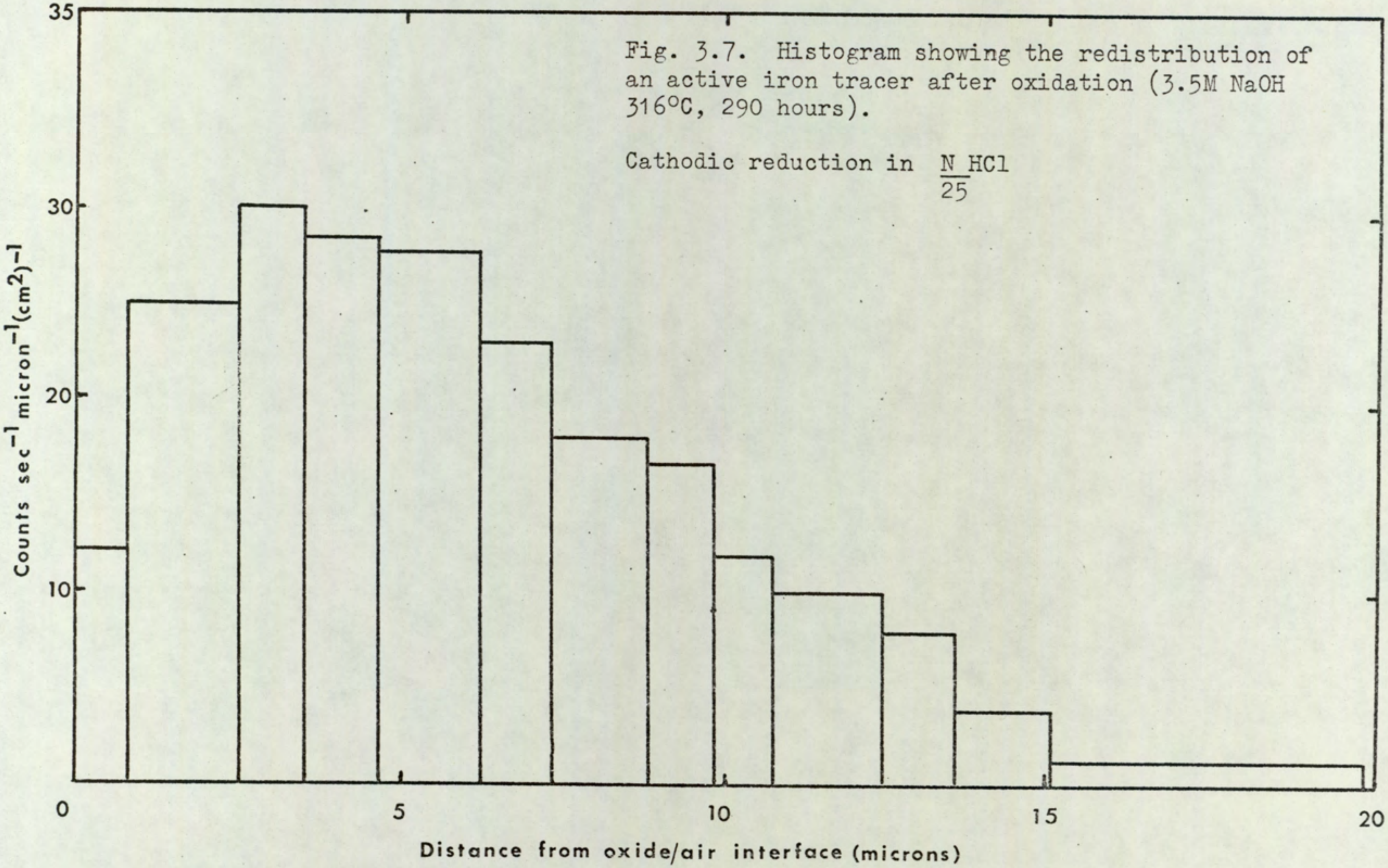

Fig. 3.7. Histogram showing the redistribution of an active iron tracer after oxidation (3.5M NaOH 316°C, 290 hours).

Cathodic reduction in $\frac{N}{25}$ HCl

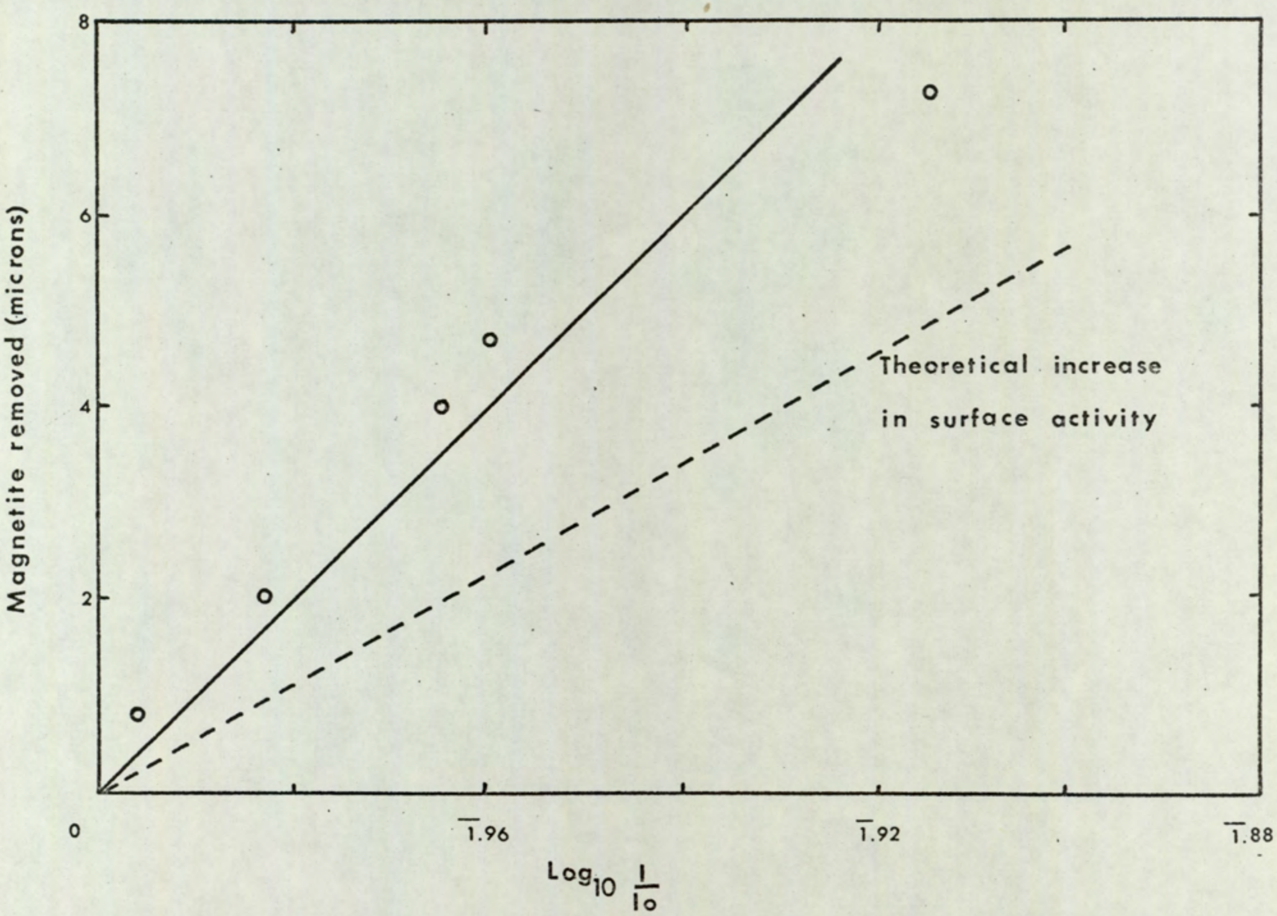

Fig. 3.8. Showing increase in surface activity after removal of successive magnetite layers compared to theoretical increase for a planar active tracer.

3.4. Electron microscopy.

3.4.1. Growth in 3.5M NaOH at 316°C.

All the specimens were annealed and electropolished before oxidation. The structure of the iron surface after electropolishing is shown in Fig. 3.9. for comparative purposes. The electropolished surface had a fine substructure that showed grain orientation dependency. On some grains there were ridges between 200 and 500Å across, whilst on others there appeared to be bumps of similar size. There was some difficulty in distinguishing between the nucleating oxide and the polishing substructure especially in the early stages.

After 12 minutes oxidation the specimen was observed to have a uniform yellow interference tint; no change in structure was observed at this stage by either scanning or transmission electron microscopy. After 30 minutes the interference tint had changed colour and was now a grey-brown; it was at this stage that changes in structure were observed (Fig. 3.10.). If a comparison was made with the electropolished structure, it appeared that many of the facets of the latter had been retained but their depth had increased. This suggested that after 30 minutes the air formed ferric oxide film was being thickened by solid state diffusion. It is known however from radioactive experiments that dissolution of the ferric oxide is taking place simultaneously. The thickness of the oxide film can be calculated from interference colours[56] if it is

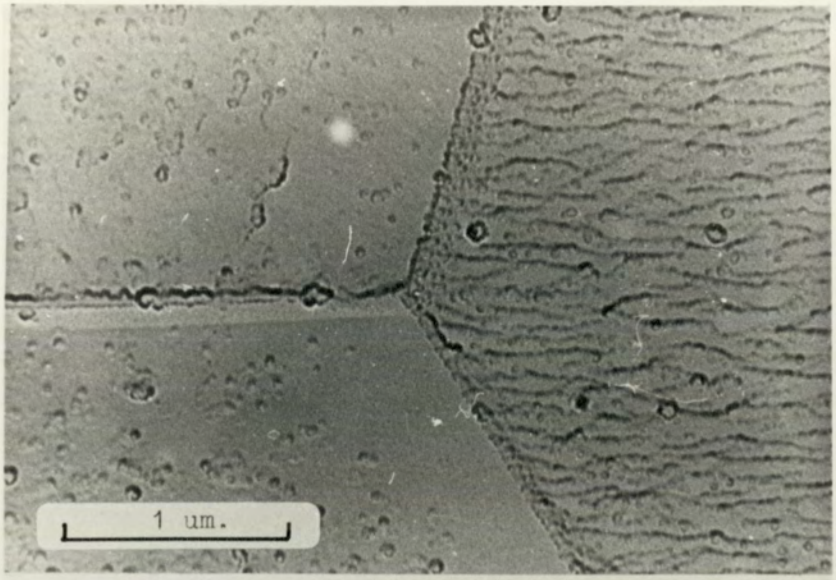

Fig. 3.9. Surface of steel electropolished in 10% perchloric acid in acetic acid solution.

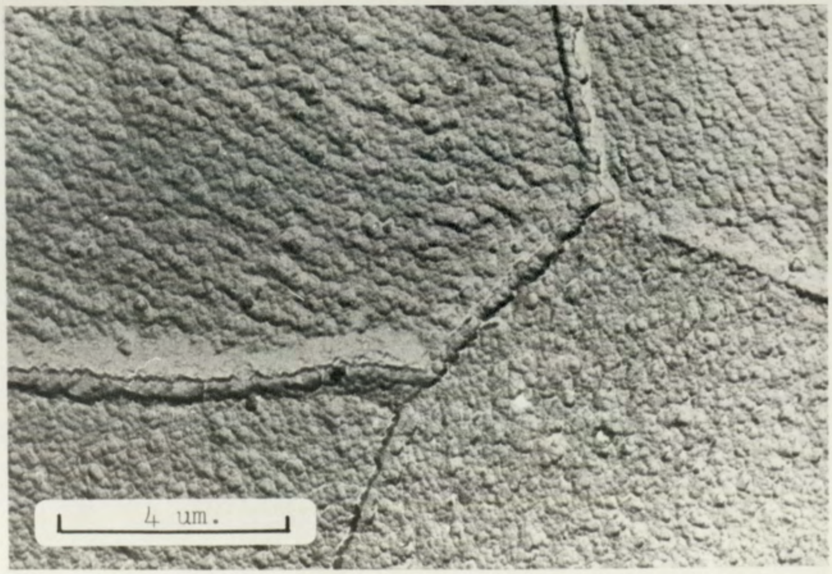

Fig. 3.10. Transmission electron micrograph of a carbon replica of steel surface oxidised in a conditioned pressure vessel. (3.5M NaOH, 316°C, 30 minutes).

assumed to be Fe_2O_3. At this stage the oxide is calculated to be about 325Å thick. After 40 minutes the oxide surface showed no interference colours whatsoever, but examination of the surface revealed a structure consisting of individual crystallites about 1000Å across (Fig. 3.11.); there was also evidence of some of these crystallites increasing in size more rapidly than others. Fig. 3.12. shows the surface after 1 hour oxidation, in some areas very large crystals have appeared at isolated sites which most probably have grown from solution and constitute the outer layer.

Scanning electron microscopy studies of the same samples did not show any resolvable changes in structure until after 50 minutes when areas of the surface were covered with oxide platelets identified as haematite[57] (Fig. 3.13). The part played by these is uncertain, they are not however observed to the same extent when steel is oxidised in deionized water, nor do they provide sites for magnetite crystals subsequently grown from solution[57]. After 24 hours oxidation the surface of the steel was seen to be thickly covered with magnetite tetrahedra (Fig. 3.14.) and there was no sign of the haematite platelets. The haematite was only present within the first 60 minutes when there was residual oxygen present.

The results of an S.E.M. examination of a bulk oxide formed after 250 hours are shown in Fig. 3.15. The oxide and metal substrate was flexed through about 5 degrees causing a certain

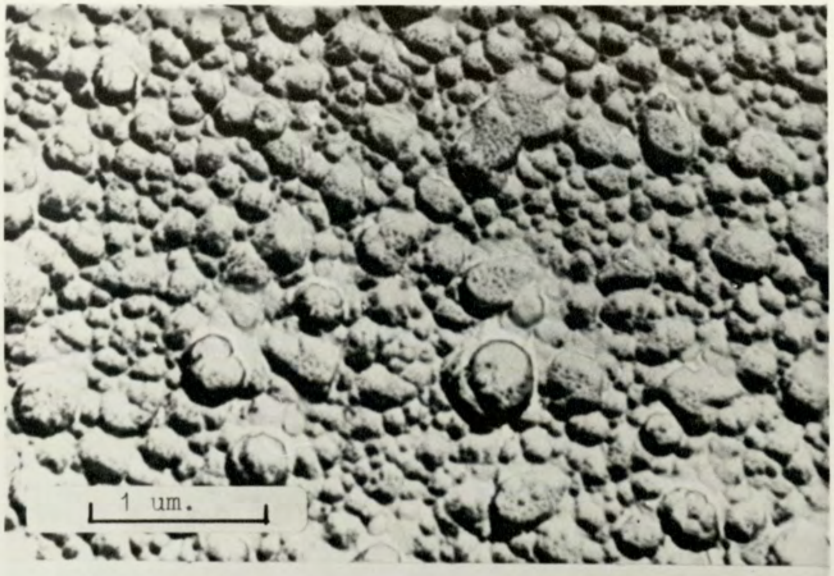

Fig. 3.11. As Fig. 3.10. but oxidised for 40 minutes, showing initial magnetite crystallites.

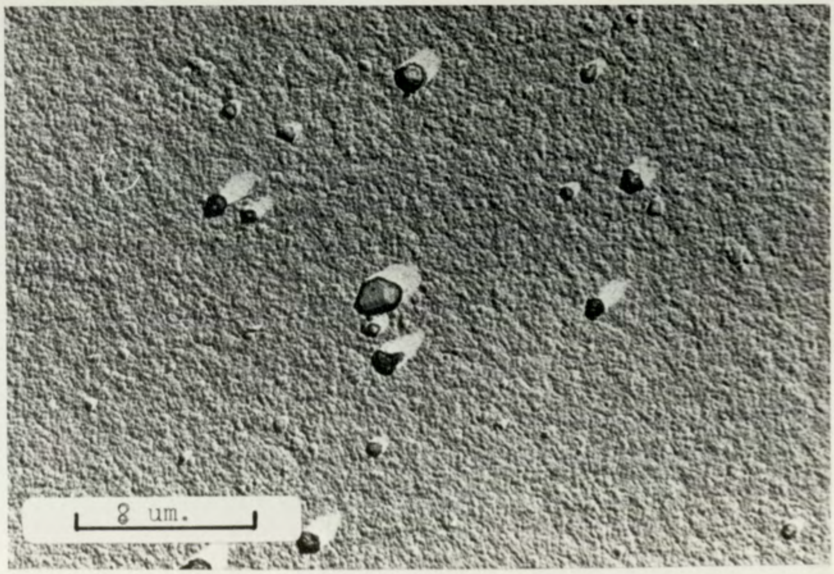

Fig. 3.12. As Fig. 3.10. but oxidised for 60 minutes. Nucleation of outer layer has taken place.

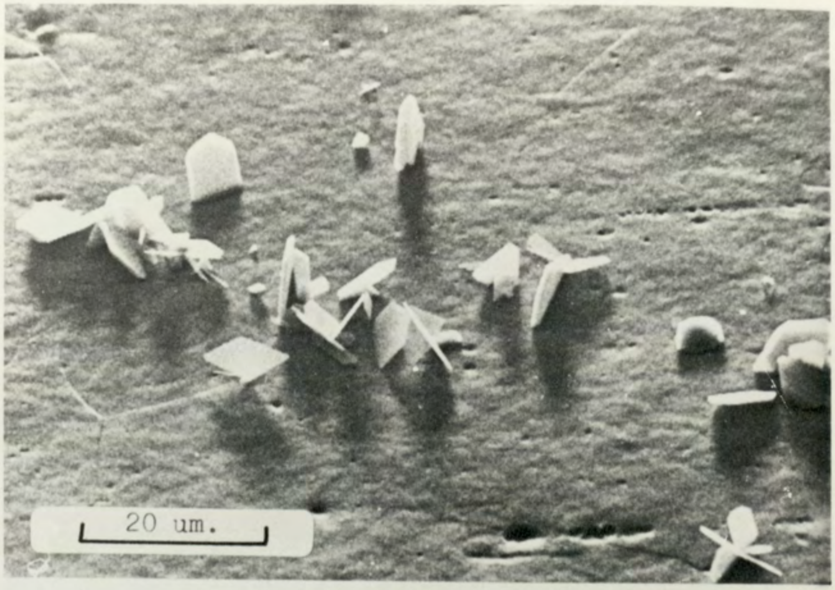

Fig. 3.13. Scanning electron micrograph of steel surface oxidised for 50 minutes at 316°C in 3.5M NaOH, showing an area supporting haematite growth.

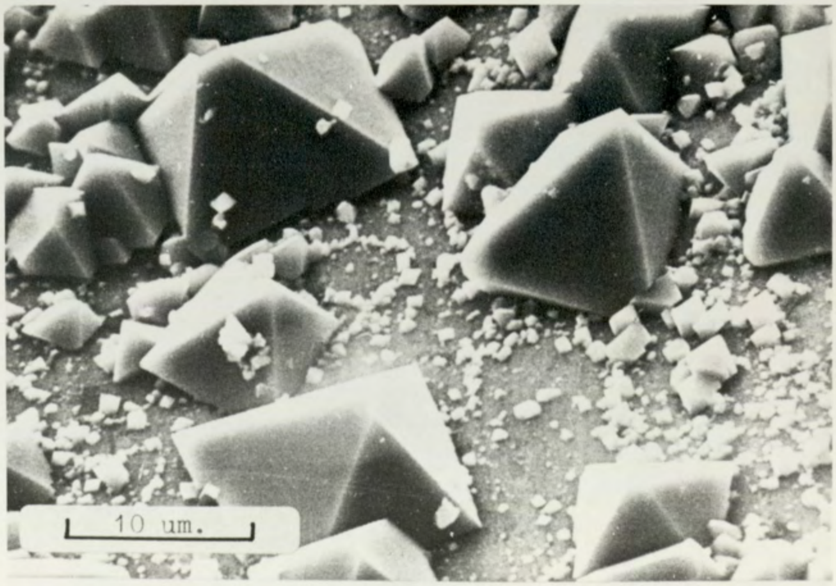

Fig. 3.14. As Fig. 3.13. but oxidised for 24 hours. The surface is thickly covered with magnetite crystals.

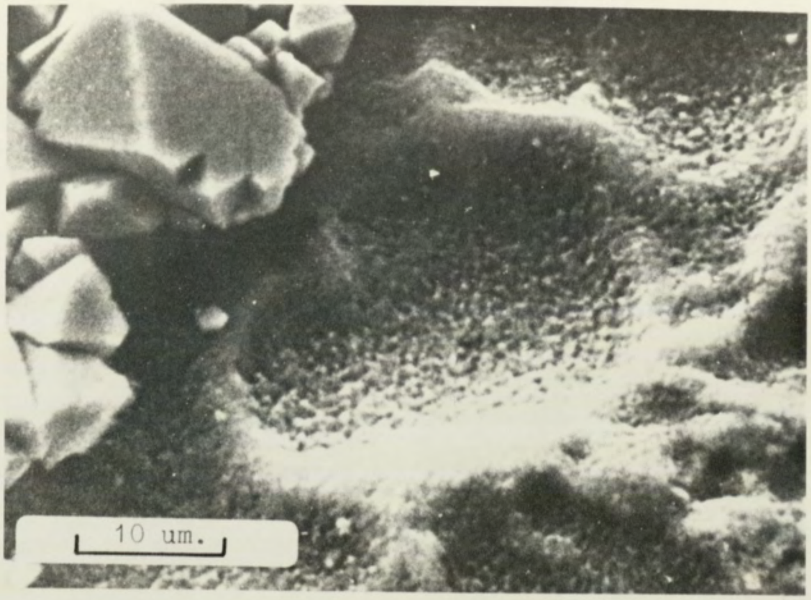

Fig. 3.15. Structure of inner/outer layer interface of Potter and Mann oxide revealed by flexing sample.

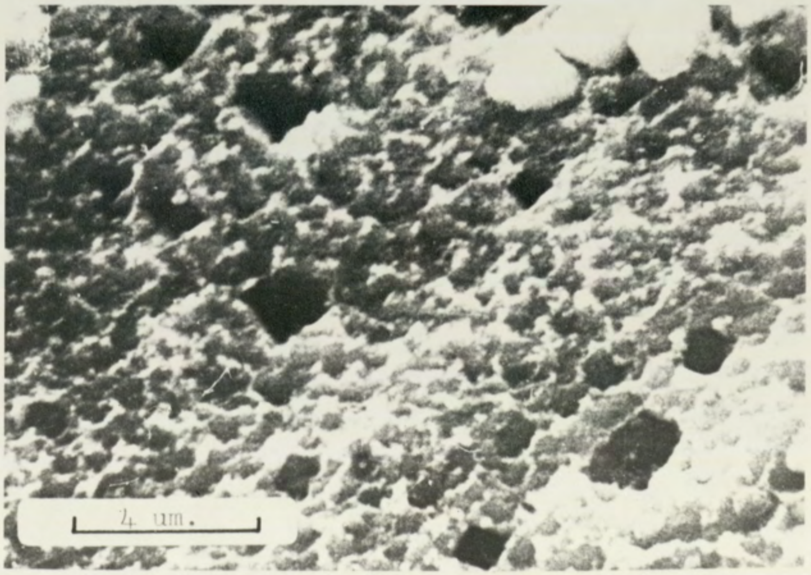

Fig. 3.16. As Fig. 3.15.

amount of spalling of the oxide layers. At low magnifications depressions could be seen in the inner layer surface and appeared to be associated with groups of outer layer crystals. This effect invariably occurred in annealed samples of large grain size and was usually associated with outer layer crystals. It was because of this non uniformity of the inner layer that the large grain steel was not used in the radioactive experiments. The reasons why these depressions are formed are not really known but could arise from either (1) some form of interaction between the inner and outer layer or (2) they may be extensions of the original surface since the inner layer forms with zero volume change. Some of the iron that is ionized at the metal oxide interface forms the inner layer whilst the rest is transported away. Thus the inner layer/outer layer oxide interface would represent the original metal surface after oxidation. A small grain size might therefore approximate to a uniform surface on oxidation. Even under these conditions departures from the ideal arise because triangular shaped pits that could conceivably have been the seat of an outer layer crystal are often found (Fig. 3.16.).

The suggestion that some form of interaction occurs between the electrolyte permeating the porous layer, and the porous layer itself, does seem credible in view of the saucer shape of the depressions. The depressions would then be extended once a large crystal occupied it by a movement of solution around the crystal attempting to find a site for deposition of iron as magnetite.

3.4.2. Growth in deionized water at 316°C.

In contrast to the oxidation of iron in sodium hydroxide solution, in deionized water the surface is covered with small nuclei after only 9 minutes oxidation; the temperature inside the pressure vessel after 9 minutes is only 210°C. The oxide particles at this stage were amorphous (Fig. 3.17a.) and were not epitaxially orientated as in later stages. Fig. 3.17b. shows the structure after 15 minutes oxidation. Some of the crystallites appeared to be growing outwards from the original nucleated layer and were approximately $\frac{1}{4}$-1μ in size. The growing particles were just beginning to show some crystallographic form. After 25 minutes oxidation these larger particles had increased in size and assumed a definite crystallographic shape that was dependent on the metal substrate (Fig. 3.18.). Even at this stage the original layer of loose porous nuclei could still be seen between the growing particles. These larger particles increased in size and merged until the whole surface became covered with an oxide that showed a whole variety of definite crystallographic forms which were completely dependent on the metal substrate (Fig. 3.19.). Even the grain boundaries were in evidence, being marked by a thickening of oxide formed from one of the more prominent grains making up the

Surface of steel electropolished in 10% perchloric acid/acetic acid.

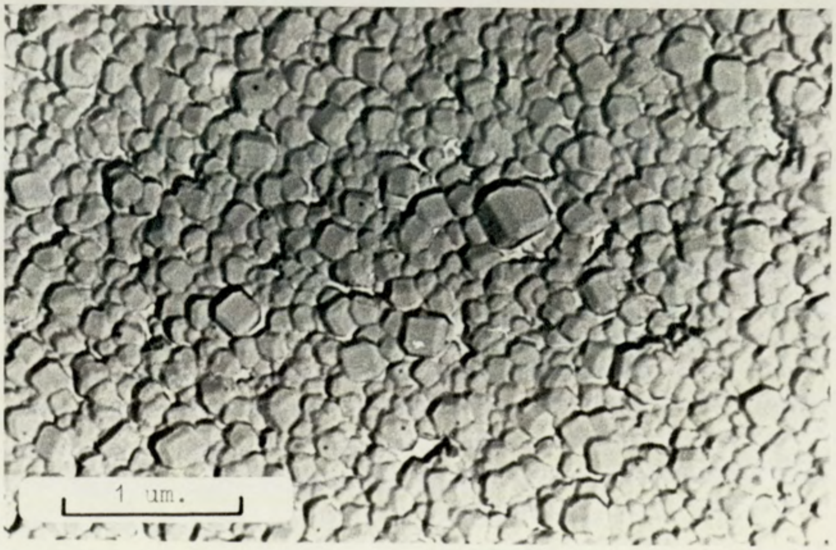

Fig. 3.17.a Transmission electron micrograph of a carbon replica of steel surface after oxidation. (deionized water, 316°C, 9 minutes).

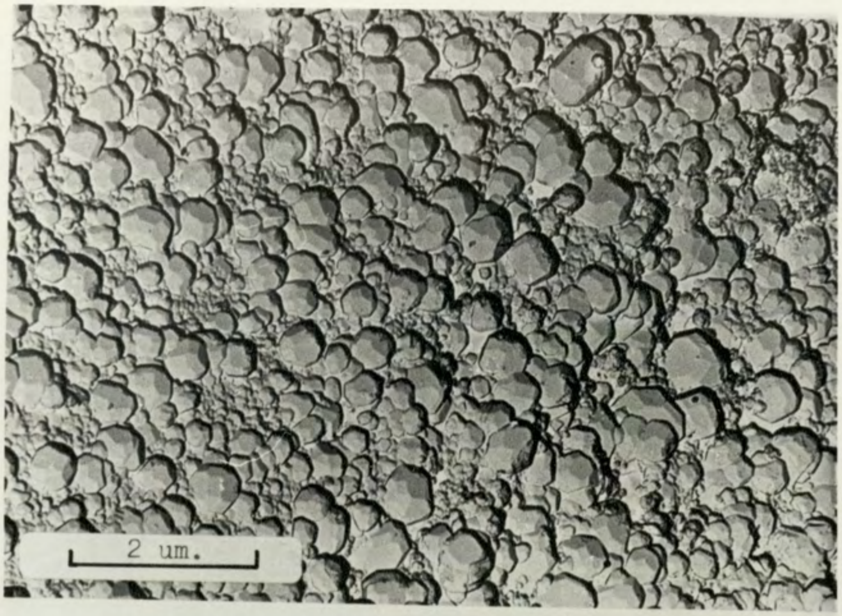

Fig. 3.17b. As Fig. 3.17. but oxidised for 15 minutes.

Fig. 3.18. As Fig. 3.17., oxidised for 25 minutes.

Fig. 3.19. As Fig. 3.17. but after 35 minutes oxidation.

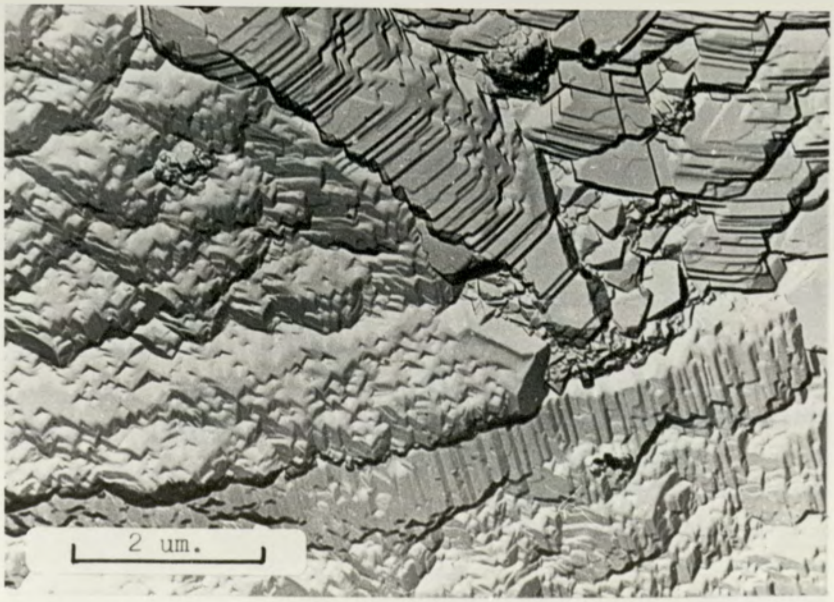

Fig. 3.20. As Fig. 3.19.

boundary. This was not always the case however, reference to Fig. 3.20. shows that the oxide layer adjacent to the boundaries is of some intermediate form. Figs. 3.21. and 3.22. are photomicrographs of the oxide after 45 and 60 minutes respectively; large particles appeared to be nucleated quite randomly on the surface. The particles showed evidence of rapid growth from solution, since each crystal face was characterised by parallel layers of magnetite. This would explain the mode in which the outer crystals grow and readily impinge with neighbouring crystals. After 1 hour oxidation very few crystals had an appearance of platelet growth; it would seem that crystals formed in this manner became smoothed over and an outline formed that was characteristic of magnetite after prolonged oxidation times. Figs. 3.23a. and 3.23b. show an electron diffraction pattern of a crystal extracted from a surface after 50 minutes oxidation. The only phase that could be identified with any certainty was cubic magnetite.

Variations in the nucleation of magnetite were observed when the ratio of surface area to volume was altered. Figs. 3.24. to 3.29. show the stages in oxidation as described previously but where the ratio of surface area to volume (3 cm^2./6 mls.) was approximately half of that used in the previous experiments.

The chief differences observed were:-

(1) there was less tendency for the surface to be covered

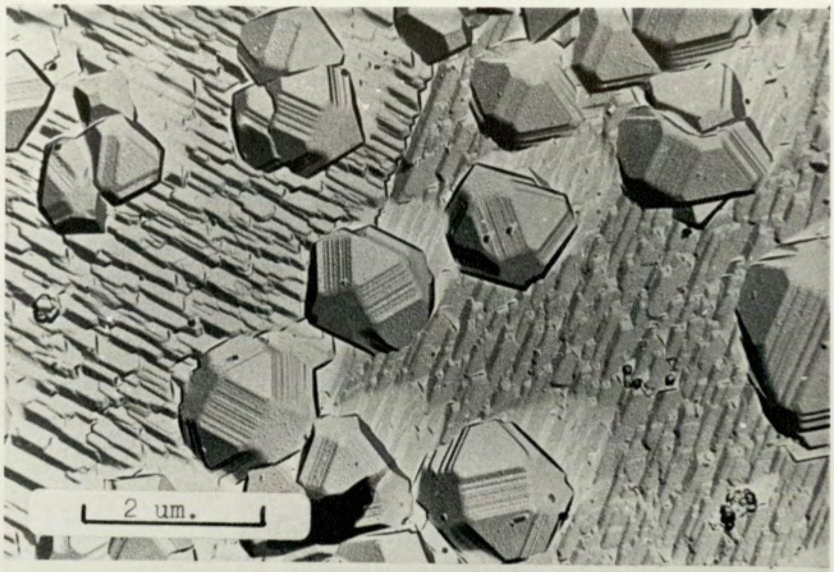

Fig. 3.21. Transmission electron micrograph of a carbon replica of an oxidised steel surface showing growth of outer layer nuclei. (deionized water, 316°C, 45 minutes.)

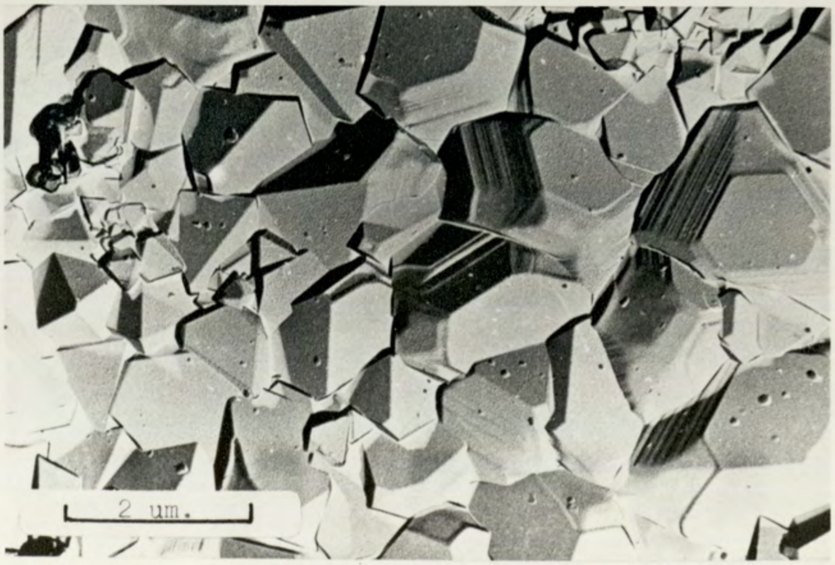

Fig. 3.22. As Fig. 3.21. but after 60 minutes oxidation.

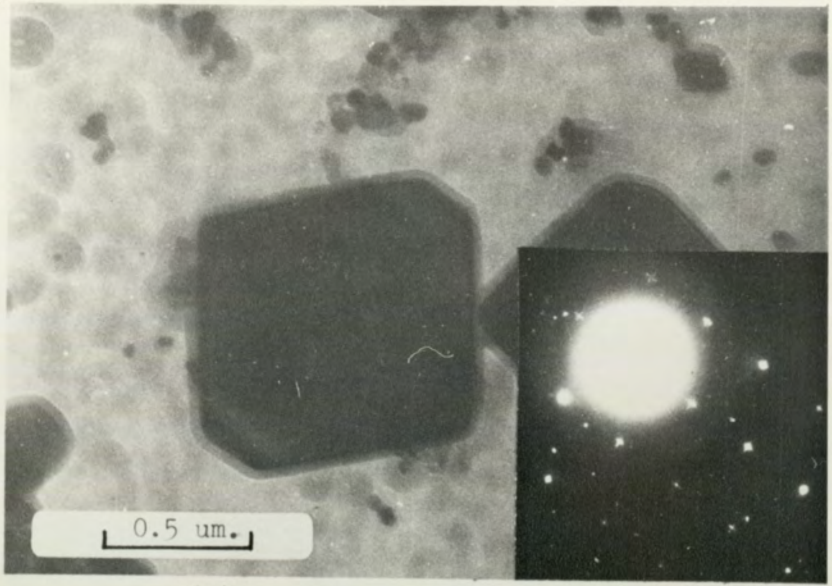

(a) (b)

Fig. 3.23(a). Transmission electron micrograph of a magnetite film stripped from oxidised iron. (deionized water, 316°C, 20 minutes.)

Fig. 3.23(b). Electron diffraction pattern of LHS crystal shown in Fig. 3.23(a).

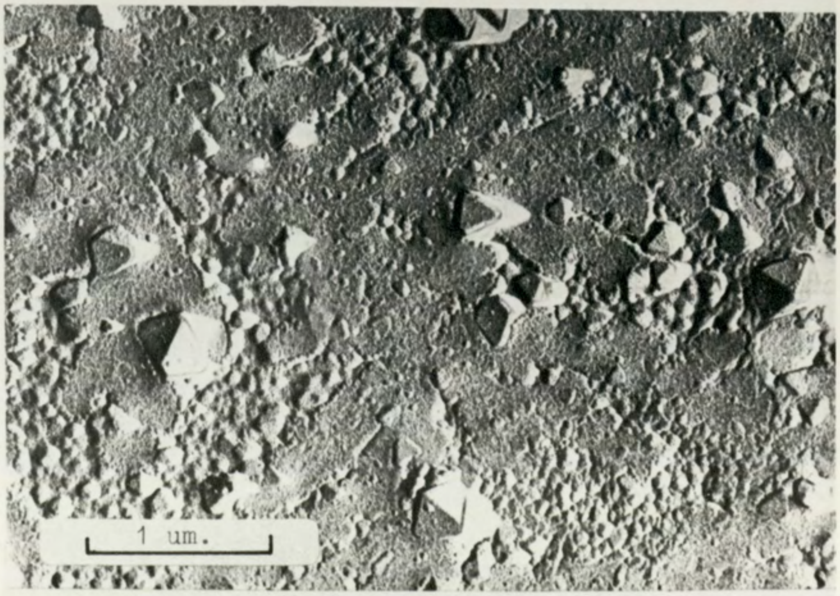

Fig. 3.24. Transmission electron micrograph of a direct carbon replica of an oxidised steel surface. (deionized water, 316°C, 15 minutes, surface:volume 3 cm^2/6 mls.)

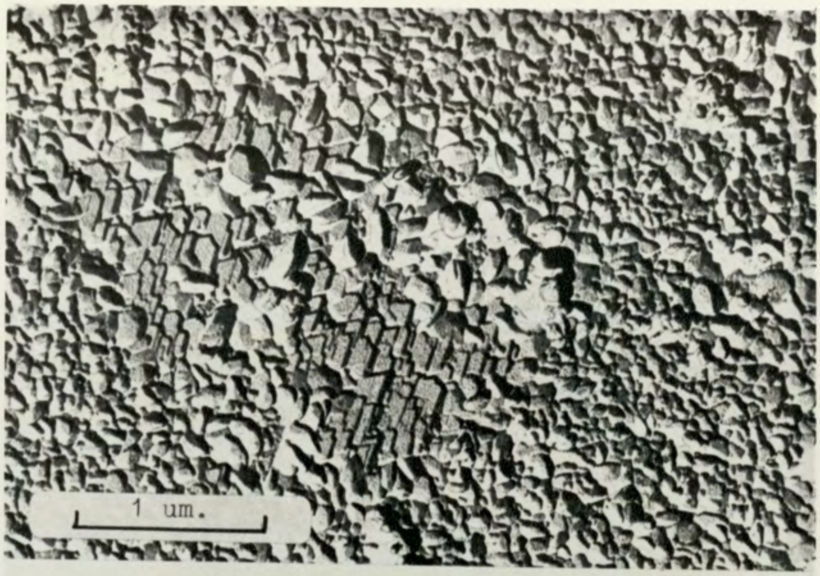

Fig. 3.25. As Fig. 3.24. but after 20 minutes oxidation, showing nucleation of magnetite.

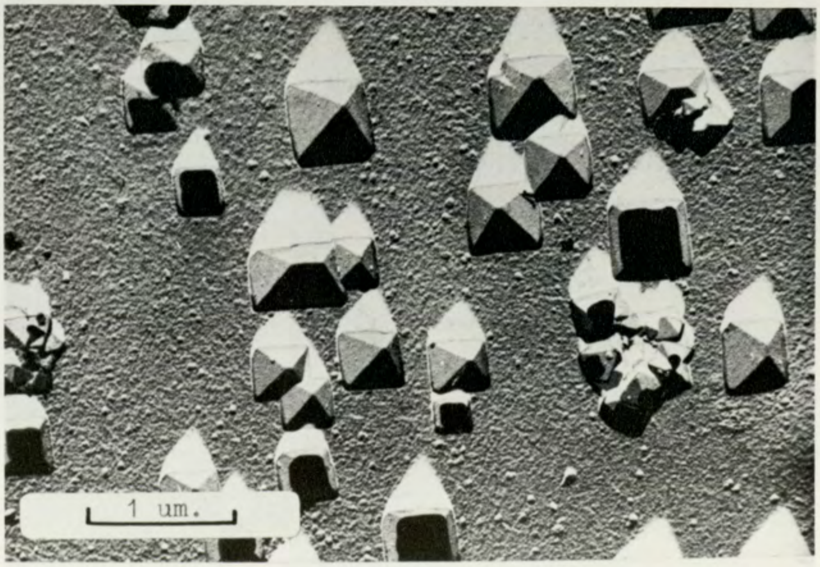

Fig. 3.26. As Fig. 3.24. but after 25 minutes. Outer layer nuclei are well formed, the black squares represent magnetite nuclei still adhering to the carbon replica.

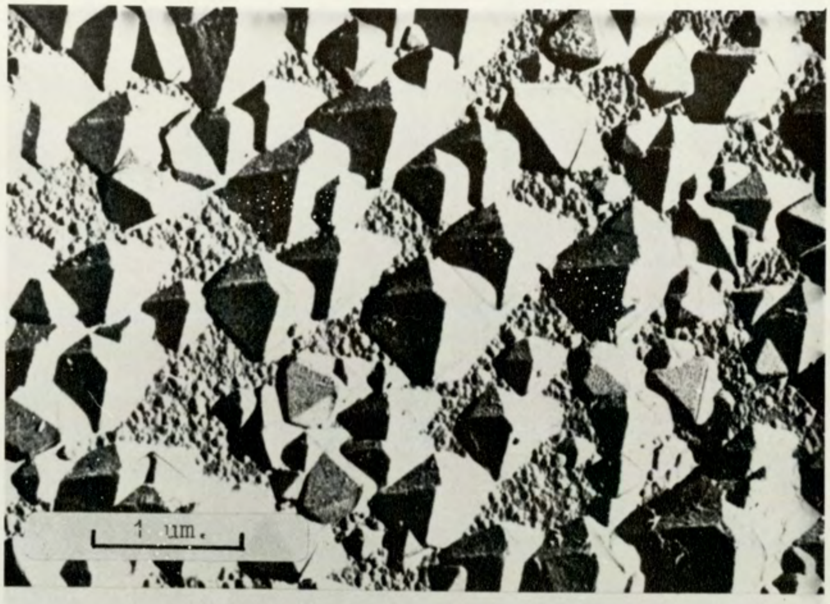

Fig. 3.27. As Fig. 3.24. but after 45 minutes oxidation.

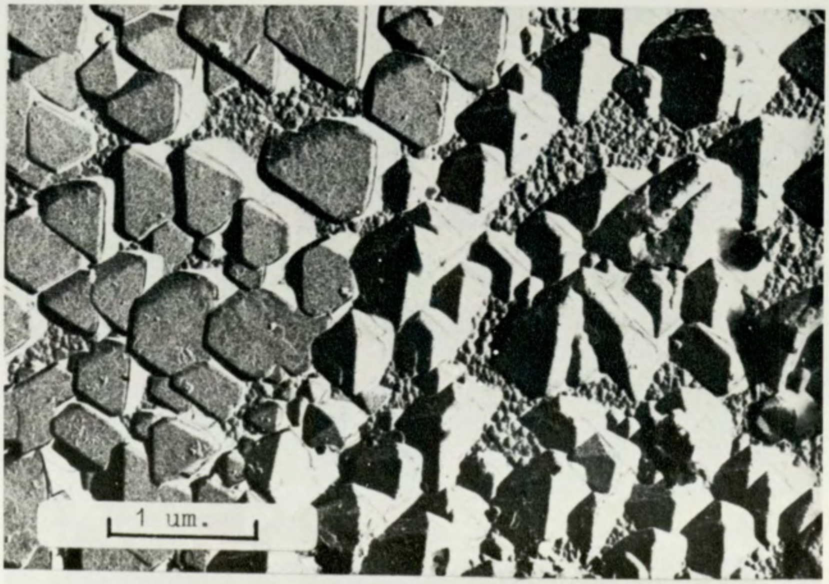

Fig. 3.28. As Fig. 3.24 but after 45 minutes oxidation.

Fig. 3.29. As Fig. 3.24. but showing the structure formed after 4 hours oxidation. The outer layer crystals are well developed.

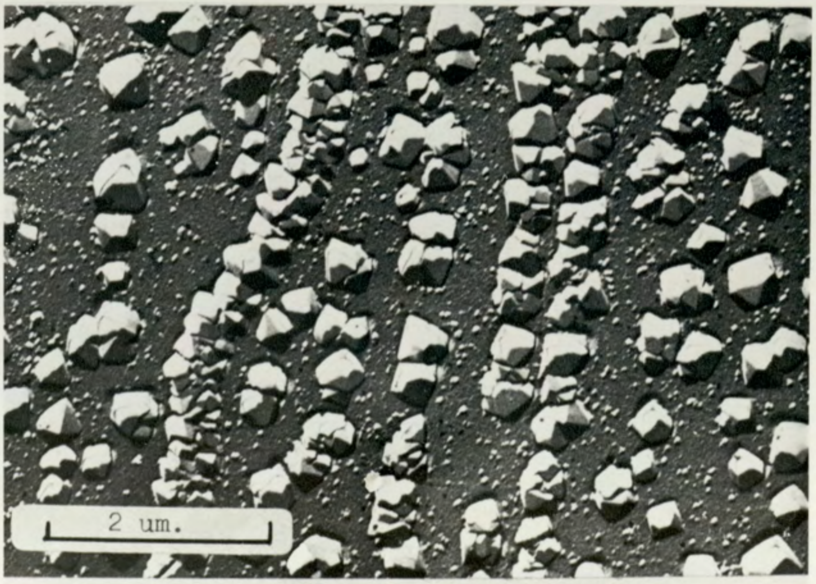

Fig. 3.30. Transmission electron micrograph of a direct carbon replica after 30 minutes oxidation. Outer layer magnetite has nucleated preferentially on surface scratches.

with the highly orientated intermediate layer (compare Fig. 3.19. with Fig. 3.26.).

(2) the large outer crystals showed no evidence of the parallel platelet growth, although the nucleation and the surface at times in excess of 1 hour were very similar (compare Fig. 3.21. with Fig. 3.27.).

A feature of these outer layer crystals is that they could be promoted by local working of the surface. Fig. 3.30. illustrates the preferential growth on a lightly scratched surface; this is a further indication of the sensitivity that the deposition of magnetite has for changes in electrochemical character of a particular site.

Scanning electron microscopy.

Figs. 3.31 to 3.34. illustrate and confirm the stages of growth described previously. Whilst lacking in resolution compared to the electron microscope, the Stereoscan was most useful since the whole of the oxidised sample could be examined. The presence of the intermediate layer as described earlier was confirmed in the S.E.M. study. The chief difference between oxidation in deionized water and sodium hydroxide solutions was the relative slowness for a sample oxidised under the latter conditions to produce large outer crystals, yet the kinetics of oxidation in sodium hydroxide solution are much faster than oxidation in deionized water.

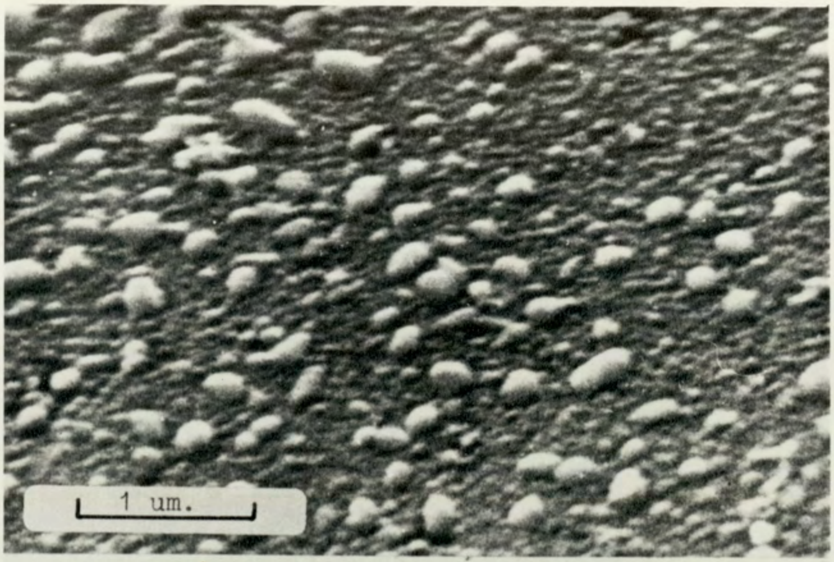

Fig. 3.31. Scanning electron micrograph of an oxidised steel surface (deionized water, 316°C, 25 minutes.)

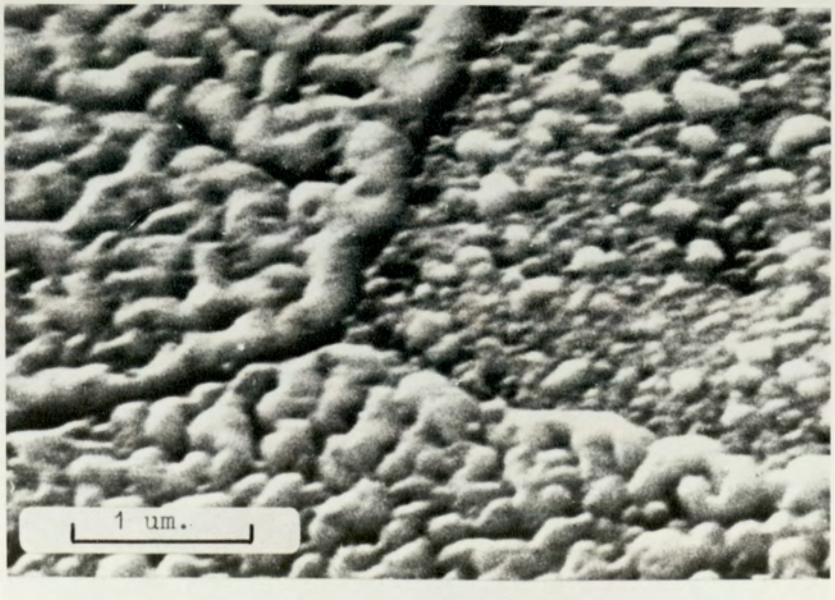

Fig. 3.32. As Fig. 3.31. but after 35 minutes oxidation.

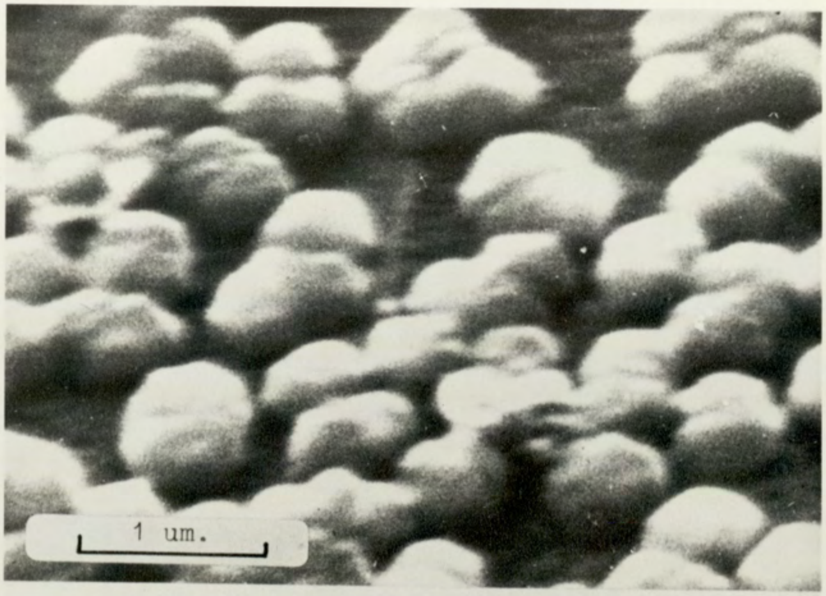

Fig. 3.33. As Fig. 3.31. but after 45 minutes.

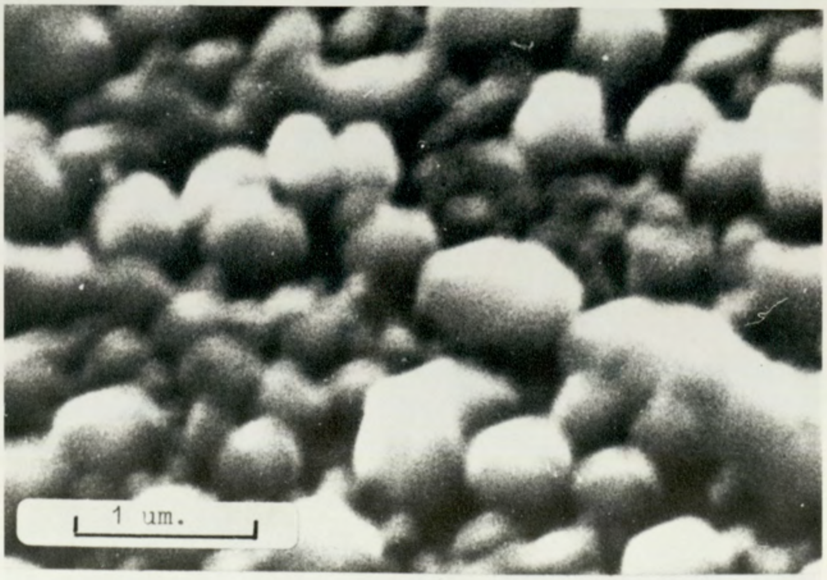

Fig. 3.34. As Fig. 3.31. but after 60 minutes.

CHAPTER IV

RESULTS: GROWTH IN P.T.F.E. LINED PRESSURE VESSELS

4.1. Introduction.

The differences in morphology of bulk oxides formed in both conditioned and P.T.F.E. lined pressure vessels which have been described in Chapter I, are of particular interest to research workers in high temperature oxidation. Relatively small changes in environment can make vast differences to the nature and kinetics governing the oxidation product. For this reason the precise conditions responsible for these changes must be understood for successful steam generator corrosion control.

The first part of this chapter is devoted to a scanning and transmission electron microscopy investigation of the nucleation and growth of oxides on steel test pieces measuring 2.5 x 0.8 x 0.056 cms., grown in P.T.F.E. capsules containing 2.5 mls. of either deionized water or 3.5M sodium hydroxide solution. Explanations of the various structures are made from radioactive tracer surface activity studies and also weight change studies in the second and third part respectively. Finally, all the experimental evidence is used to describe the oxidation by a mathematical rate law that is consistent with self pore blocking.

4.2. Nucleation and growth studies.

4.2.1. 3.5M NaOH.

After 12 minutes oxidation very small oxide particles which had probably formed by the competing processes of solid state diffusion and dissolution were observed on the surface, the majority falling in the size range 500-2000Å (Fig. 4.1.). These particles rapidly merged and became both larger and randomly shaped (Figs. 4.2a. and b.). This lateral growth was in a similar way to that reported by Friggens and Holmes[14] from a transmission electron microscopical investigation of stripped oxides. It certainly seemed that if this was the origin of an inner layer, its porosity would be limited; it still appeared to allow access of some electrolyte to the metal/oxide interface at this stage. After 40 minutes the oxide showed some signs of the formation of magnetite tetrahedra similar to those found on substrates oxidised in conditioned pressure vessels (Fig. 4.3.). An S.E.M. study of the oxide formed under these conditions, confirmed the formation of magnetite tetrahedra after 40 minutes (Fig. 4.4a.). Some of the magnetite crystals grew preferentially (Fig. 4.4b.) in such a way that after 1 hour the surface was well covered with quite large crystals (Fig. 4.5.). These observations were in accord with the weight change data. In the absence of an external cathode (e.g. a magnetite covered pressure vessel wall) all the iron that dissolved in the electrolyte would ultimately return to the specimen surface as magnetite; the most rapid increase in weight occurring over the first 40 minutes. It appeared that both dissolution and the deposition of magnetite from solution occurred simultaneously during

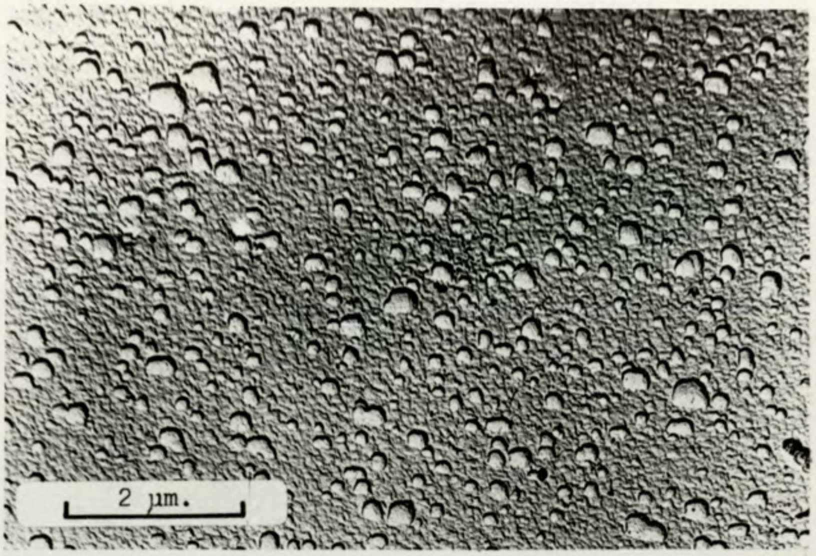

Fig. 4.1. Transmission electron micrograph of a carbon replica of a steel surface oxidised in a P.T.F.E. lined pressure vessel, showing initial magnetite nuclei (3.5M NaOH, 316°C, 12 minutes).

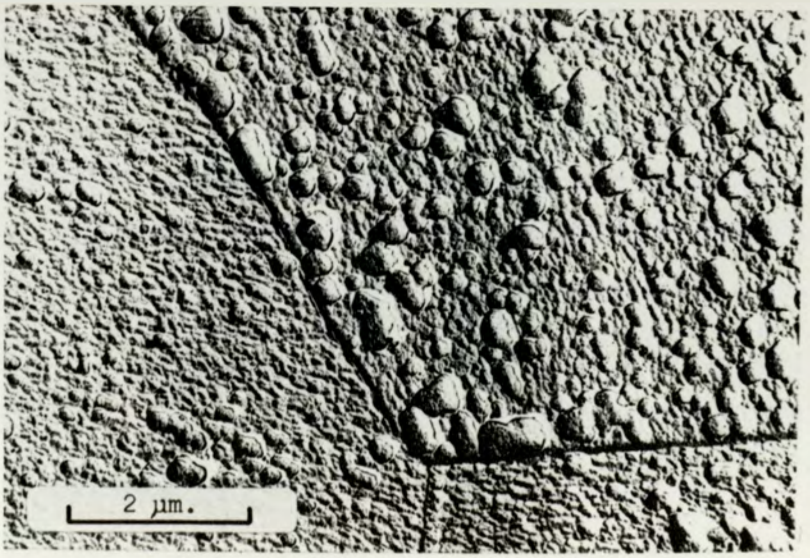

Fig. 4.2a. As Fig. 4.1. but after 30 minutes.

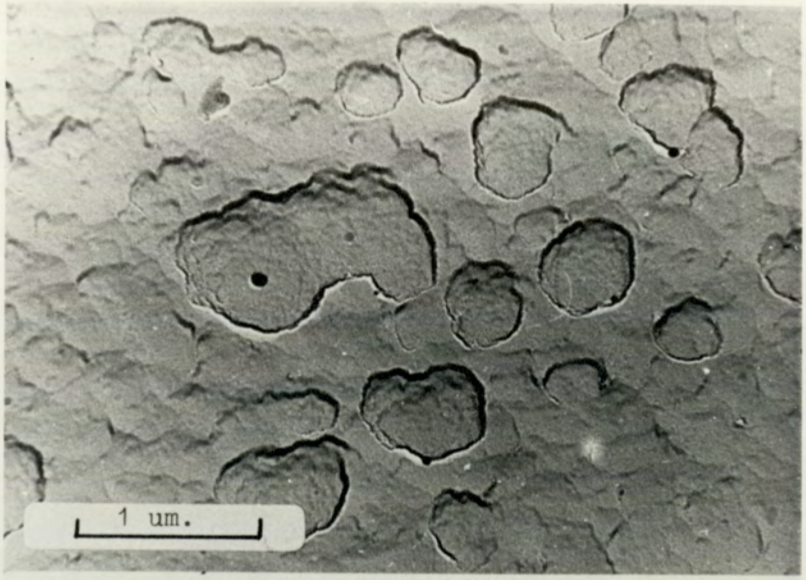

Fig. 4.2b. As Fig. 4.1. but after 30 minutes oxidation, showing pore closure.

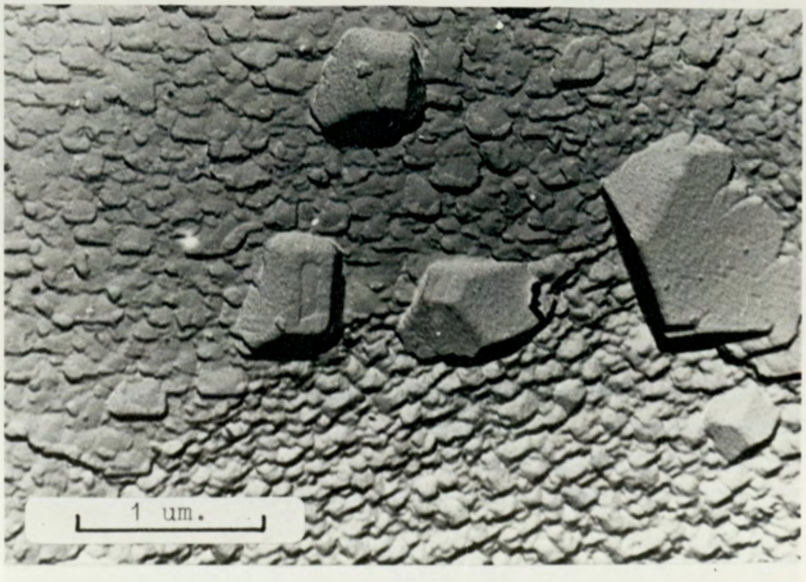

Fig. 4.3. As Fig. 4.1. but after 40 minutes oxidation.

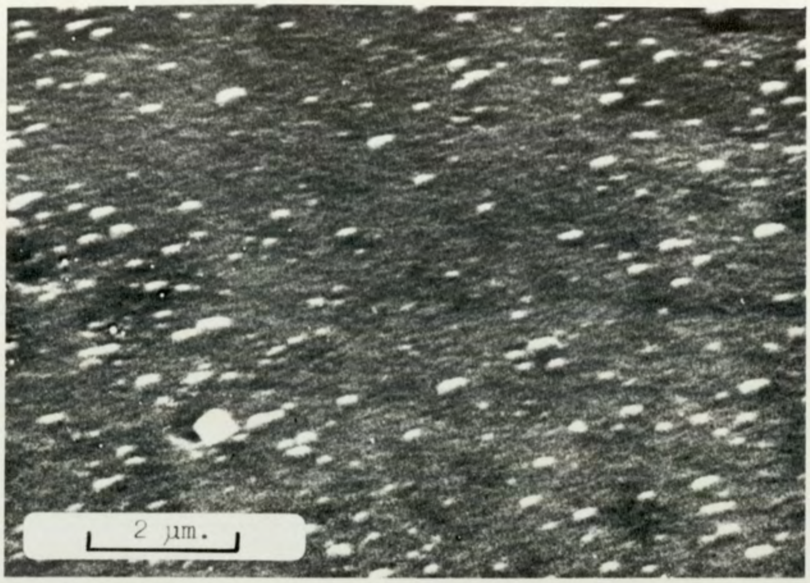

Fig. 4.4a. Showing a scanning electron micrograph of a steel surface oxidised in a P.T.F.E. lined pressure vessel (3.5M NaOH, 316°C, 40 minutes).

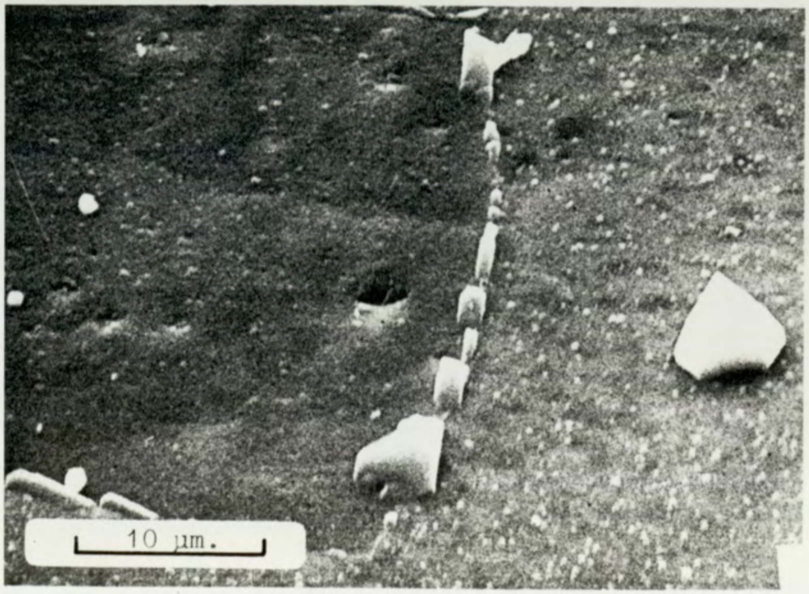

Fig. 4.4b. As Fig. 4.4a.

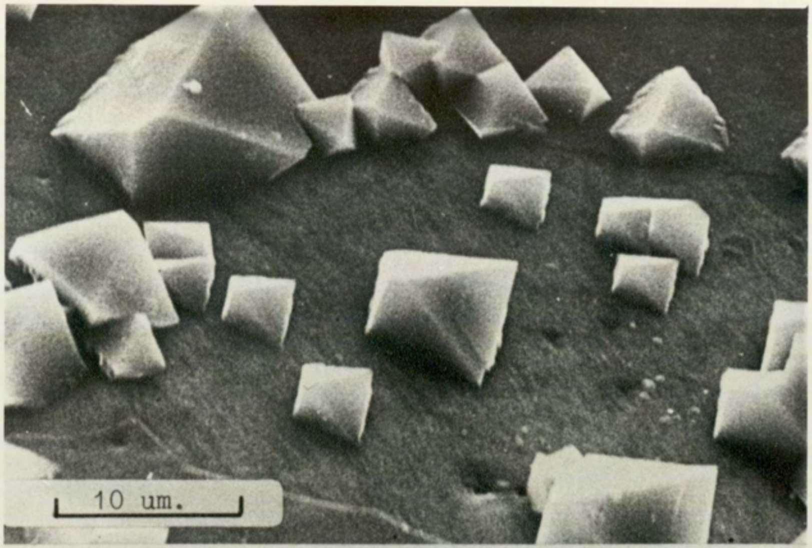

Fig. 4.5. As Fig. 4.4a., but showing well formed magnetite crystals after 60 minutes oxidation.

these early stages. This was readily explained because the amount of iron saturating the solution (90 ppm)[58] would only account for an increase in weight of 0.07 mgm./cm^2. of sample surface. The falling off after 2 hours in the weight change/time plot indicated a retardation of dissolution, or alternatively the mechanism responsible for dissolution. This is illustrated if Fig. 4.6a. is compared with Fig. 1.6b. and Fig. 4.6b. is compared with Fig. 1.2b. This shows that there is very little change in the topography of an oxide grown in a P.T.F.E. lined pressure vessel after 3 hours, yet there is quite a remarkable difference between the surfaces produced under Potter and Mann conditions after these times.

4.2.2. Deionized water.

The initial stages of oxidation were quite similar to those described earlier for iron oxidised in a conditioned pressure vessel containing deionized water. The surface was covered after 12 minutes with magnetite nuclei whose density appeared to be dependent on the metal substrate grain, (Fig. 4.7.). These particles merged together quite readily with increasing time (Fig. 4.8.). After merging had been completed, which took about 35 minutes, very little structural change was observed; in fact, little or no change could be observed between 45 and 60 minutes (Figs. 4.9. and 4.10.) yet in a conditioned pressure vessel large outer crystals would have rapidly formed after this time.

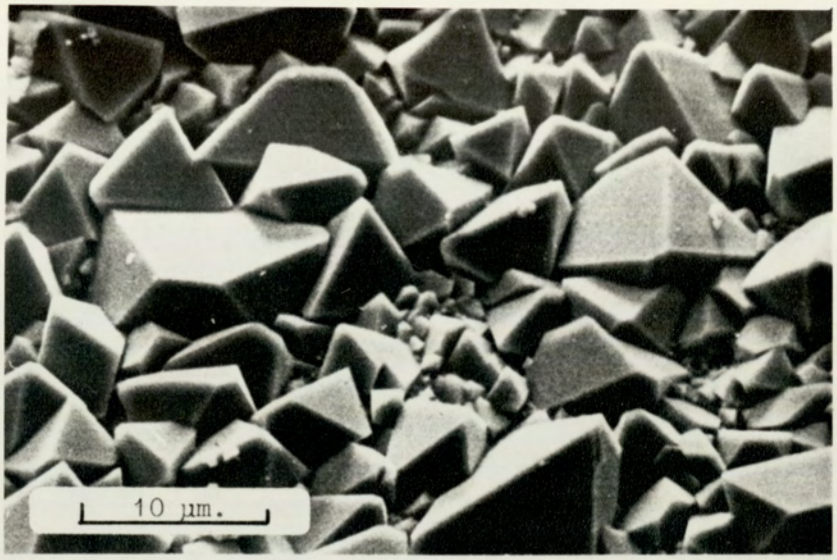

Fig. 4.6a.

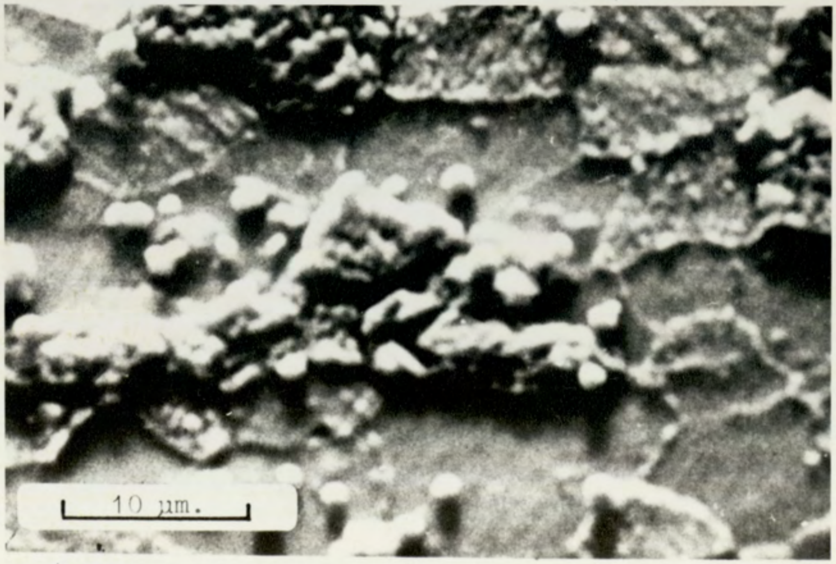

Fig. 4.6b.

Fig. 4.6. showing comparison between the oxide produced after 3 hours in 3.5M NaOH at 316°C in (a) a P.T.F.E. lined capsule and (b) a conditioned pressure vessel.

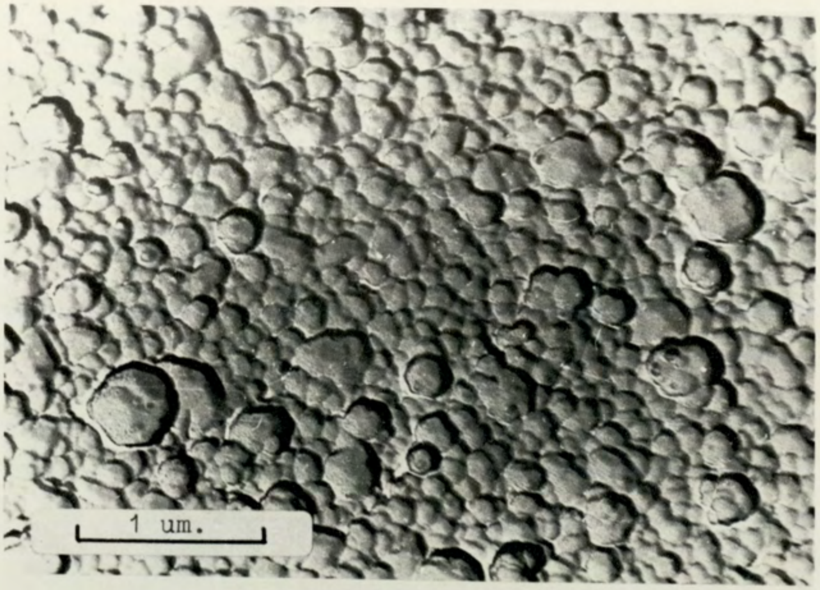

Fig. 4.7. Transmission electron micrograph of a direct carbon replica of steel oxidised in a P.T.F.E. capsule showing initial magnetite nuclei (deionized water, 316°C, 12 minutes).

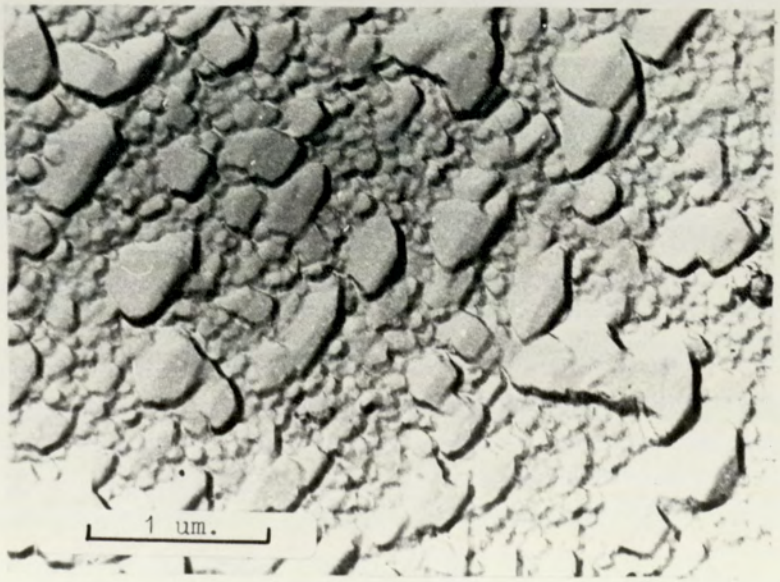

Fig. 4.8. As Fig. 4.7. but after 20 minutes.

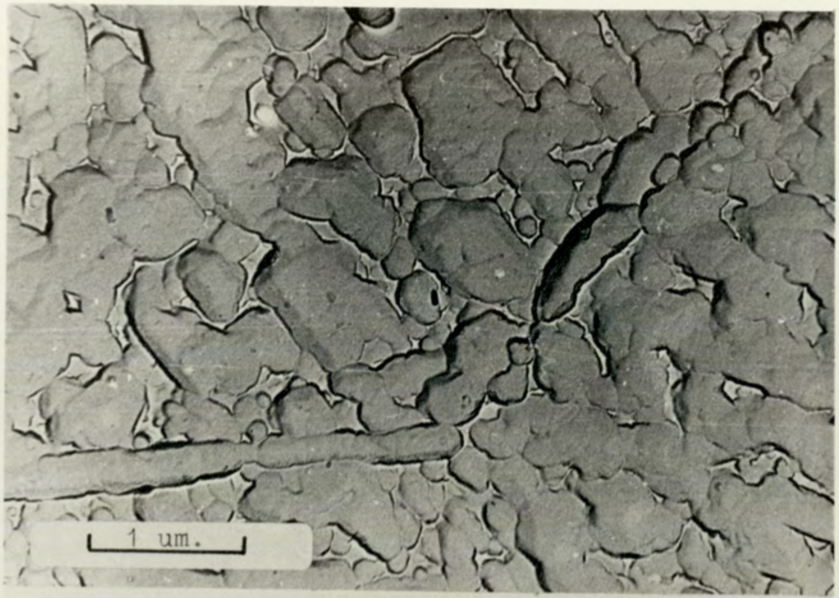

Fig. 4.9. As Fig. 4.7. but after 45 minutes oxidation. Pore closure is taking place.

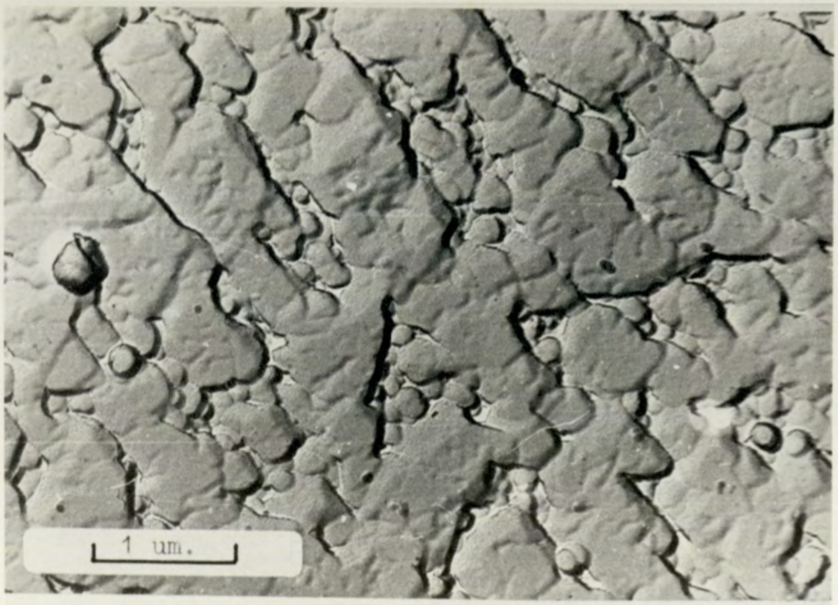

Fig. 4.10. As Fig. 4.7. but after 60 minutes oxidation. No outer layer magnetite nuclei have formed.

Figs. 4.11. and 4.12. are photomicrographs of an S.E.M. study of the early stages of oxidation. Although similarities exist between Potter and Mann and Bloom growths, such as the difference in oxidation behaviour between individual grains (Fig. 4.11.) the most notable difference was the complete absence of large tetrahedra that were characteristic of Potter and Mann oxidation after 50 minutes in deionized water. In this S.E.M. study very little difference in topography was observed from 45 minutes oxidation onwards.

4.3. Radioactive tracer experiments.

4.3.1. Surface activity measurements.

Table V gives data of surface activity measurements with time. When this data was plotted in the same way as for growth

TABLE V

Oxidation of iron in a P.T.F.E. capsule (3.5M NaOH, 316°C).

time (hrs)	$(\frac{I}{Io})$	Z (see p.43)	thickness of magnetite (mgm/cm.^{2})
2	0.984	-	0.25
19	0.926	-	1.11
60	0.910	0.006	1.35
152	0.860	0.022	2.05
317	0.856	0.023	2.15
530	0.856	0.023	2.15

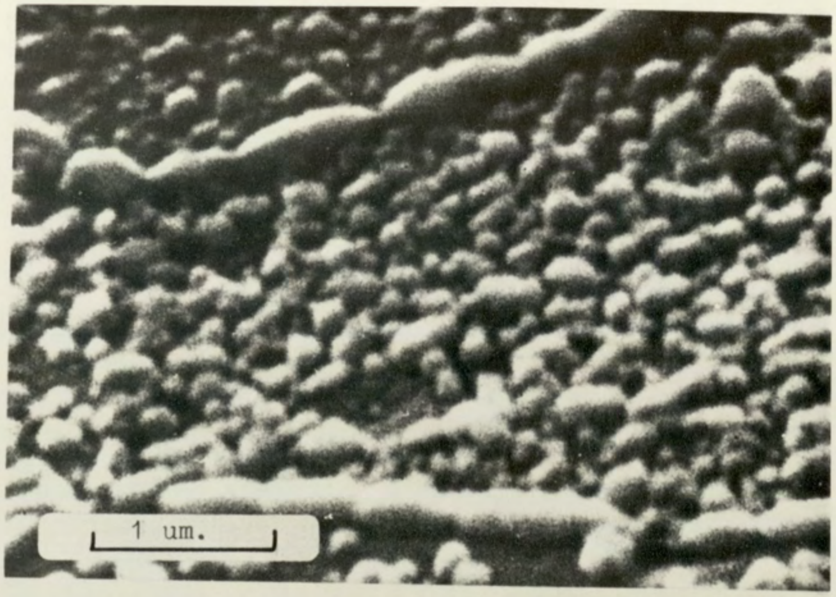

Fig. 4.11. Scanning electron micrograph of steel surface oxidised in a P.T.F.E. lined pressure vessel (deionized water, 316°C, 20 minutes).

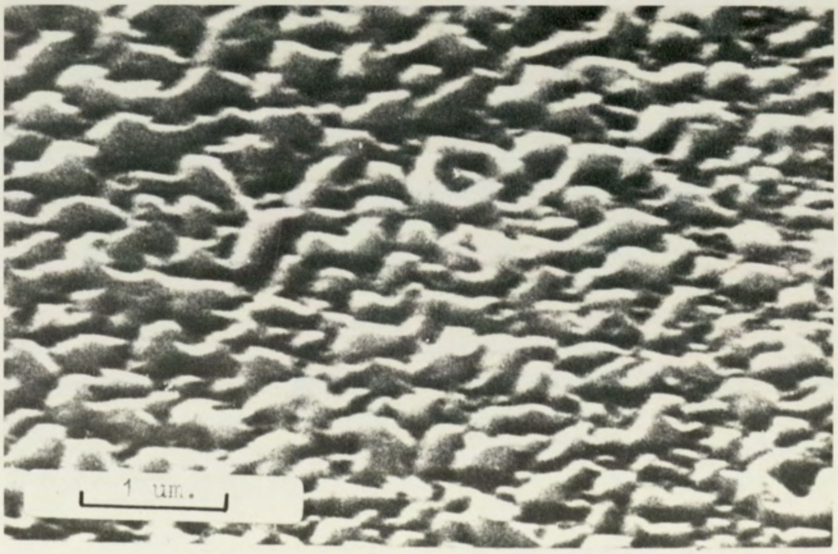

Fig. 4.12. As Fig. 4.11. but after 45 minutes.

under Potter and Mann conditions, linearity was not found. This suggested that some mechanism other than solution transport via solution filled pores was operative. Care is needed in interpreting these results because the active layer was laid down under Potter and Mann conditions involving 90 minutes oxidation. When the sample was later reoxidised in a P.T.F.E. capsule, the specimen had the origins of a two layered oxide, this would certainly modify the oxidation mechanism in that the most rapid decrease in surface activity occurred over the first 100 hours. The weight change data for iron oxidised in P.T.F.E. capsules is shown in Fig. 4.13. and in this instance the most rapid increase occurred over the first 100 minutes. This weight change data agrees with the thickness of oxide observed (4-6 microns) if the increase in weight is assumed to occur from the conversion of iron into magnetite; e.g. after 5 hours oxidation a 4-6 micron layer formed, compared to 6 micron calculated from weight change data after the same time.

4.4. Kinetics and oxidation mechanisms.

Electron microscopy has shown the presence of pores during the early stages of oxidation of iron in a P.T.F.E. capsule; but in contrast to oxidation in a conditioned pressure vessel the pores appear to be short lived, there being little evidence of pores after 45 minutes. A blocking pores process might well explain the differences between the two types of oxidation mechanisms in the

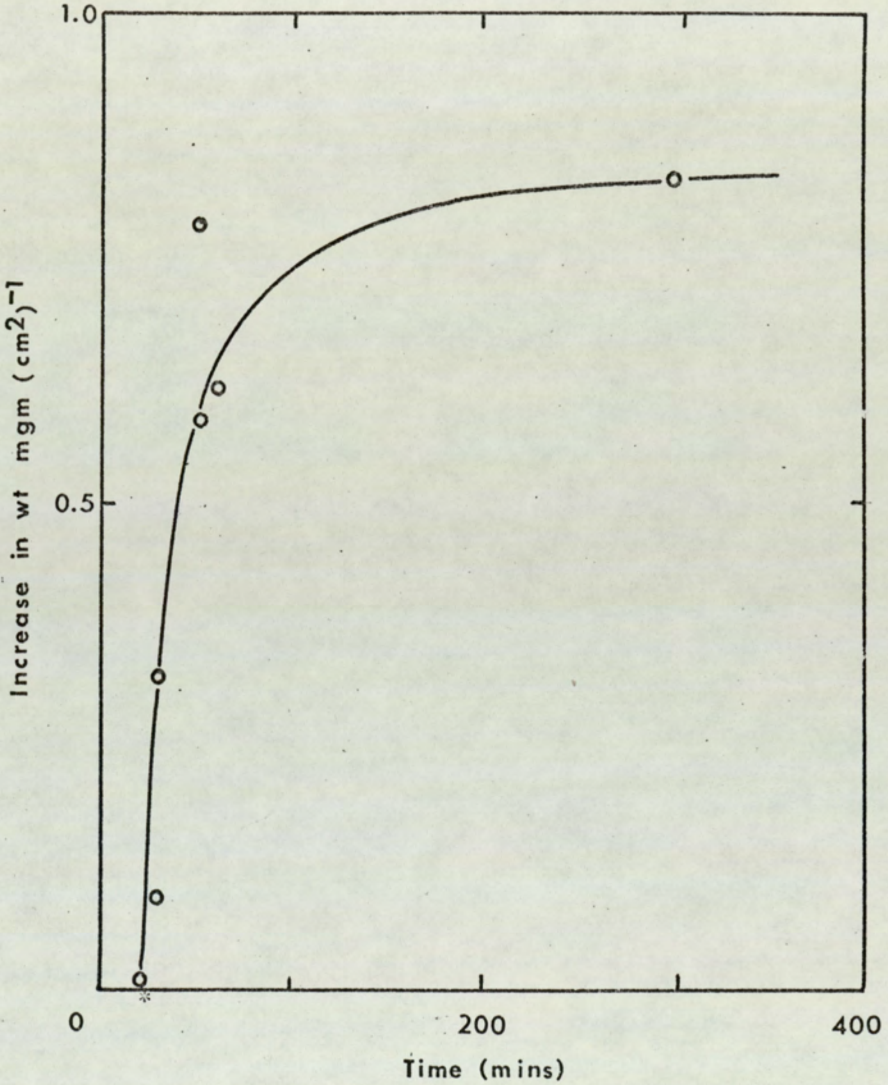

Fig. 4.13. Oxidation of iron in a P.T.F.E. capsule in 3.5M NaOH at 316°C.

* In the mathematical analysis zero time was taken to be the time that the first increase in weight was observed i.e. 20 mins.

early stages. Regarding the surface activity data, it is doubtful that if a sample with a much thicker porous oxide than that formed after 2 hours had been reoxidised in a P.T.F.E. capsule, whether such differences would have been observed.

After the pores had been blocked, oxidation by solid state diffusion would be rate controlling. If the data of Table V is substituted into the formula:-

$$F = e^{Z}\left[1 - \theta(\sqrt{Z})\right]$$

where $Z = \mu^2 Dt$

μ is the absoption coefficient

D is the diffusion coefficient

θ is the Gauss error integral

t is the time

$F = \frac{I}{Io}$ and is the fractional decrease in surface activity

then D can be calculated for different values of time; using times of 60 and 530 hours, D is calculated to be 1.92×10^{-13} $cm^2 . sec^{-1}$ and 8.3×10^{-14} $cm^2 . sec^{-1}$ respectively. These calculated values of D (the diffusion of iron in magnetite) are several orders of magnitude too high from the extrapolated values of Himmel et al[26], but more important the values diminish with increasing time. Clearly D should be constant at a given temperature. This is further evidence of a two stage process, i.e. oxidation by a self blocking pore mechanism followed by solid state diffusion. It would be expected therefore that the experimental values of D derived from surface activity measurements would approach the true value of D for iron diffusion in magnetite at infinity.

4.4.1. Self blocking pores.

The weight change results have been examined over the period 20-300 minutes, and are found to be consistent with the rate law:-

$$y = k_1 (1 - e^{-k_2 t}) \quad ....(I)$$

where y is the increase in weight due to oxidation (mgm./cm.^{2}) after time t (mins.)

and k_1 and k_2 are constants of oxidation.

From equation (I) let $u = (1 - e^{-k_2 t})$

therefore $y = k_1 u$

therefore $\frac{dy}{du} = k_1$

but $u = (1 - e^{-k_2 t})$

therefore $\frac{du}{dt} = -e^{-k_2 t} \times -k_2$

$= k_2 e^{-k_2 t}$

now $\frac{dy}{dt} = \frac{dy}{du} \times \frac{du}{dt}$

therefore $\frac{dy}{dt} = k_1 (k_2 e^{-k_2 t})$

$\frac{dy}{dt}$ is the tangent of the total oxidation/time curve at any point.

Let $\frac{dy}{dt} = n$ then

$$n_1 = k_1 \, (k_2 e^{-k_2 t_1})$$

therefore $$k_1 = \frac{n_1}{(k_2 e^{-k_2 t_1})}$$

and $$n_2 = k_1 \, (k_2 e^{-k_2 t_2})$$

substituting $$n_2 = \frac{n_1}{(k_2 e^{-k_2 t_1})} \, (k_2 e^{-k_2 t_2})$$

taking logs $$\ln n_2 - k_2 t_1 = \ln n_1 - k_2 t_2$$

therefore $$\ln n_2 - \ln n_1 = -k_2 t_2 + k_2 t_1$$

therefore $$-k_2 = \frac{\ln n_2 - \ln n_1}{t_2 - t_1}$$

Substituting values of y and t from Fig. 4.13. k_1 and k_2 are calculated to be 0.83 and 0.042 respectively. The equation describing oxidation between 20-300 minutes is

$$\underline{y = 0.83 \, (1 - e^{-0.042t})}$$

This law which was first suggested by Evans[27] mathematically describes oxidation through pores where the oxidation product is active in blocking the pores with increasing time. The equation is asymptotic such that y never becomes greater than k_1.

In this study there has been evidence from electron microscopy that pores are present initially but appear to become blocked over the period 20-150 minutes. Whilst the increase in weight of the steel sample is due to the formation of magnetite from solution, it is considered that the rate at which this occurs is reflected in the rate and effectiveness of pore closure. There is the further possibility that magnetite crystals formed from solution are instrumental in preventing dissolution.

CHAPTER V

RESULTS: OXIDATION IN CHLORIDE ENVIRONMENTS

5.1. Introduction.

In this study oxidation was carried out in 0.1M $FeCl_2$ + 0.001M $NiCl_2$ solutions, these environments are known to produce rapid rates of oxidation. The type of oxide produced is considered by some workers[11,58] to be analagous to the oxide formed in boilers suffering on-load corrosion; for this reason its study is extremely important. Fig. 5.1. shows a cross section of an oxide formed after 40 hours. The average thickness in uniform areas was about 100 microns. On each cross section there were many areas showing an oxide of a non uniform character. These areas were either heavily pitted with hemispherical pits up to three times deeper than the uniform oxide (Fig. 5.2.) or alternatively heavily spalled as in Fig. 5.3. In some of the heavily spalled areas voids were left whose widths were equal to the adjacent layers of oxide (Fig. 5.4.). There appeared to be a high degree of blending of both crystalline and porous oxide.

A study of nucleation and growth of the oxide was made by scanning and transmission electron microscopy. The results from the S.E.M. were much more informative than the study by replicas, since it was possible to observe at all times the growing pitted and spalled areas, and obtain information on the effect of nickel. The carbon replicas did not cover these areas very well and replica damage invariably occurred at these sites. However, they did

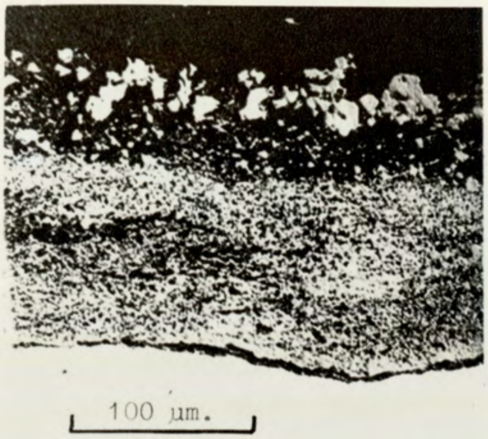

Fig. 5.1.

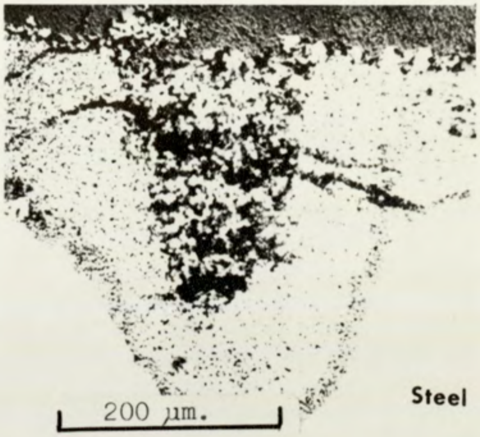

Fig. 5.2.

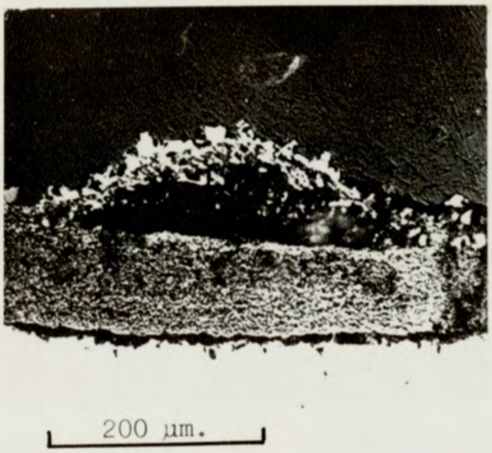

Fig. 5.3.

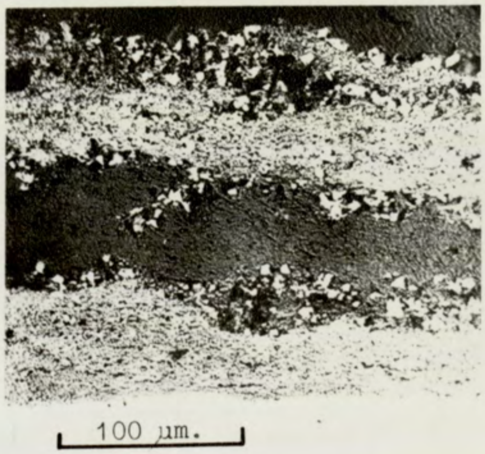

Fig. 5.4.

Fig. 5.1. Cross section of steel after oxidation in 0.1M $FeCl_2$ + 0.001M $NiCl_2$ (316°C, 40 hours).

Fig. 5.2. As Fig. 5.1. but showing a pitted region.

Fig. 5.3. As Fig. 5.1. but showing non uniform oxide growth.

Fig. 5.4. As Fig. 5.1.

illustrate the mode of uniform growth.

Experiments to determine the redistribution of active iron tracers after oxidation in these ferrous chloride environments are described; the results are used to discuss the effects of high ferrous ion environments on iron transport.

5.2. Electron microscopy.

Almost immediately after placing an iron sample into a ferrous chloride/nickel chloride environment the nickel in solution was deposited onto the sample which lost an equivalent amount of iron to the solution. The volume to surface area in the pressure vessel being approximately 1 ml:1 cm^2. would result in a layer of nickel 0.66 microns thick (if all the nickel was uniformly deposited onto the iron surface). Fig. 5.5. shows the surface after 12 minutes oxidation, it is seen to be covered with a finely divided layer of nickel. Even at this stage crystallites of magnetite could be seen distributed quite randomly over the surface. It was not found possible to resolve the very small magnetite nuclei because of the interference from the nickel deposit. The layer of nickel that was present between the metal substrate and the growing oxide must have been responsible in eliminating the epitaxy observed in other growths. Figs. 5.6. - 5.8. show the structure after 20, 30 and 60 minutes respectively. The stages of growth were quite similar to those found in sodium hydroxide environments although the intermediate

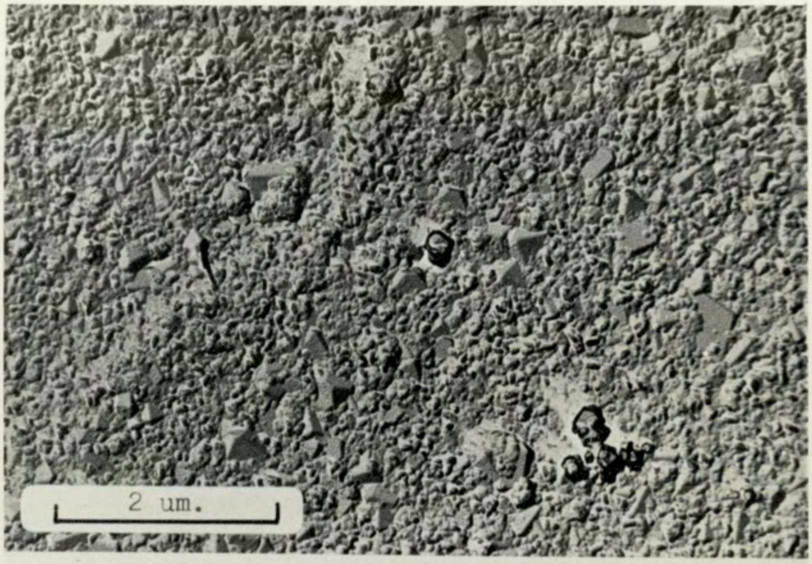

Fig. 5.5. Transmission electron micrograph of a direct carbon replica of steel oxidised in 0.1M $FeCl_2$ + 0.001M $NiCl_2$ (316°C, 12 minutes).

Fig. 5.6. As Fig. 5.5. but after 20 minutes oxidation.

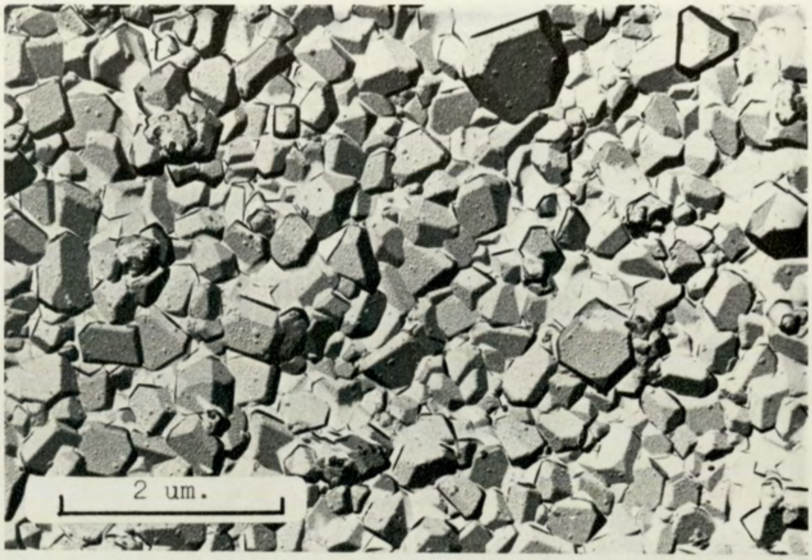

Fig. 5.7. As Fig. 5.5. after 30 minutes oxidation.

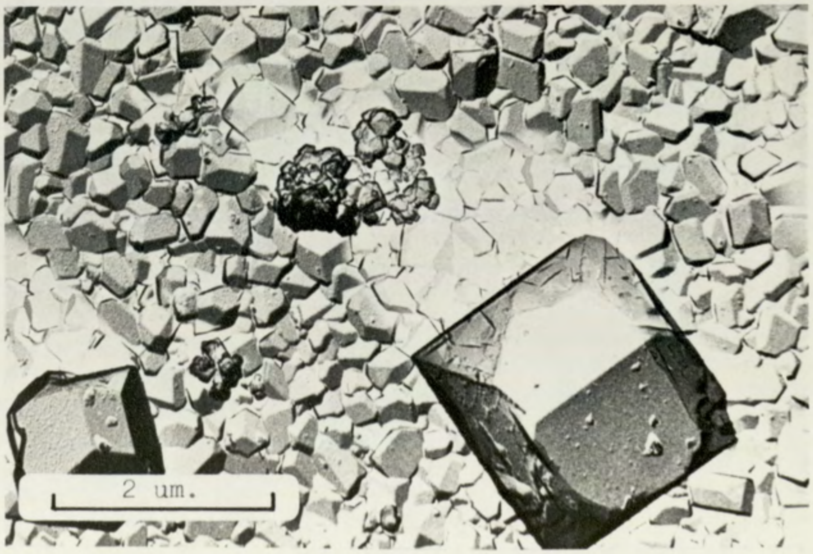

Fig. 5.8. As Fig. 5.5. but after 60 minutes oxidation.

layer of magnetite tetrahedra appeared to be very much looser in packing and therefore more permeable to electrolytes.

An S.E.M. study of the same specimens was very much more informative since a detailed study could be made of areas supporting non uniform growth.

It is evident that initiation of pits occurred very early on in the oxide growth history. Fig. 5.9. illustrates the surface after 12 minutes oxidation. The surface had the appearance of a finely divided structure and probably consisted of a mixed layer of nickel and magnetite nuclei. The physical properties of the nickel deposit are expected to be very poor indeed, and it would not be protective in its own right. It was also expected that the electrolyte had a relatively easy access to the metal beneath the deposit. After 20 minutes oxidation cracks had become apparent at many sites in the mixed oxide/nickel layer (Fig. 5.10.). These cracks occurred at defects in the metal and led to discontinuities in the nickel layer; the oxidation process itself also enhanced the cracking once it had started. Furthermore, electrochemical processes occurring at or adjacent to these sites were aggravated in a high chloride iron environment. The exposed iron underneath the pit would be ionized according to $Fe \rightarrow Fe^{++} + 2e$ and under these conditions the corrosion would be under cathodic control, i.e. the rate depending on the area of nickel sustaining the cathodic

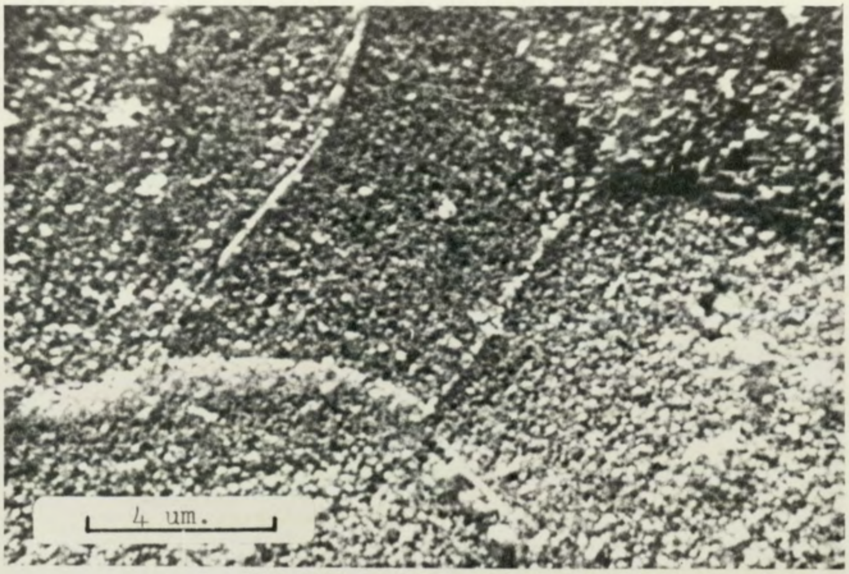

Fig. 5.9. Scanning electron micrograph of an oxidised steel surface (0.1M $FeCl_2$ + 0.001M $NiCl_2$, 316°C, 12 minutes).

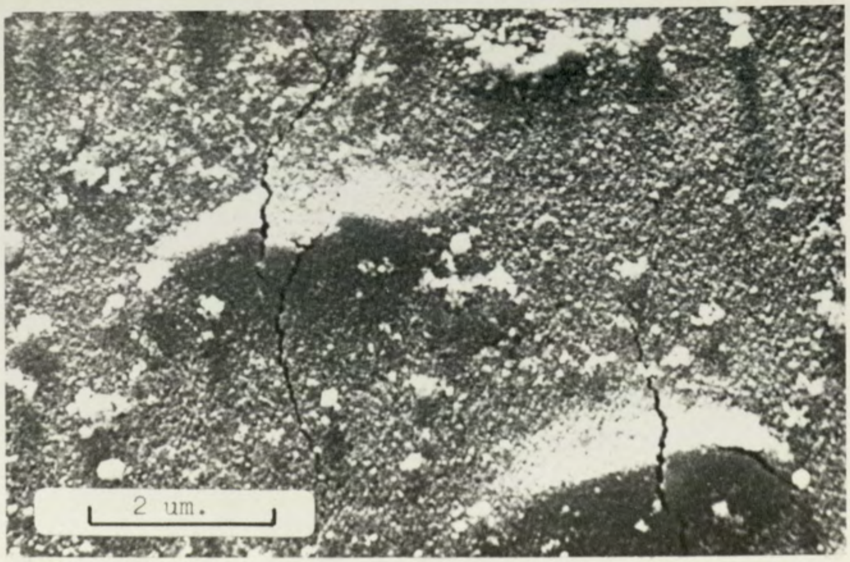

Fig. 5.10. As Fig. 5.9. but after 20 minutes showing defects in nickel/oxide layer.

reaction:-

$$2H^+ + 2e \rightarrow H_2$$

In Fig. 5.11. the oxide surface is seen to be covered with humps, these are thought to be associated with the defects in the nickel layer described earlier, they soon became covered with a layer of oxide. After oxidation times in excess of 1 hour, some of these humps were surrounded by a ring of very coarse magnetite crystals (Fig. 5.11.); the surface as a whole however had many humps present that were not surrounded with these crystals. The ones that were surrounded eventually opened up (see Fig. 5.12.). On examination of the hole (Fig. 5.13.) the base was observed to be quite thickly covered with magnetite crystals; this would represent the banded structure seen in the cross sections. Even after 40 hours oxidation there were still only a few humps that had actually opened up (Figs. 5.14a and b.) but by now the whole of the surface was covered thickly with magnetite crystals. Examination of the underside of a small piece of oxide removed from a hole (Figs. 5.15a and b.) showed a mixed crystalline porous structure.

5.3. Radioactive tracer experiments.

5.3.1. Distribution of iron within the experimental system.

Fig. 5.16. illustrates the relationship between activity on the specimen, pressure vessel and electrolyte for different times of oxidation. The first readings that were taken indicated that

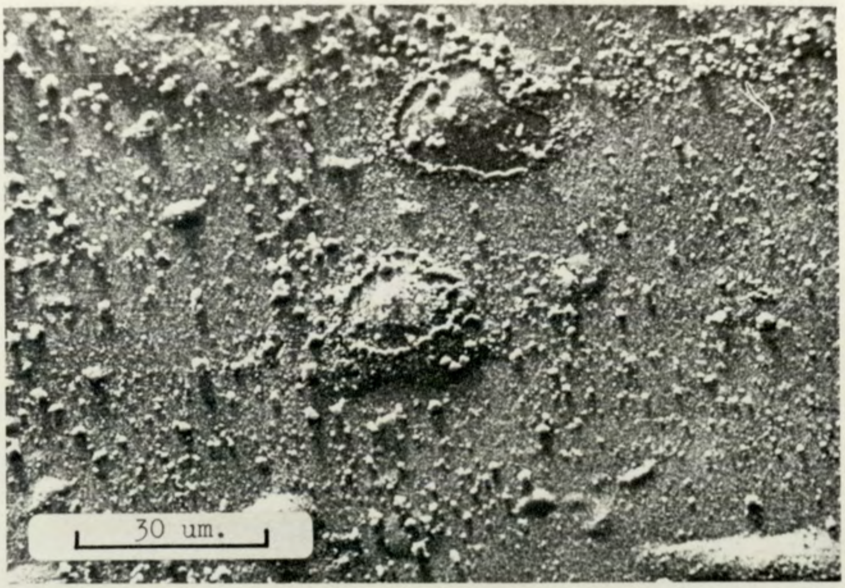

Fig. 5.11. Showing oxide structure after 60 minutes oxidation in 0.1M $FeCl_2$ + 0.001M $NiCl_2$ at 316°C.

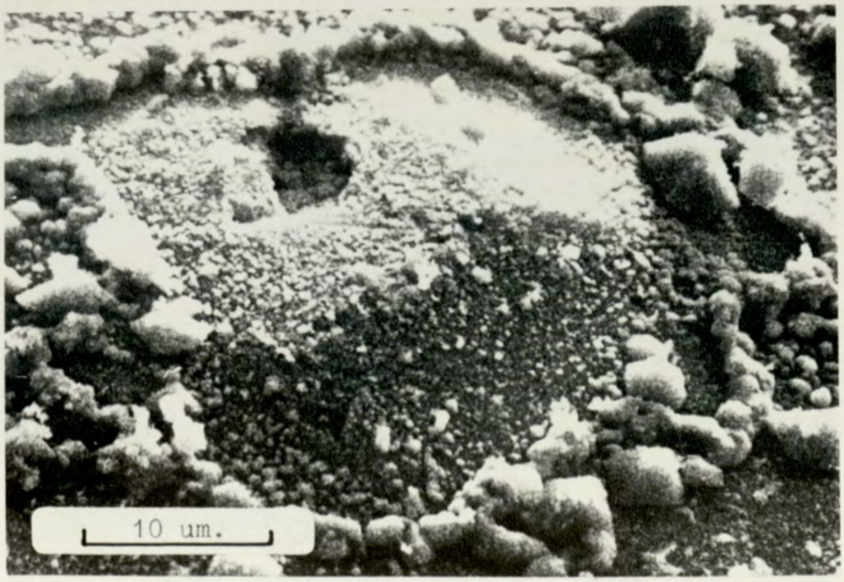

Fig. 5.12. As Fig. 5.11. but illustrating a different area.

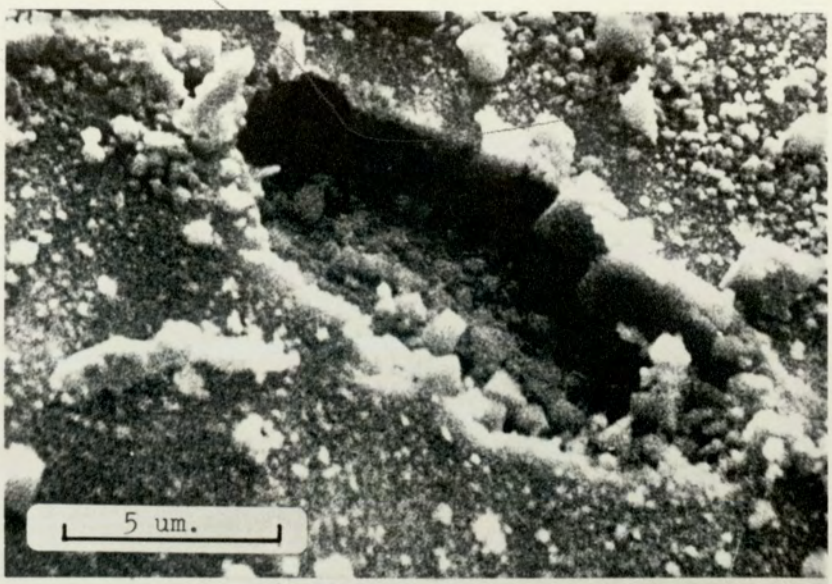

Fig. 5.13. As Fig. 5.11. but illustrating a different area.

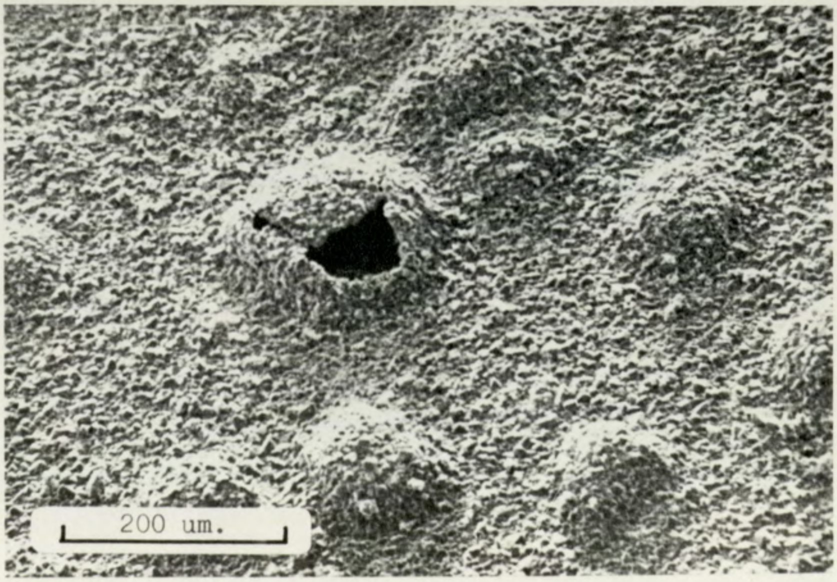

Fig. 5.14a. Oxide structure after 40 hours oxidation in 0.1M $FeCl_2$ + 0.001M $NiCl_2$ at 316°C.

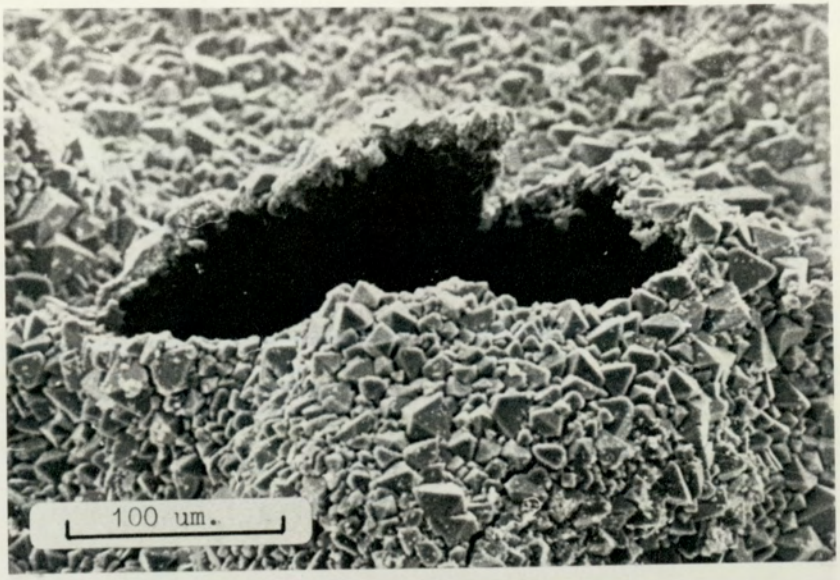

Fig. 5.14b. As Fig. 5.14a.

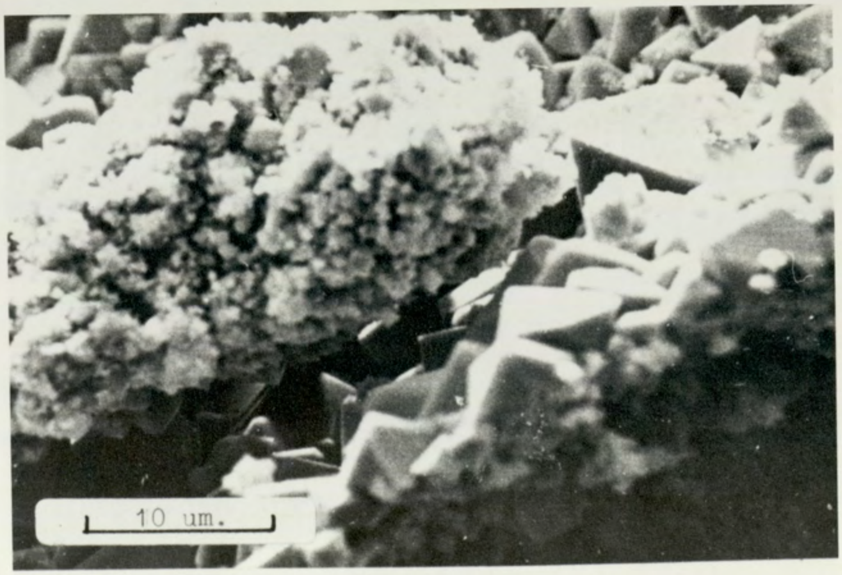

Fig. 5.15a. As Fig. 5.14a. showing structure of oxide removed from a blister.

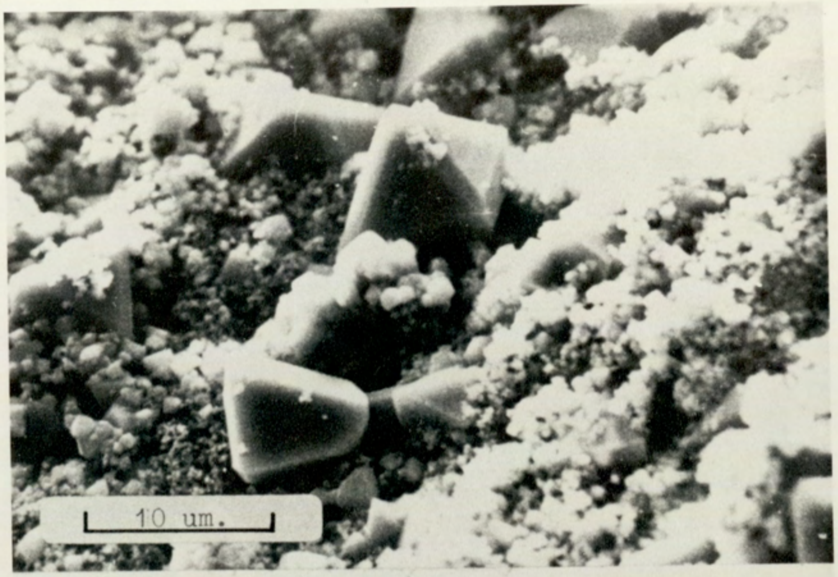

Fig. 5.15b. As Fig. 5.15a.

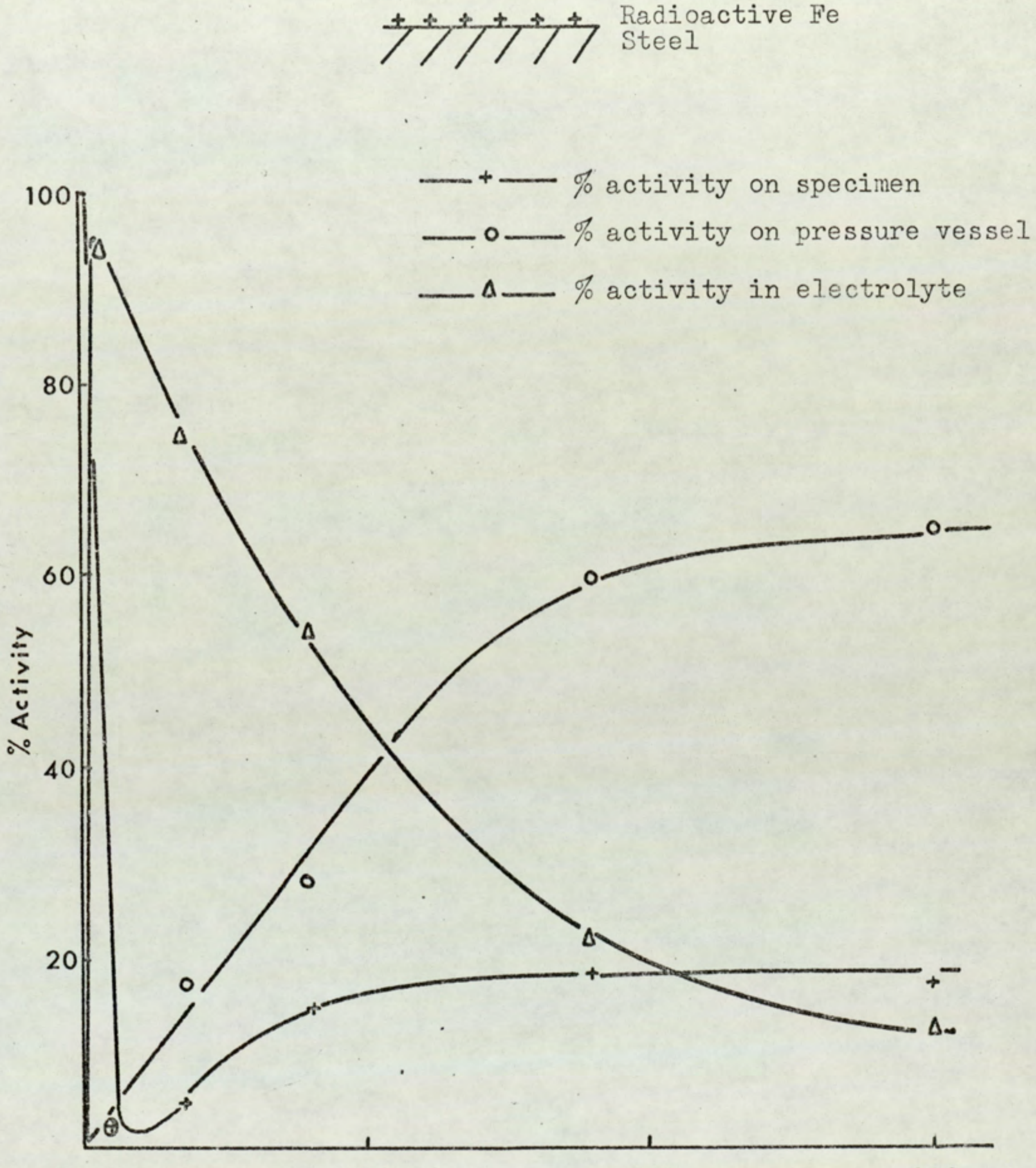

Fig. 5.16. The redistribution of an active Fe^{59} tracer after oxidation in 0.1M $FeCl_2$ + 0.001M $NiCl_2$ at 316°C.

there had been almost immediate total ion exchange between the nickel in solution and an equivalent amount of iron from the surface of the sample. Within 5 minutes the activity of the sample had dropped from 100% to 3% whilst the electrolyte had increased its activity from 0% to 94%, the balance being retained by the internal surfaces of the pressure vessel walls. With increasing oxidation times the activities of both the sample and the pressure vessel increased at the expense of the activity in the electrolyte, until fairly constant conditions were achieved after 280 minutes. The ratios at this point were 20% electrolyte, 20% sample and the balance pressure vessel walls.

Initially the electrolyte contained 0.1M Fe^{++}. If it is assumed that both the pressure vessel wall and the specimen corrode at the same rate, then it would be possible to predict the reduction in activity of the electrolyte. If it is further assumed:-

(1) there is free and constant exchange of ions between the solution, pressure vessel wall , and specimen

(2) the level of ferrous ions in the pressure vessel remain constant then change in activity,

$$\frac{dA}{dt} = k_1 A \qquad \text{.........} \ (I)$$

where k_1 is a constant of ion exchange

and A is activity after time t.

Let $A = 1$ in equation (I)

then $k_1 = (-\frac{1}{A})(\frac{dA}{dt})$ this is the form of a first order reaction.

Let a be the initial activity of A, and x be the decrease in activity of A due to ionic exchange and dilution in the pressure vessel up to time t.

therefore $A = (a - x)$ at time t

therefore $-\frac{dA}{dt} = -\frac{d}{dt}(a - x) = \frac{dx}{dt}$

equation (I) becomes

$$\frac{dx}{dt} = k_1(a - x)$$

when $t = 0$. i.e. at the start of oxidation, $x = 0$ and when $t = t$, $x = x$

integrating to limits $$\int_{x=0}^{x=x} \frac{dx}{(a - x)} = \int_{t=0}^{t=t} k_1 dt$$

therefore $$\Big[-\ln(a - x)\Big]_{x=0}^{x=x} = \Big[k_1 t\Big]_{t=0}^{t=t}$$

therefore $$\ln \frac{a}{(a - x)} = k_1 t \quad ....(II)$$

rearranging equation (II) in order to test graphically

then $$\ln(a - x) = -k_1 t + \ln a$$

or $$\log_{10}(a - x) = \left(\frac{-k_1}{2.303}\right)t + \log_{10} a \quad .....(III)$$

Equation (III) is the equation of a straight line when $\log_{10}(a - x)$ is plotted against t.

Fig. 5.17. shows this plot from data derived from Fig. 5.16. the relationship is in fact found to be linear. Statistical regression analysis of the results show the degree of fit to be extremely good with a product moment correlation coefficient[55] of 0.99. The constant is found to be 0.0030.

This result suggested that there is virtually perfect ion exchange in the electrolyte, providing of course the total ferrous ion content stayed constant*. This would seem reasonable in view of the high chloride ion content present. The concentration of Fe^{++} ions was not determined after oxidation, such determinations would be most useful in assessing the validity of these proposals.

5.3.2. Surface activity experiments.

Decrease in surface activity experiments were performed on samples that had been activated by oxidising for 2 hours in an Fe^{55} environment. This activation treatment was followed by a further treatment involving a 200 hours oxidation in sodium hydroxide solution; this was necessary to reduce to a minimum any solution/magnetite exchange that might occur in a high chloride environment.

---

* The molar concentration refers to the solution added to the pressure vessel at room temperature. The molality could change at the test temperature by expansion and saturation vapour effects.

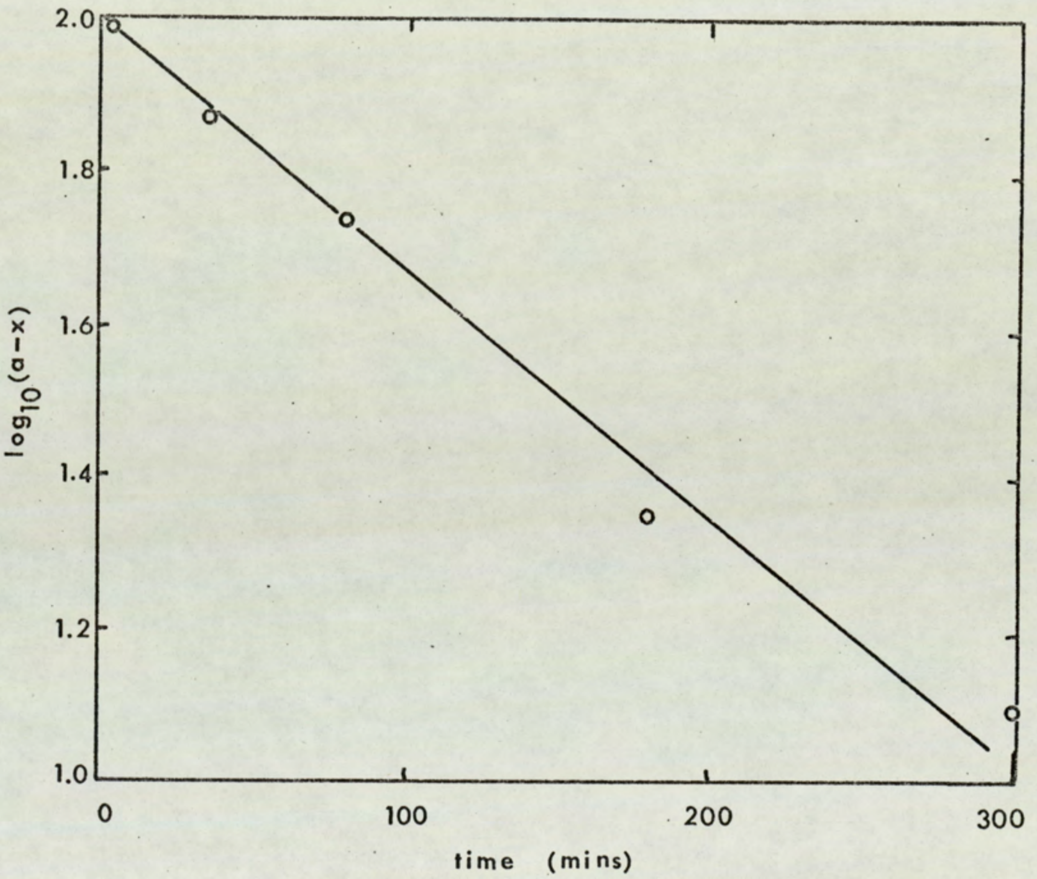

Fig. 5.17. Plot of $\log_{10}$ (activity in electrolyte) with time for iron oxidised in 0.1M $FeCl_2$ + 0.001M $NiCl_2$ solution at 316°C.

It has been shown previously[60] that an initial duplex oxide does not affect the oxidation performance in a ferrous chloride/nickel chloride environment.

The test pieces would therefore have the active layer at the interface between the inner and outer layer oxide. Duplicate test pieces were used, withdrawals being made at approximately 15 hour intervals. Fig. 5.18. shows the change in surface activity with time; linearity was obtained if log(activity) was plotted against time. Providing that there was no magnetite dissolution, a linear build up of magnetite with time at the solution/oxide interface is inferred. These results confirm the previous radioactive experiments and microscopy of the oxide grown in these environments. After 50 hours, spalling of the oxide occurred to such an extent that activity measurements after this time were invalidated.

The decrease in surface activity measurements implied a further 10 microns layer on top of the existing oxide in a period of 50 hours. In view of the periodic loss of adhesion exhibited by oxides formed in chloride environments, caution must be exercised before any categorical explanations are made.

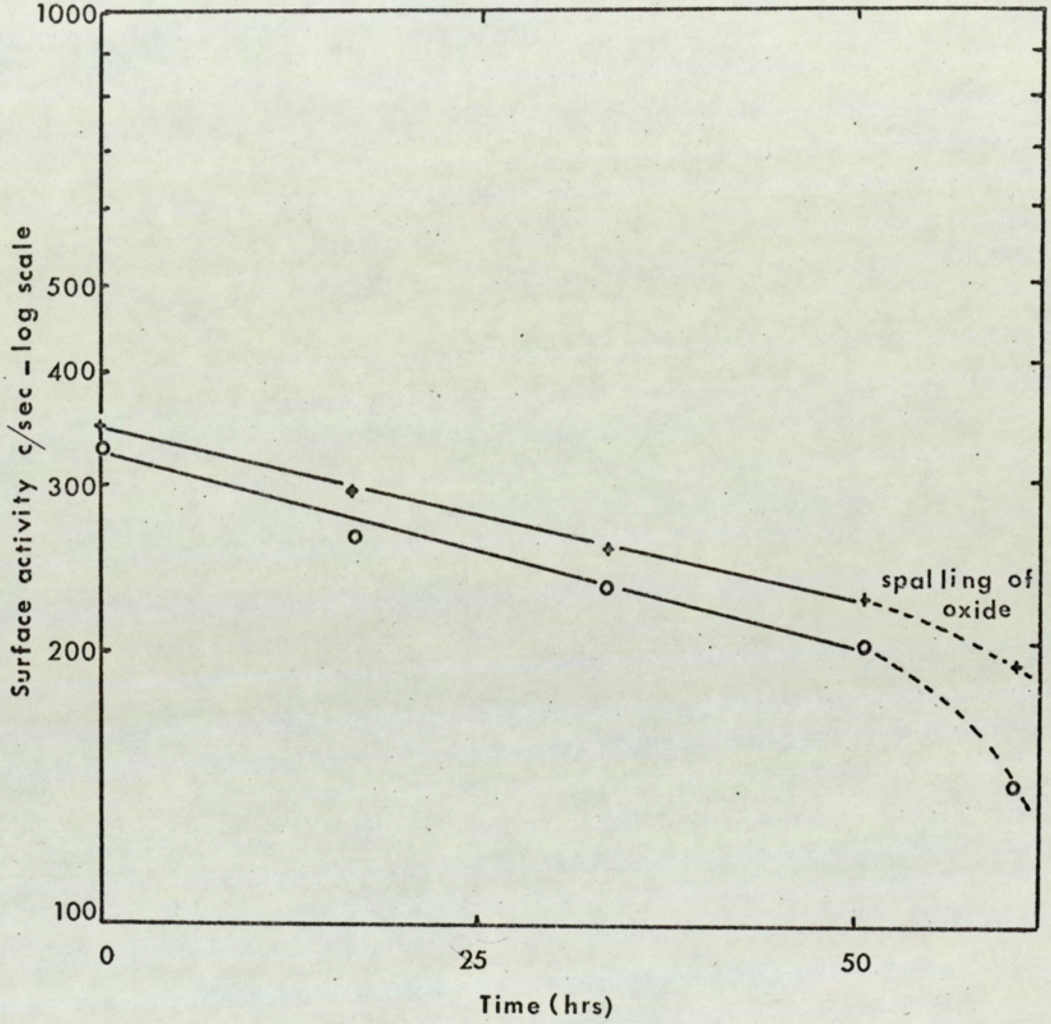

Fig. 5.18. Surface activity data for iron oxidised in a ferrous chloride/nickel chloride environment at 316°C.

CHAPTER VI

RESULTS: OXIDATION OF IRON ELECTRODEPOSITS

6.1. Introduction.

During some ancillary work on the oxidation of electrodeposited iron, it was noticed that there was a departure from the normal pattern regarding the morphology of the outer layer. A short series of experiments were undertaken to resolve these differences and thereby increase our knowledge on the factors affecting oxidation.

Two electroplating baths were used; they are fully described in Chapter II, and for the present purpose they may be differentiated as (a) ferrous ammonium sulphate bath and (b) ferrous chloride bath. The deposits were plated onto mild steel substrates to a nominal thickness of 12 microns. (The steel was from the same stock used in all the other oxidation experiments.

6.2. Properties of electrodeposits.

The deposit from the ferrous chloride bath was quite ductile and had a much larger grain size than the brittle sulphate deposit. Figs. 6.1a and b. which show scanning and transmission electron micrographs of both of these deposits illustrate these differences.

X-ray studies of the two electrodeposits indicated a fibre texture in both cases; Fig. 6.2. shows radial scans of the two deposits and it is seen that although both have a (111) texture, the texture of the deposit from the sulphate bath is much stronger.

Fig. 6.1a.

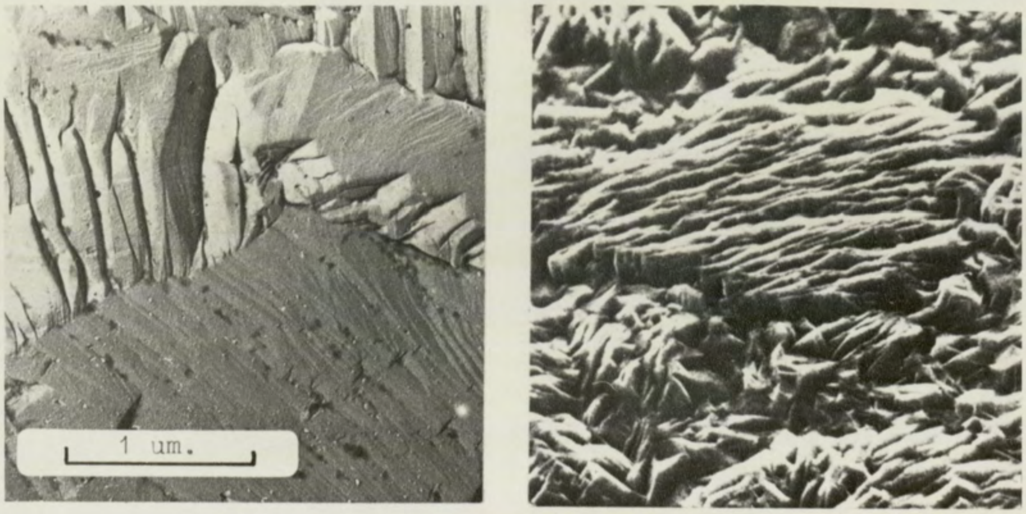

Fig. 6.1b.

Fig. 6.1a. showing electron micrograph (LHS) and an S.E.M. (RHS) of iron electrodeposited from ammonium ferrous sulphate solution.

Fig. 6.1b. showing electron micrograph (LHS) and an S.E.M. of iron electrodeposited from ferrous chloride solution.

Fig. 6.2

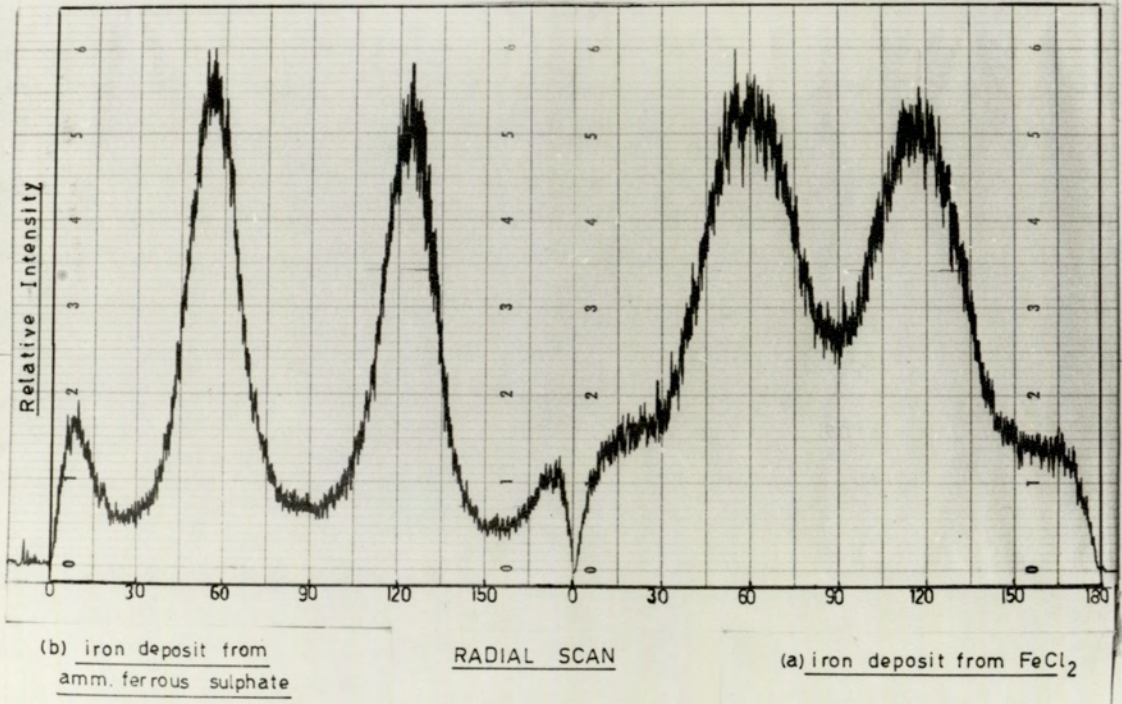

(b) iron deposit from amm. ferrous sulphate

(a) iron deposit from $FeCl_2$

6.3. Oxidation of iron deposits.

All the samples oxidised were in the form of strips 3 cm. x 1 cm. Oxidation was carried out in 3.5M NaOH at 316°C using a surface area to volume of 1 cm^2./ml.

It was noticed that if a mild steel sample plated one side was then oxidised, the plated side invariably grew a single porous layered oxide; a normal two layered oxide formed on the non plated side (Fig. 6.3.). If however both sides were plated, a two layered oxide formed on both sides (Fig. 6.4.). Weight change data for the latter case are shown plotted against time in Fig. 6.5. They confirm that the rate of oxidation is quite similar to that of steel.

Samples were prepared with an interface between the plated and non plated regions. This was achieved by stopping off one half of the iron with "Lacomit"; after plating the "Lacomit" was stripped off and the samples were washed with several changes of acetone. Figs. 6.6a. and b. show an S.E.M. and a corresponding cross section of an oxidised ferrous chloride deposit interface. The deposit side of the interface is covered with a thin layer of small magnetite crystals, whilst the iron side has oxidised quite normally and quite large crystals are in evidence; the inner layer oxide in both cases is quite similar. Figs. 6.7a and b. are corresponding micrographs of an iron/iron sulphate deposit

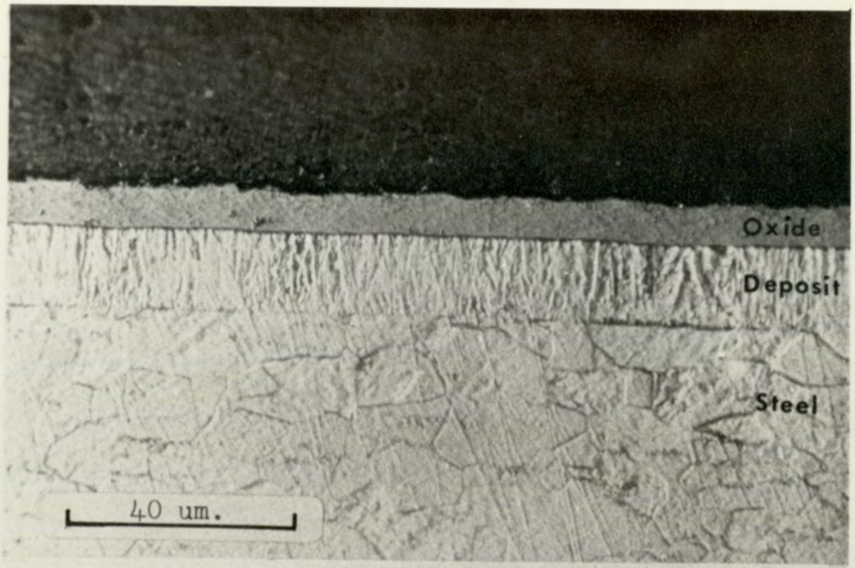

Fig 6.3. Single layered oxide produced on a mild steel sample plated on one side with iron.

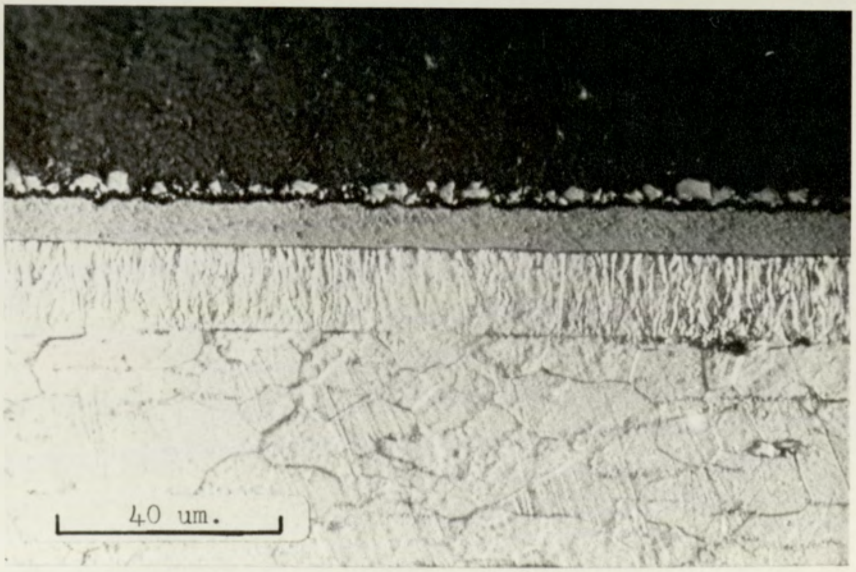

Fig. 6.4. Duplex layered oxide formed on a mild steel sample plated both sides with iron.

Fig. 6.5. Oxidation of iron plated both sides with iron from ammonium ferrous sulphate solution, in 3.5M NaOH at 316°C.

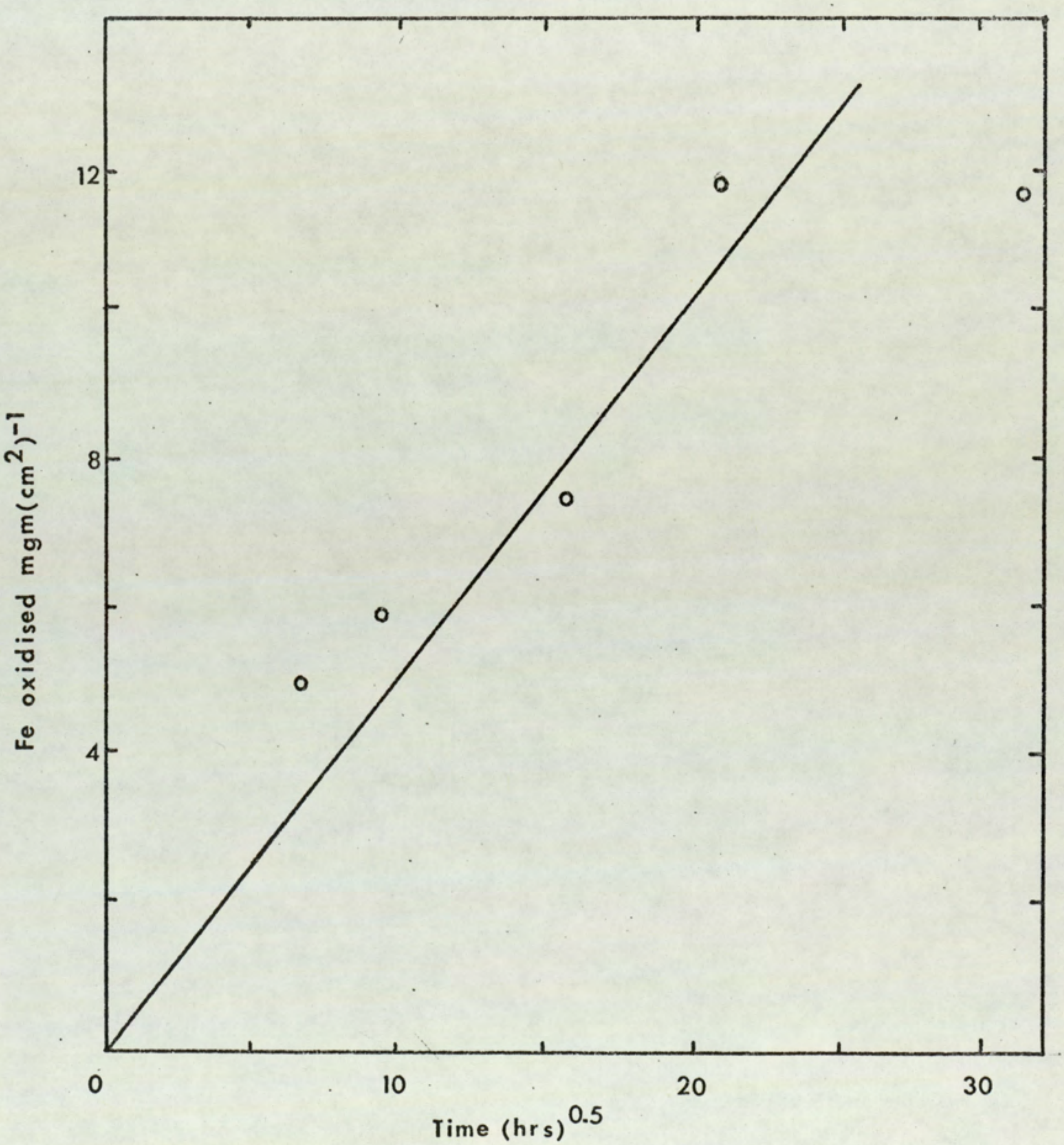

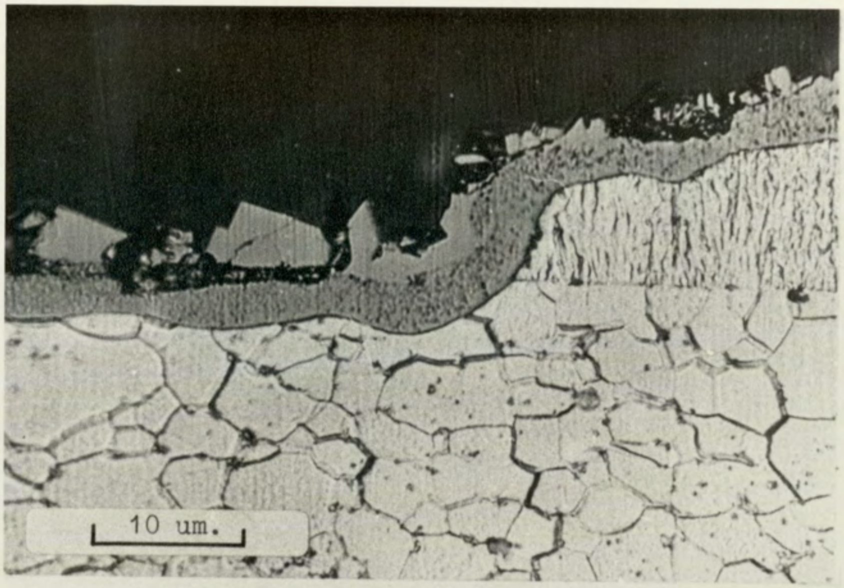

Fig. 6.6a. Cross section of the interface between plated and non plated regions. (Iron plated from ferrous chloride solution.)

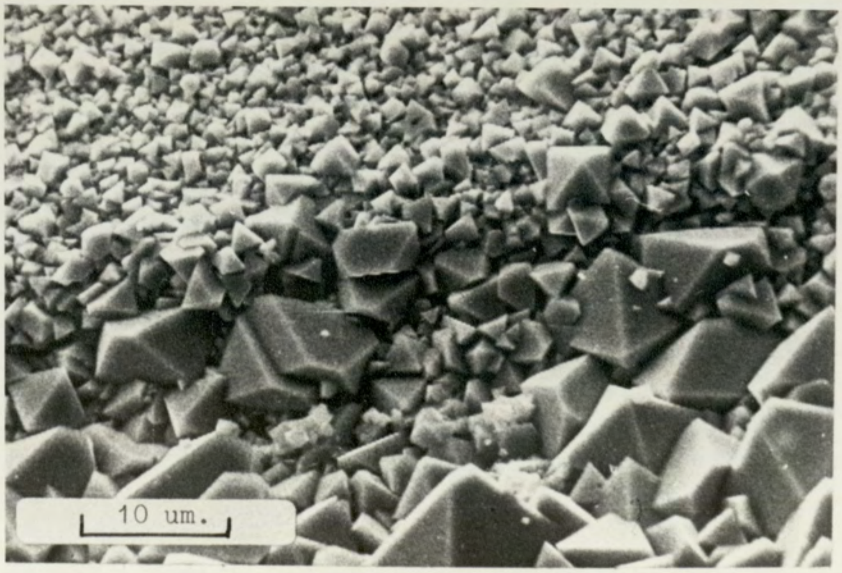

Fig. 6.6b. Scanning electron micrograph of the interface shown in Fig. 6.6a.

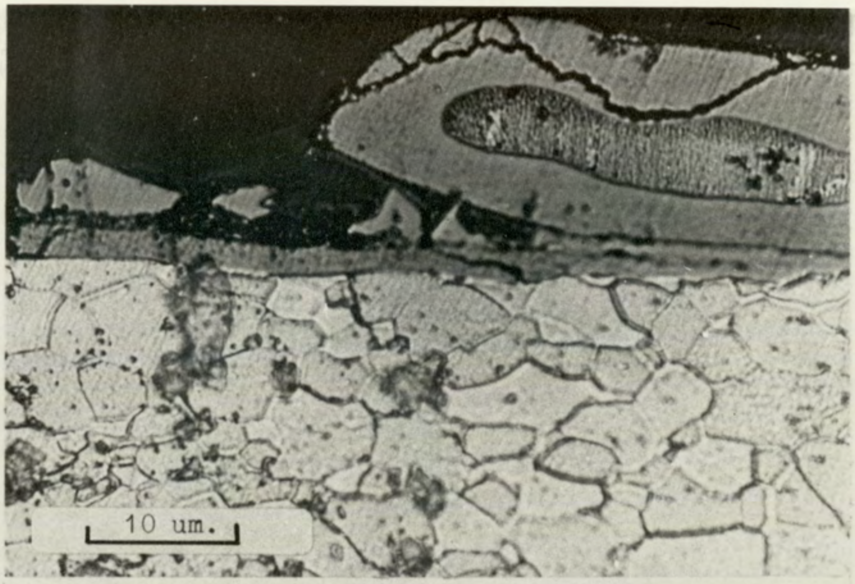

Fig. 6.7a.

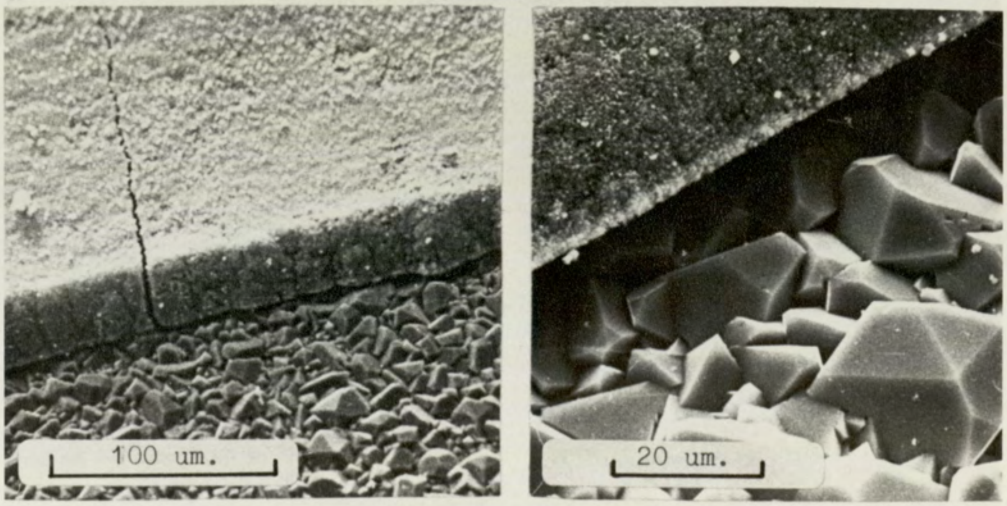

Fig. 6.7b.

Fig. 6.7a. showing a cross section of the oxide produced at the interface between mild steel and iron electrodeposited from ferrous ammonium sulphate solution.

Fig. 6.7b. Scanning electron micrograph of the surface shown in Fig. 6.7a.

interface.

The interface has become separated from the underlying metal, this would be caused by a combination of edge effect and lack of ductility in the electrodeposit. The factors operative in the suppression of the outer layer were more active in this case. Even cracks in the oxide were not able to heal or support the formation of outer layer; in Fig. 6.9a. just the occasional magnetite crystal can be observed in the many cracks in the porous layer. S.E.M.s of the plated layer at intervals of distance away from the interface showed a steady increase in the amount of crystalline magnetite (Figs. 6.8. a,b,c and d.); both the size and crystal density (numerically) increase with distance from the interface.

Defects in the deposit that allowed electrolyte to reach the steel provided a special case. Figs. 6.9a. and b. are cross sections of one such defect. A central pore that was the start of the defect is observed to be open to the surface of the steel. The oxide was found to be thickest at the steel/oxide interface, presumably because electrolyte could permeate the poor bond between the steel and the plate. The zero volume change of iron conversion into oxide had been obeyed since the original interface between the steel and deposit could still be observed.

All the defects observed in the electrodeposit were very

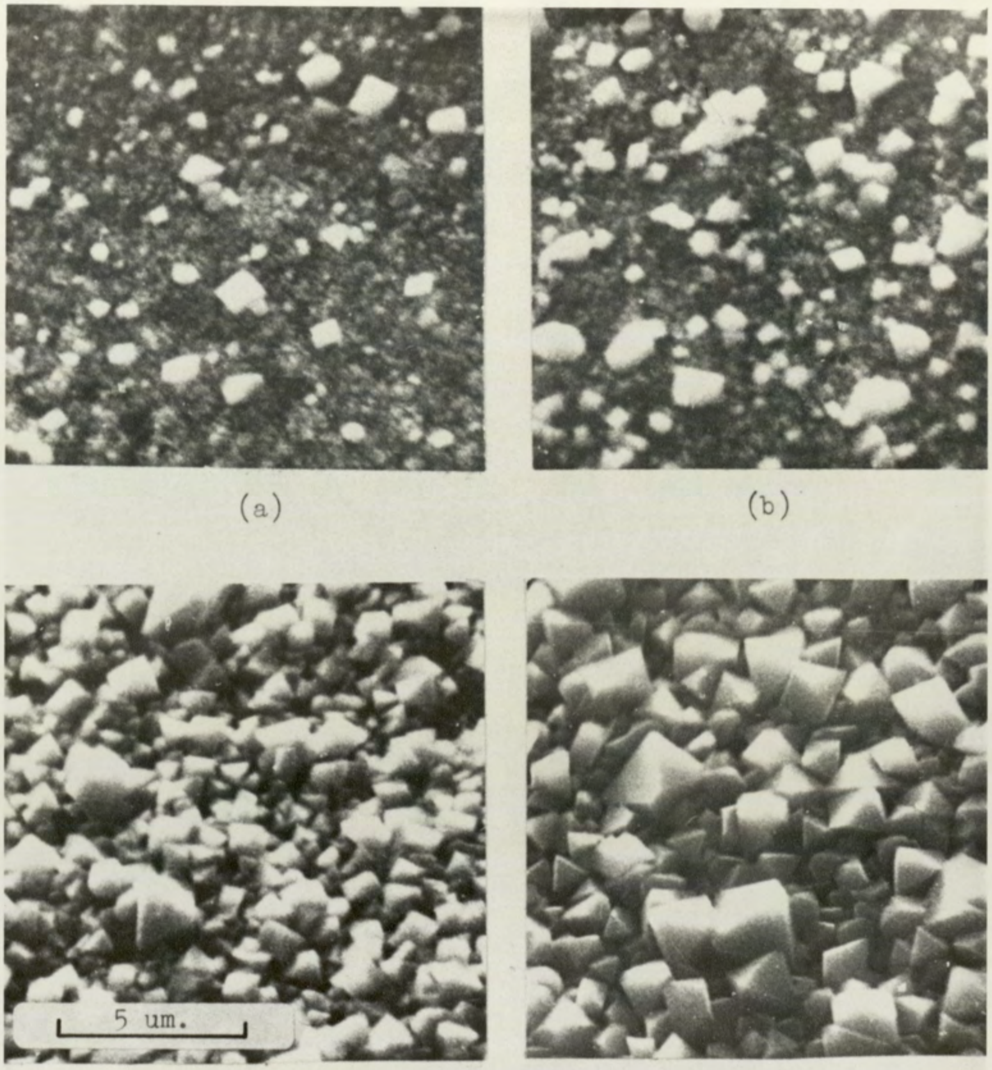

(a) (b)

(c) (d)

Fig. 6.8. Illustrating the variation in amounts of outer layer at increasing distances from such an interface as shown in Fig. 6.7a.

Fig. 6.9a. Scanning electron micrograph of the oxide formed on iron electrodeposited from ammonium ferrous sulphate solution showing defects in the oxide.

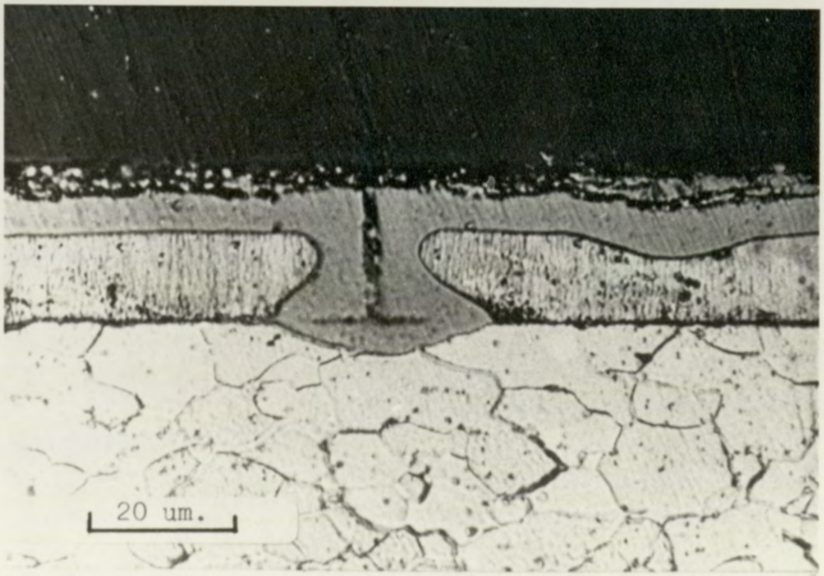

Fig. 6.9b. Cross section of the defect illustrated in Fig. 6.9a. The crack penetrates through to the underlying steel.

much smaller than the central pore in Fig. 6.9b. It might be expected therefore that the same mechanism that kept this pore open is identical to one that inhibits the nucleation of magnetite crystallites in the porous inner layer in Potter and Mann oxidation. Conversely, if this mechanism was not operative, Bloom growth might be expected to take place.

To confirm the differences observed in the oxidation of iron electrodeposits, a 1 x 1½ cms. piece of steel was placed in electrical contact with a 1 x 1½ cms. piece of steel plated on both sides with iron from an ammonium ferrous sulphate bath; the combined specimen was oxidised for 150 hours. Figs. 6.10a and b. show that the steel is thickly covered with magnetite crystals whilst the deposit is virtually crystal free, thus confirming the previous results.

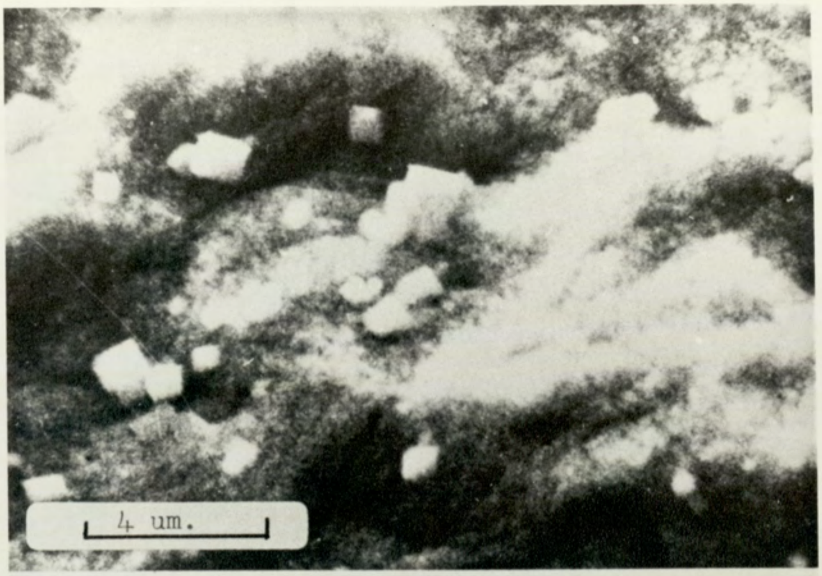

Fig. 6.10a. Showing an S.E.M. of iron electrodeposit side of a steel interface; very little outer layer oxide has formed.

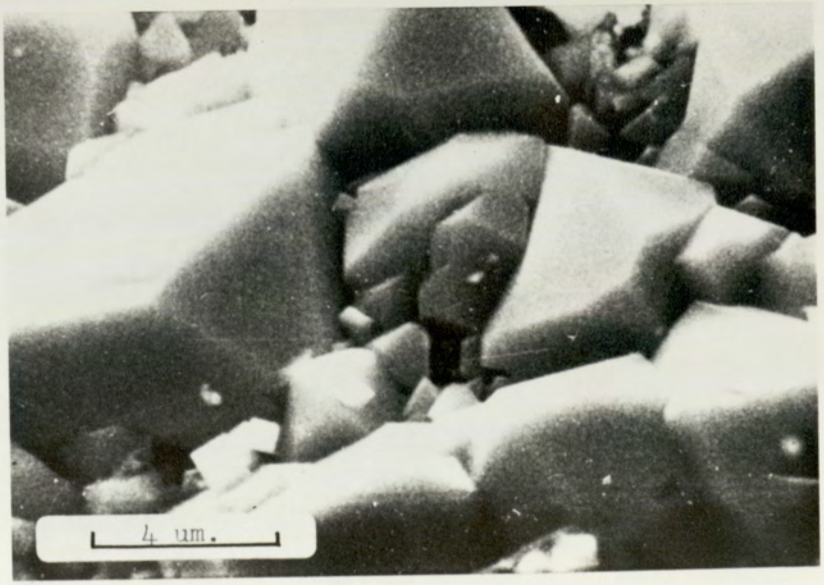

Fig. 6.10b. S.E.M. of steel side of interface showing a well formed outer layer.

CHAPTER VII

DISCUSSION

7.1. Introduction.

In this chapter an attempt is made to discuss the important features abstracted from each system. Although each chapter is considered in the same order as it appears in the text, information from a different system is often drawn on to strengthen the discussion of a particular issue. In dealing with the oxidation of steel in conditioned pressure vessels, emphasis is placed on outer layer formation and the transport of iron within the experimental system. This is followed by new ideas on oxidation in P.T.F.E. capsules, where structures are described in conjunction with a schematic representation of oxide growth. There follow two sections, one devoted to a discussion of transport processes and the role of nickel in ferrous chloride environments and the second one to the oxidation of iron electrodeposits.

7.2. Oxidation in conditioned pressure vessels.

7.2.1. Kinetics.

There is evidence from sectioning experiments, that an active iron tracer originally present on the surface resides in the region of the inner/outer layer interface during oxidation. If this result is applied to the surface activity measurements, then the rate at which an active Fe^{55} tracer is covered with magnetite is given by $y = kt^n$, where t is time (hours) and k and n are found to be 0.22 and 0.49 respectively from statistical treatment. The agreement between outer layer thickness derived from surface activity measurements and weight loss data is only fair; this could most likely be attributable to experimental errors in the weight loss experiments since the experimental procedure was more complex than in surface activity measurements. The value of n (0.49) that was determined from surface activity measurements is in good agreement with the value of n derived from total iron oxidised. It is postulated therefore, that outer layer formation is a function of total oxidation and forms according to $y = kt^{0.5}$. The state of the surface is thought to have a profound affect on k since variation in k occurred when the surface was pretreated e.g. by abrading or etching. Attempts to determine the effect of pretreatment on variations of k were discontinued because of the difficulty in obtaining a reproducible surface. Whilst confidence can be placed on the parabolic formation of outer layer, the value of k however only refers to the steel and pretreatment used in this investigation. Nevertheless this is very strong evidence that iron transport processes are predominating over solid state diffusion under these conditions.

In the absence of solid state diffusion the iron tracer might be expected to behave in a similar way to an inert marker, and in fact Douglas and Zyzes[1] observed a decrease in surface activity of an inert radioactive marker during the oxidation of iron in deionized water; they did not differentiate between two layers in the oxide, presumably because the layers produced in deionized water are extremely thin.

In order to obtain maximum information from the surface activity measurements, it is helpful to consider the form of the active layer. The procedure used to activate the samples would result in the formation of active iron contained in magnetite at the interface between an inner and outer layer formed after 2 hours oxidation. It is thought that the majority of the active iron would be contained in the first formed crystals, although there may be some present in the inner layer adjacent to the outer layer which may have formed by solution interaction during the early stages. On reoxidation, the distribution of the tracer will depend largely on the mode in which the outer crystals grow; three possible ways are shown in Fig. 7.1. Fortunately, each mode would produce different decreases in surface activity for a given time of oxidation, i.e. $a > b > c > d$. The evidence from electron microscopy is that during the initial stages of

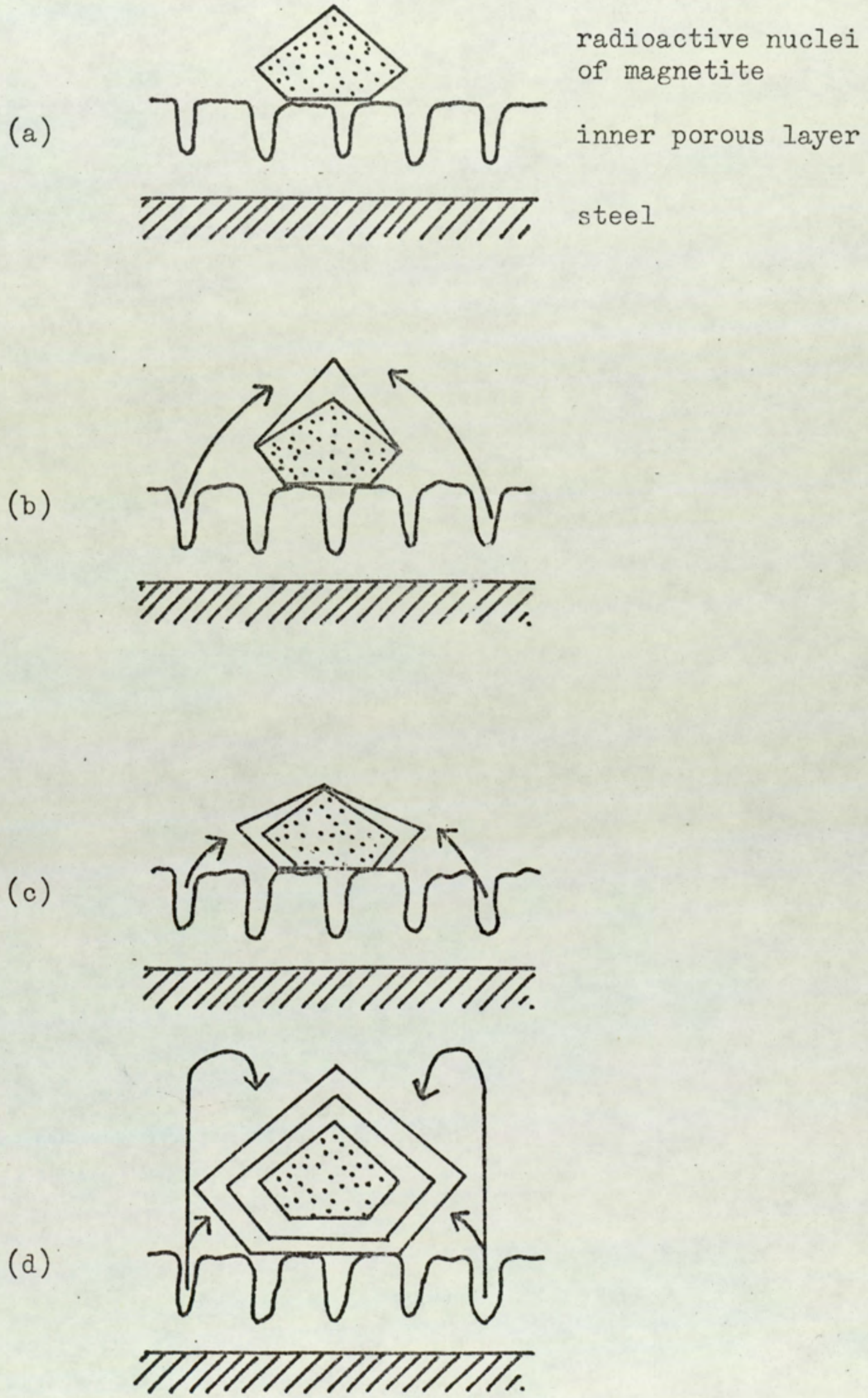

Fig. 7.1. Showing possible growth mechanisms of a magnetite layer under Potter and Mann[7] conditions.

oxidation a mixture of b and c occurs until interaction between growing crystals takes place and the inner porous layer is completely covered. This is then followed by growth on any exposed faces; at this stage the decrease in surface activity would be a function of outer layer growth. Evidence of this is shown in Fig. 7.2. which is an S.E.M. of a polished and etched oxide face; voids can clearly be seen between outer layer crystals allowing access of solution.

7.2.2. Nucleation and growth.

There is strong evidence both in the present work (p.54 Ch. III) and from other research workers[61] that nucleation of a magnetite layer is preceded by dissolution at the iron surface. Obviously in the absence of an electrolyte capable of causing iron dissolution, the rate of oxidation would be governed purely by solid state diffusion. Kato and Arai[33] conclude that oxidation between 15° and 200°C in environments selected for their lowest corrosion rates, oxygen dissolved in the electrolyte reacts directly with the steel and the corrosion mechanism approximates to one of dry oxidation.

If a piece of iron is placed in sodium hydroxide solution at room temperature, considerable length of time would be required for the solution to become saturated with iron.

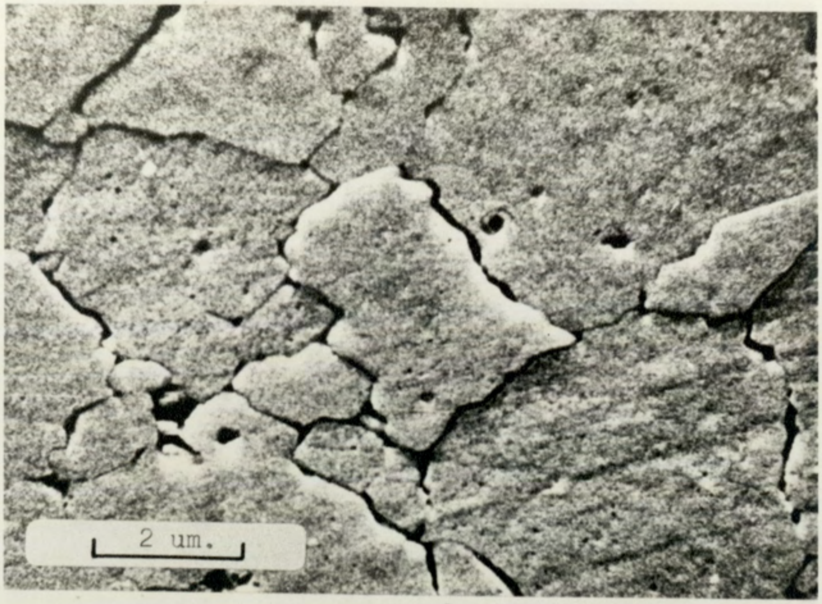

Fig. 7.2. Showing voids between outer layer crystals revealed by polishing and etching. Potter and Mann conditions (3.5M NaOH, 316°C, 500 hours.)
Etchant: HCl vapour.

However with increase in temperature this state of affairs would not continue i.e. the ratio between the solubility product and the dissolution rate would not be constant. A variable factor in this argument would of course be the effect of convection currents within the electrolyte of which very little is known. Reference to Fig. 3.1. shows that there is a very rapid rise in the amount of iron dissolved in the electrolyte with increasing time. The maximum amount of iron in solution is reached after about 12 minutes; the temperature at this stage is about 150°C, at this temperature decomposition of ferrous hydroxide to magnetite would occur by the spontaneous reaction[19,20]:-

$$3Fe(OH)_2 = Fe_3O_4 + H_2 + 2H_2O \quad ....(I)$$

on any convenient surface capable of supporting it. This reaction would certainly represent a driving force for the dissolution of iron.

The ratio of solubility to the rate of dissolution could affect the nucleation and growth of the crystalline outer layer. In Chapter III the results of the oxidation of iron using two different surface area to volume ratios are described. In the experiments involving a reduced surface area, the nucleation and growth of the magnetite crystals is very much retarded. Obviously the solution will not saturate so rapidly at a given temperature as in the experiments involving larger surface areas. In sodium hydroxide solution the outer layer crystals form at a very much later stage than in deionized water. If we apply the criterion already used, the pressure vessel wall, itself an efficient cathode, will play a much greater part as a cathodic surface for reaction (I) because of the electrolyte's ability to hold more iron in solution and also because of its higher conductivity. In fact the radioactive tracer experiments demonstrate this (p.54, Ch. III.) where the pressure vessel is observed to contain 80% of the total activity after about 50 minutes oxidation.

7.3. Oxidation in P.T.F.E. capsules.

Bloom or non porous magnetite which has been grown in P.T.F.E. capsules has certain similarities with Potter and Mann growth. Firstly, the topographies are almost identical in that they are covered with crystalline magnetite after oxidation in NaOH, and secondly the first 10 minutes of oxidation generally occurs in a similar way by the formation of a somewhat porous oxide. However, many differences exist between the oxides formed under these two conditions and any theory must adequately account for these differences. Whereas in Potter and Mann conditions pores could be observed between crystallites that had impinged right up to the time until they were covered with a magnetite outer layer, in Bloom growths they were observed to close. During oxidation in deionized water under Potter and Mann conditions well formed outer layer magnetite crystals were formed, these were notably absent under Bloom conditions i.e. iron oxidised in P.T.F.E. capsules containing deionized water. In 3.5M NaOH however large outer layer crystals formed on iron oxidised in a conditioned pressure vessel (Potter and Mann conditions) much later than if the oxidation was performed in a P.T.F.E. capsule.

The fact that pores were observed in both cases in the early stages suggested that dissolution occurred in the same way. Once again variations of solubility and dissolution rates with temperature can be envisaged. At the temperature responsible for the breakdown of ferrous hydroxide or sodium ferrate to magnetite, pore blockage begins to take place. It is not considered that it occurs instantaneously but occurs over a period of time depending on various factors especially the experimental system and the electrolyte. This would explain the absence of outer crystals in deionized water, the solubility of iron being very much lower than for caustic soda solution at high temperatures. It also explains why the outer crystals form in a P.T.F.E. capsule with a sodium hydroxide environment and also why they form much earlier than under Potter and Mann conditions. In a P.T.F.E. capsule the sample is the only surface capable of supporting the Schikorr reaction. In the presence of an external cathode (i.e. Potter and Mann conditions), iron from solution will be attracted at a very much earlier stage to this cathode, and it will only be when the solubility/dissolution rate ratio increases e.g. by an increase in temperature, that the sample surface will obtain a share of the iron. When this occurs the sample itself will be able to offer a more suitable surface for the magnetite depositing reaction in competition with the external cathode. This would further explain the observation that although the formation of outer layer is a function of total oxidation*, the rate at which it forms depends on the ability to provide a surface suitable for magnetite deposition in competition with other cathodes.

The weight change data were found to fit the logarithmic kinetic law proposed by Evans[27] for self blocking pores extremely well. This would confirm the observations from

---

* Refer to Ch. VII, p.90 where it is shown that orientation, grain size and state of surface can affect the mode in which the outer layer forms.

scanning and transmission electron microscopy already described in Chapter IV. Fig. 7.3. shows schematically a tentative model describing the stages of oxidation of iron in a P.T.F.E. capsule in both deionized water and sodium hydroxide solutions.

The thickness of the porous layer that initially forms on dissolution is considered to be extremely critical, since it is recalled that a porous layer formed after 1½ hours oxidation in sodium hydroxide behaved somewhat differently when reoxidised in a P.T.F.E. capsule. This limiting thickness of porous layer above which Potter and Mann growth could occur even in the absence of an external cathode, could account for many of the intermediate growths observed[13]. If this were the case, there could be much latitude on this limiting thickness and would involve competition between pore closure, dissolution rates and the solubility of iron. Once pore blocking had started to take place and dissolution rate was decreasing, the iron already in solution would form magnetite on the specimen and further oxidation would only occur by solid state diffusion. This would explain the similar topographies that exist between iron oxidised in conditioned and P.T.F.E. lined capsules containing sodium hydroxide solutions. Oxidation by solid state diffusion is

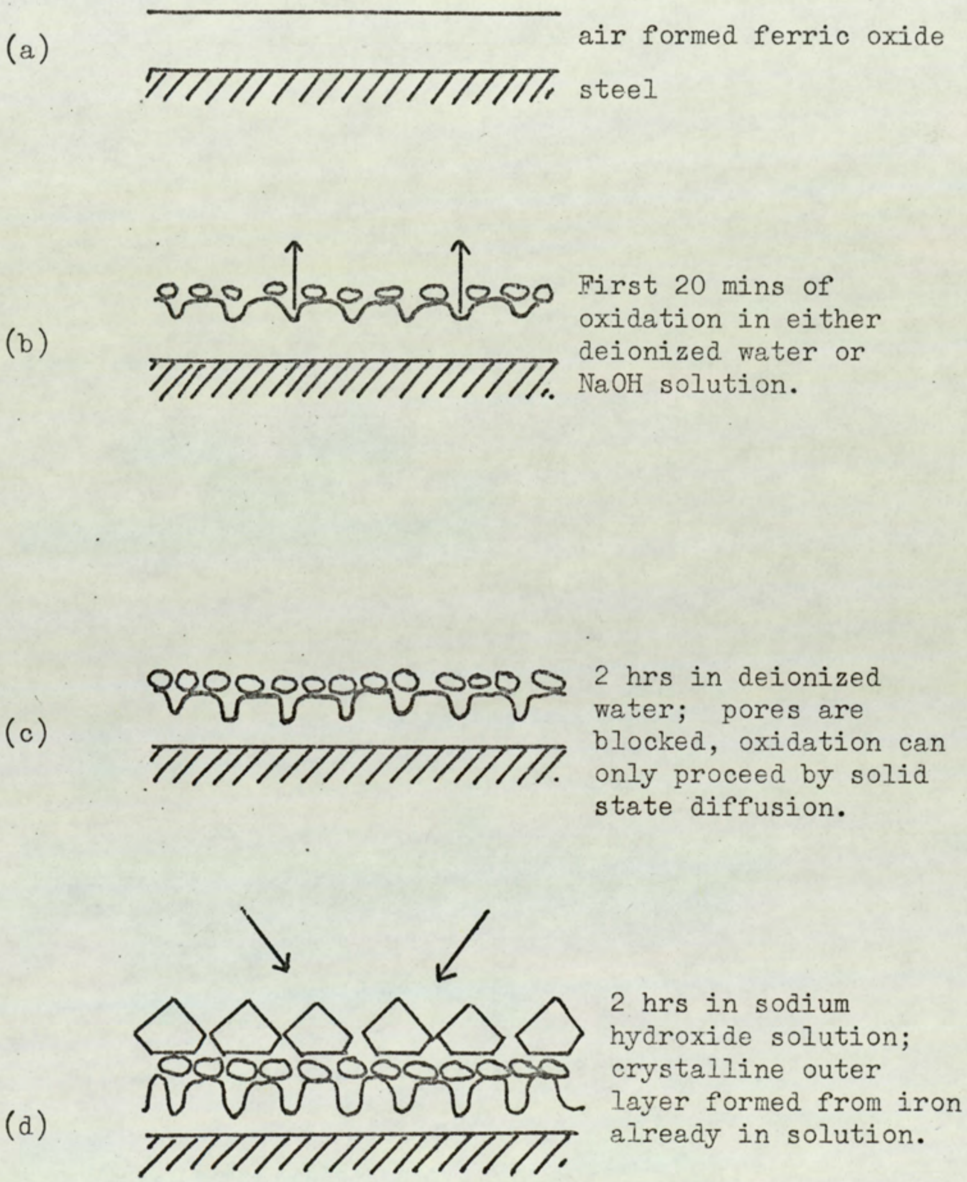

First 20 mins of oxidation in either deionized water or NaOH solution.

2 hrs in deionized water; pores are blocked, oxidation can only proceed by solid state diffusion.

2 hrs in sodium hydroxide solution; crystalline outer layer formed from iron already in solution.

Fig. 7.3. Schematic representation of oxidation in a P.T.F.E. capsule in both sodium hydroxide solution and deionized water.

very slow compared to oxidation by solution transport at 316°C and hence explains the asymptotic shape of the weight change/time relationship.

The structures described by Moore and Jones[62,63] for the oxidation of iron in lithium and sodium hydroxide solutions at 316°C resemble the structures reported in this investigation of the oxidation of iron in a P.T.F.E. capsule. They were able to resolve a crystalline oxide which covered a thin, fine grained, randomly orientated base film. Whereas their results were consistent with the corrosion rate decreasing logarithmically with time, the results reported here are described by an oxidation process decreasing asymptotically with time. The difference is only of academic interest when the experimental conditions are taken into account. Moore and Jones used "Bloom" type capsules for their experiments; these experimental conditions have been shown to give irregular oxides, for example, some samples have pitted areas with the magnetite in the pits being of a porous nature.

An explanation for the amorphous oxide formed under these conditions (Figs. 4.1. to 4.3.) may be obtained from the work of West[64] who postulates that when a metal is undergoing passivation a non crystallographic oxide will be produced, providing its formation is diffusion controlled; this would appear to be the mechanism during the early stages of oxidation.

The irregular oxide/metal interface that exists on iron oxidised in a P.T.F.E. capsule containing sodium hydroxide solution still requires explaining. Referring to the cross section of such oxides (Fig. 1.6a.) it is seen that the oxide is thickest at those regions where dissolution of metal has occurred, this is consistent with a dissolution/deposition mechanism with local high concentrations of iron in solution. Under Potter and Mann conditions the presence of a porous layer between the outer layer and the metal interface ensures a regular metal/oxide interface, since it promotes uniformity of dissolution.

7.4. Oxidation in ferrous chloride solutions.

The results of investigations in this environment are extremely important to the operation of large scale steam generation plant where high concentrations of chloride ions may occur (see Appendix I).

The striking similarity between boiler surfaces suffering internal corrosion and oxides produced in chloride environments in the laboratory cannot be ignored. The areas that had spalled and blistered were generally adjacent to those areas on the steel containing defects. The areas adjacent to the defects appeared to be a better cathode for the deposition of nickel and thicker deposits were generally laid down on these sites. The nickel, being porous had very poor physical properties and did not obstruct the oxidation mechanism but enhanced it by presenting an excellent surface for the cathodic reaction; the extent can be gauged from Fig. 5.12. which shows a ring of magnetite crystals around a nickel induced blister. These enhanced corrosion rates have resulted in periodic loss of adhesion between oxide layers resulting in the formation of blisters.

The decrease in surface activity measurements was consistent with a linear production of magnetite with time, and since Potter and Mann[11] observed linear weight gains with time there is no reason to believe that the oxidation mechanism in ferrous chloride environments is fundamentally different to oxidation in water or sodium hydroxide solutions. The experiments involving the distribution of an Fe^{59} isotope about the experimental system confirmed these observations since they showed that there was continuous iron ion exchange between the corroding sample, pressure vessel and the ferrous chloride environment.

7.5. Oxidation of iron electrodeposits.

Experiments involving the oxidation of iron electrodeposits provided much variation in the formation of outer layer magnetite. The highest reductions in the formation of outer layer were observed when the electrodeposit was in electrical contact with the steel.

These reductions may be explained in three ways:-

(1) the outer layer may form but does not adhere,

(2) the steel may act as a sink for magnetite deposition (because it may present a more suitable surface),

(3) some form of preferential electronic conduction occurs across the interface and supports a cathodic reaction occurring favourably on the steel.

Explanation (1) hardly seems credible in view of the variation in amounts of adherent outer layer varying at distances from the interface which were recorded in some experiments. If only the state of the surface affects adhesion there should be no variation in outer layer. Whilst mode (2) would explain the variation in amounts of outer layer from the interface, it does not explain why the pressure vessel wall does not have the same effect on samples plated both sides.

If unplated iron functions as a superior cathode for the reaction $2e + 2H_2O \rightarrow 2OH^- + H_2$ to plated iron, then at an interface between these two species electrons would be preferentially conducted across the interface to support this reaction and hence accompany subsequent deposition of magnetite[31] on the steel. This implies that the ability of an inner layer oxide to compete for magnetite deposition depends to a large extent on the grain size and texture of the substrate from which it was formed. This would explain the variation in amounts of adherent outer layer at varying distances from the interface.

CONCLUSIONS

Potter and Mann conditions, 316°C.

1. Nucleation of magnetite was preceded by dissolution of iron.
2. The iron dissolved in the early stages was transported quite readily about the experimental system via the electrolyte.
3. After 15 minutes oxidation in deionized water magnetite nuclei (varying in size between 1000 and 2500Å) were formed on the surface in conjunction with the dissolution process. A secondary nucleation process occurred after 25 minutes, these subsequently grew to be outer layer. In sodium hydroxide solutions the two nucleation processes occurred after 30 and 60 minutes respectively.
4. Radioactive iron tracers originally present on the surface were found to reside at the interface between the inner and outer layer. Growth of outer layer was characterised by laminar build up of oxide on exposed crystal faces until impingement with neighbouring crystals occurred. The growth could be described by:-

$$y = 0.22t^{0.49}$$

where y = outer layer (mgm./cm^2.)

t = time (hours)

This information is consistent with oxidation controlled by solution transport.

5. Surface conditions such as grain size and texture affect its ability to support the cathodic reaction accompanying magnetite deposition. In this respect randomly orientated mild steel was superior to iron having a (111) fibre texture electrodeposited from ferrous chloride solution which in turn was superior to a strong (111) textured iron electrodeposited from a ferrous sulphate solution.

6. After 60 minutes oxidation of iron in 0.1M ferrous chloride + 0.001M nickel chloride solution at 316°C, local concentrations of nickel were responsible for pitting and spalling of the oxide. The most severe pitted and spalled areas were characterised in the early stages by rings of crystalline magnetite.

   When a portion of the ferrous ions in the ferrous chloride was replaced with iron ions containing Fe^{59} they were found to be removed exponentially with time during oxidation.

This implied free and continuous iron exchange between the environment and the corroding sample. This confirmed that solution transport processes were operative.

Oxidation in a P.T.F.E. lined pressure vessel (Bloom conditions) at 316°C.

1. Oxidation commenced by dissolution of iron, resulting in local concentrations of iron at regions adjacent to the dissolution sites.
2. Nucleation of a porous oxide accompanied the dissolution process but was only transient and pore blocking occurred after 45 minutes in 3.5M NaOH. Oxidation was then rate controlled by the slow process of solid state diffusion. The growth could be described by the law

   $$y = 0.83\,(1 - e^{-0.042t})$$

   where y = increase in weight (mgm./cm^2.)

   t = time (hours)

   over the period 20-300 minutes and may be interpreted by a consideration of self blocking pores, since the increase in weight due to the magnetite formed from solution is proportional to the rate of dissolution of iron.

APPENDICES

APPENDIX I

Practical issues concerning internal corrosion.

On-load corrosion has been a growing problem in boiler operation for 30 years, simply because of the rapid increase in the size of generator units; many papers have been published on internal corrosion during this period[65-69].

The common feature of this corrosion is that the oxide layer adjacent to the steel is of hard grey magnetite, whilst the outer layers are covered with a loose reddish-brown material; analysis of the material has shown the presence of Fe_3O_4, Fe_2O_3 CuO and Cu metal plus small amounts of nickel, the copper and nickel being derived from feed-water preheaters. Many pits have been examined and in general they tend to show a laminated structure. The pits are either found singly or multiple but the extent of the corrosion is often sufficient for the steel to have lost most of its strength from hydrogen damage. The corrosion is caused by rogue growth and calculations show that of all the working boiler surfaces, one part in 10^8 is affected in this way. The normal thickness of magnetite in a working boiler is approximately 30-50 microns and is of a form successful in protecting the underlying steel.

Internal corrosion has been observed to affect practically all parts of immersed boiler surfaces, but experience has shown that a higher than normal incidence occurs in the following areas:-

(1) zones of high heat transfer

(2) at or near welds and particularly bad welds i.e. those that have not been properly reamed

(3) tube bends

(4) areas allowing salt concentration such as the steam water interface or regions containing porous deposits.

These factors have been amply reviewed by Holmes and Mann[69].

Examination of a boiler tube.

A boiler tube that has been in service for 4000 hours in a 120 MW unit has been examined. The results have been included in this thesis so that the recommendations of laboratory tests may be brought into true perspective regarding large scale plant.

The tube was removed because it had suffered acute fire side corrosion on the side adjacent to the heat source; the wall thickness in this region was found to be very much thinner

(Fig. A1.1.). Sections cut from both sides were examined by optical microscopy. The section cut from the thicker side of the tube wall is an example of protective magnetite, the layer varied between 20 and 35 microns and followed the contours of the tube (Fig. A1.2a.). It had the appearance of normal inner layer magnetite. If this layer remained stress free, then during its formation an equivalent amount of iron must have been lost to the system; the formation of a normal outer layer most likely being suppressed in a dynamic system such as an operational boiler. The average chemical conditions for the water contained by the tube were 5 ppm. of sodium hydroxide resulting in a pH 10 at 25°C. The iron that entered solution during the formation of protective magnetite would either be removed early in the life of the boiler during frequent changes of water, or alternatively promote the formation of porous deposits in parts of the boiler having reduced water flow.

The section cut from the heat affected side of the boiler tube is seen to carry a much thicker oxide layer of approximately 70-90 microns thick (Fig. A1.2b.). Adjacent to the metal is a magnetite layer between 15 and 20 microns thick. This side of the tube has suffered some pitting; the pits, although not presenting a major problem at this stage might well

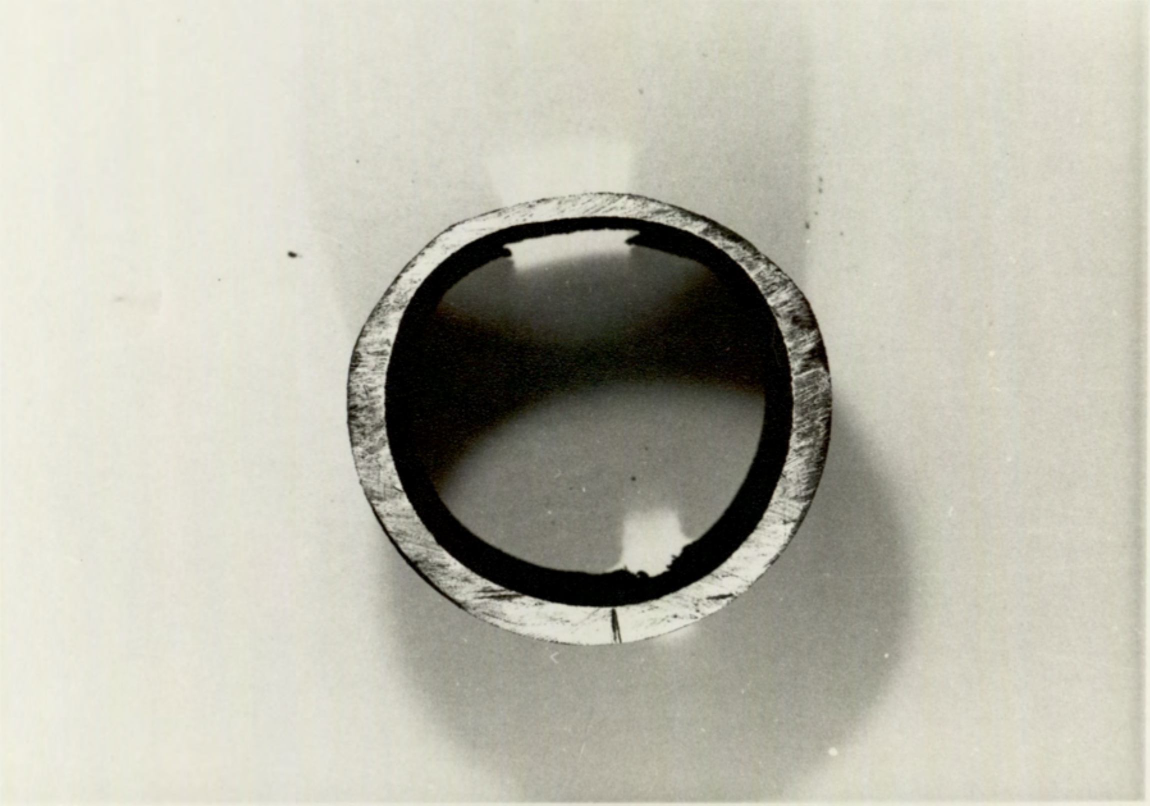

FIG. A1.1

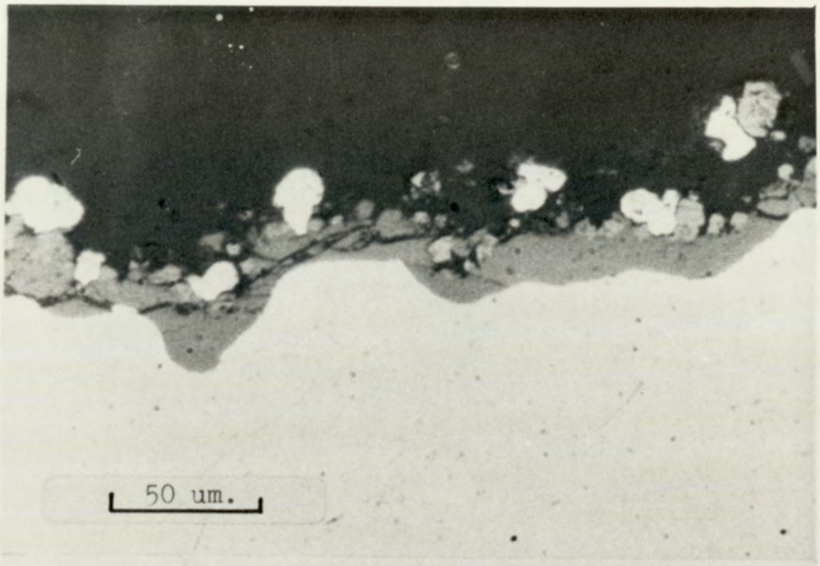

Fig. A1.2a. Illustrating a cross section of protective magnetite formed on the internal surface of a boiler tube during normal operating conditions.

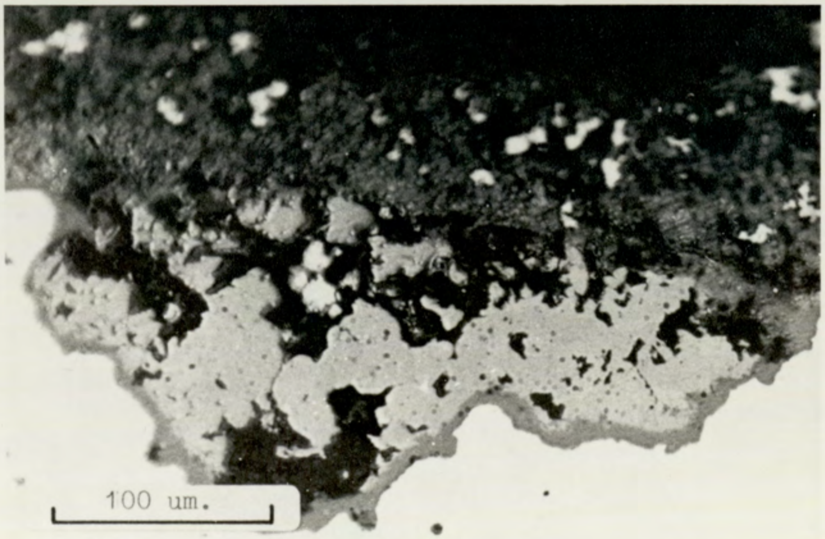

Fig. A1.2b. Showing a cross section of magnetite formed on the internal surface of a boiler tube subjected to abnormally high heat transfer.

be expected to if water conditions in the presence of nickel were allowed to develop. The outer oxide layer being porous and more important in a position of high heat transfer would promote the formation of high concentrations of boiler chemicals, that would certainly aggravate internal corrosion.

Electron microprobe analysis of scale.

The results of the microprobe analysis of samples (1) and (2) which are from the heat affected and normal sections of the boiler tube respectively are given in Figs. A1.3. and 4. The very light phases which are prominent in the optical micrographs have been identified as copper metal. It is doubtful whether the presence of copper affects corrosion to any great extent since experiments on specimens plated with copper have been unsuccessful in increasing oxidation rates in either acidic or alkaline solutions. There is however a higher concentration of nickel in the oxide from the heat affected area (compare sample (1) with sample (2); this could well become critical in stimulating the cathodic reaction and acute corrosion might be expected to occur if high chloride environments were allowed to develop.

FIG.A1.3.Electron microprobe analysis of boiler scale (sample 2)

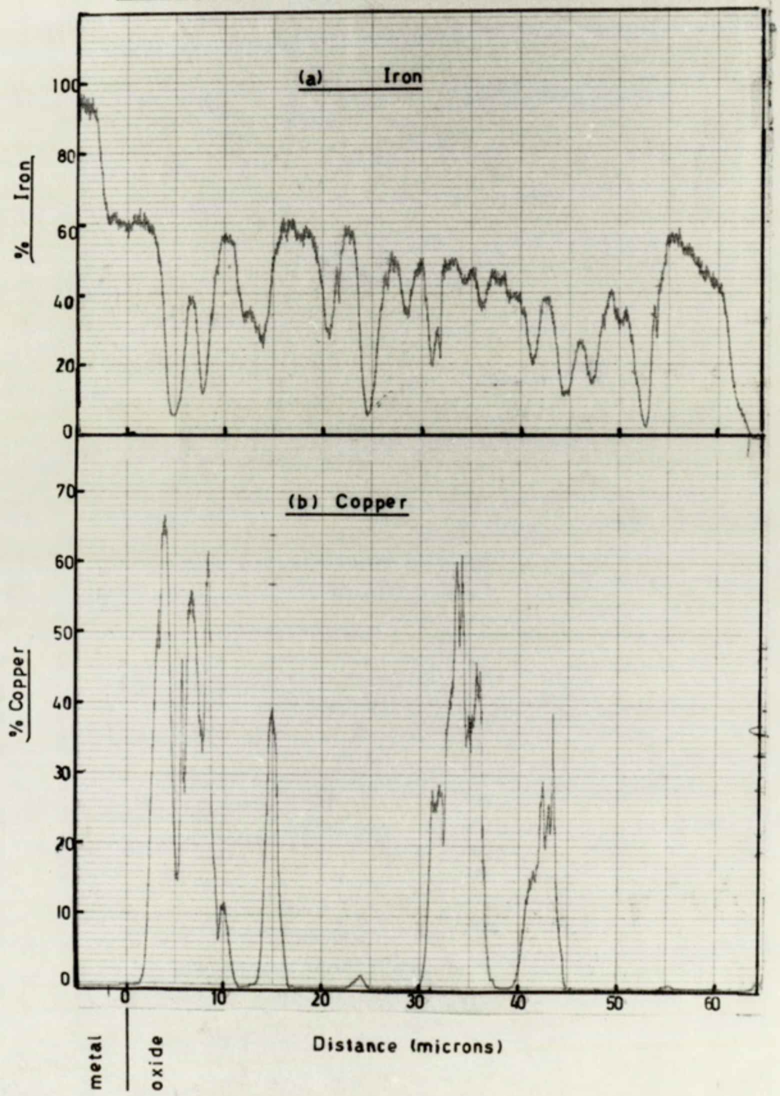

Fig. A1.4. Electron microprobe analysis of boiler scale

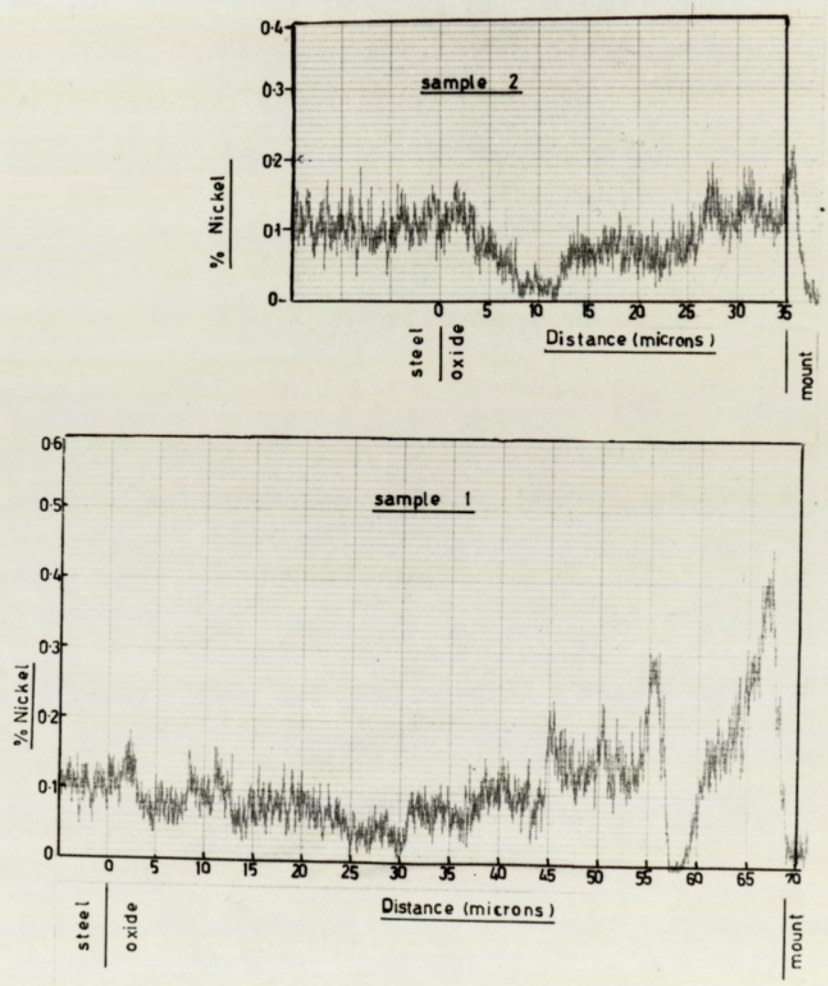

APPENDIX II

Analysis of iron.

The most satisfactory method for the determination of total iron in dilute hydrochloric acid solution was the thioglycollic acid method[70].

Reagents.

Ammonium thioglycollate: a 10% by volume solution of thioglycollic acid was neutralised with ammonium hydroxide solution.

Ammonium hydroxide: "Analar" 3M.

Method.

An aliquot of the unknown solution containing 0.01-0.1 mgm. Fe was made up to 50 mls. in deionized water. 2mls. of the ammonium thioglycollate and 10 mls. of the ammonium hydroxide solution were added to the unknown from a graduated pipette. The solution was shaken and made up to 100 mls. with deionized water. The colour intensity was compared soon after it had developed with standards similarly prepared from known ferric iron solutions. The optical intensity was measured on an E.E.L. absorptiometer in 10 cms. silica cells using a filter having maximum transmission at between 530 and 540 mu. Blank solutions were obtained for these measurements by running the potentiostat cell without the electrodes; the electrolyte was then removed and treated as described earlier. In this way reproducible accuracy better than ± 2% could be obtained.

REFERENCES

1. D.L. Douglas and F.C. Zyzes, Corrosion, 13 , 361t - 374t, 433t - 436t, June, July (1957).

2. M.C. Bloom, M. Krulfeld, W.A. Fraser and P.N. Vlannes, Corrosion, 13 , 297t (1957).

3. M. Krulfeld, M.C. Bloom and R.E. Seebold, Corrosion, 15 , 179t (1959).

4. E.C. Potter and G.M.W. Mann, Proc. 2nd Int. Congr. on Metallic Corrosion, New York, 872 (1963).

5. W.E. Ruther and R.K. Hart, Corrosion, 19 , 127t (1963).

6. Takashi Mukaibo and Shigehiko Masukawa, Corrosion Engineering, Japan, 14 (4), 163 - 167 (1965).

7. E.C. Potter and G.M.W. Mann, 1st Int. Congr. Metallic Corros., Butterworths, London, 417 (1961).

8. A.M. Adams, E.M. Field, D.R. Holmes and R.C. Stanley, 2nd Int. Congr. Metal. Corros., New York, 829 (1963).

9. J.E. Castle and H.G. Masterson, Corros. Sci., 6 , 93 (1966).

10. J.E. Castle and G.M.W. Mann, Corros. Sci., 6 , 253 (1966).

11. E.C. Potter and G.M.W. Mann, Br. Corros. J., 1 , 26 (1965).

12. M.C. Bloom, 21st A. Wat. conf. Engineers Society of Western Pennsylvania (1960).

13. T.F. Marsh, J. electrochem. Soc., 113 , 313 (1966).

14. H.A. Friggens and D.R. Holmes, Corros. Sci., 8 , 871 (1968).

15. G. Chaudron, Z. Elektrochem., 29 , 279 (1923); Ann. Chemie, 16 , 221 (1921).

16. H.E. Hömig, Tech. Überwach., 5 (11), 389 Nov. (1964).

17. V.J. Linnenbom, J. electrochem. Soc., 105 , 322 (1958).

18. W.G. Whitman, R.P. Russell and G.H. Davis, J. Am. Chem. Soc., 47 , 70 (1925).

19. G. Schikorr, Z. anorg. u. allgen. Chem., 212 , 33 (1933).

20. F.J. Shipko and D.L. Douglas, J. Phys. Chem., 60 , 1519 (1956).

21. C.E. Kaufman, V.M. Marcy and W.H. Trautman, Proc. 6th Annual Water Conference, Pittsburgh, (1945).

22. W.A. Fraser and M.C. Bloom, Corrosion, 18 , 163 (1962).

23. C.H. Desch et al., J. Iron St. Inst., 143 , 93 (1941).

24. N.B. Pilling and R.E. Bedworth, J. Inst. Met., 29 , 534 (1923).

25. M.H. Davies, M.T. Simnad and C.E. Birchenall, Trans. Amer. Inst. min. met. Engrs., 191 , 889 (1951); 197 , 1250 (1953).

26. L. Himmel, R.F. Mehl and C.E. Birchenall, Trans. Amer. Inst. min. met. Engrs., 197 , 843 (1953).

27. U.R. Evans, "The Corrosion and Oxidation of Metals", Edward Arnold Ltd., London. p.834 (1960).

28. P.L. Harrison, J. electrochem. Soc., 112 , 235 (1965).

29. E.M. Field and D.R. Holmes, Corros. Sci., 5 , 361 (1965).

30. P.W. Teare, P.L. Harrison and D.R. Holmes, C.E.R.L. Report No. RD/L/N 129 (1965).

31. U.R. Evans, "The Corrosion and Oxidation of Metals", 1st supp. volume, Edward Arnold Ltd., London.

32. M.C. Bloom, G.N. Newport and W.A. Fraser, J. electrochem Soc., 12 , 1343 (1964).

33. Jirō Katō and Yoshi Arai, J. Chem. Soc., Japan (Ind. Chem. Sect.), 63 , 1576 (1960).

34. E. Ulrich, Brennst.-Warme-Kraft, 7 (6), 241 (1955).

35. A. Rahmel, Mitt. V.G.B., 74 , 319 (1961).

36. J.E. Castle and P.L. Surman, J. Phys. Chem., 71(13), 4255(1967).

37. J.E. Castle and P.L. Surman, J. Phys. Chem., 73(3), 632 (1969).

38. P.B. Sewell, C.D. Stockbridge and M. Cohen, J. electrochem. Soc., 99 , 360 (1952).

39. W.H.J. Vernon, F. Wormwell and T.J. Nurse, J. Chem. Soc. 621 (1939).

40. R.H. Greaves, Metallurgist, 25 , 141 (1925).

41. Callendar Steam Tables, 4th edition, Edward Arnold Ltd., London.

42. The Radiochemical Manual 2nd edition, The Radiochemical Centre, Amersham (1966).

43. W.A. Macfadyen, Trans. Faraday Soc., XIV , 98 (1920).

44. P.L. Harrison, private communication (1966).

45. J. Bardeen, W.H. Brattain and W. Shockley, J. Chemical Physics 14 , 714 (1946).

46. G.W. Castellan and W.J. Moore, J. Chemical Physics, 17 , 41 (1949).

47. M.J. Pryor and U.R. Evans, J. Chem. Soc., 1259 (1950).

48. H.G. Oswin and M Cohen, J. electrochem Soc., 104 (1), 9 (1957).

49. A.M. Sukhotin and K.M. Kartashova, Corros. Sci., 5 , 393 (1965).

50. W.J. Moore and B. Selikson, J. Chemical Physics, 19 (12), 1539 (1951).

51. C.E. Birchenall and R.F. Mehl, J Metals, 188 , 144 (1950).

52. J. Steigman, W. Shockley and F.C. Nix, Physical Review, 56, 13 (1939).

53. J. Smiltens, J. Chemical Physics, 20 , 990 (1952).

54. F. Lowenheim, "Modern electroplating",2nd edition, Wiley (1963).

55. M.J. Moroney, "Facts from figures", Penguin, p.286 (1963).

56. D. Eurof Davies, U.R. Evans and J.N. Agar, Proc. Roy. Soc., (A) 225, 443 (1954).

57. J.E. Castle and H.G. Masterson, Anti-corrosion, 3, Dec. (1966).

58. D.J. Turner, C.E.R.L. Report No. RD/L/N 123/68 (1968).

59. G.M.W. Mann, Chem. and Ind., 1584 (1964).

60. J.E. Castle and H.G. Masterson, Vereinigung Der Grosskessel-besiczer, E.V. Conf, Feed-water, Essen (1965).

61. J.E. Castle, P.M. Foster and H.G. Masterson, C.E.R.L. Report No. RD/L/R 1549 (1969).

62. J.B. Moore, Jr., and R.L. Jones, J. electrochem Soc., 115 , 576 (1968).

63. J.B. Moore, Jr., and R.L. Jones, J. electrochem. Soc., 116 (8) , 1080 (1969).

64. J.M. West, "Electrodeposition and Corrosion Processes", 104, D. Van Nostrand & Co., London, (1965).

65. L.E. Hankison and M.D. Baker, Trans. Amer. Soc. mech. Engrs., 69 , 497 (1947).

66. E.W.F. Gillham and R.Ll. Rees, Bull. C.B.E.D.E. No.11,16(1951).

67. H.A. Grabowski, Trans. Amer. Soc. mech. Engrs., 77 , 433 (1955).

68. E.C. Potter and R.Ll. Rees, Bull. C.B.E.D.E. 11, No.32,73(1956).

69. D.R. Holmes and G.M.W. Mann, Corrosion, 370 (1965).

70. A.I. Vogel, "Quantitative Inorganic Analysis", 2nd edition Longmans, 647 (1960).

ACKOWLEDGEMENTS

The author wishes to record his gratitude to Dr. D.J. Arrowsmith for his continued interest in, and supervision of the research programme.

The author is also indebted to the Central Electricity Generating Board and the Science Research Council for the award of maintenance grants for the periods 1966-1967 and 1967-1969 respectively.

Thanks are also due to Dr. G. Briscoe of the Chemistry Department for continuous assistance with the radiochemical aspects of the work.